2013-09-09

Characterization of GW/P Body Components in Astrocyte and Astrocytoma Cells

Moser, Joanna Joy

UNIVERSITY OF CALGARY

Characterization of GW/P Body Components in Astrocyte and Astrocytoma Cells

by

Joanna Joy Moser

A THESIS

SUBMITTED TO THE FACULTY OF GRADUATE STUDIES

IN PARTIAL FULFILMENT OF THE REQUIREMENTS FOR THE

DEGREE OF DOCTOR OF PHILOSOPHY

DEPARTMENT OF MEDICAL SCIENCE

CALGARY, ALBERTA

SEPTEMBER, 2013

Abstract

GW/P bodies (GWB) are cytoplasmic foci that contain GW182 and Ago2 that bind micro RNA (miRNA) within the RNA-induced silencing complex (RISC) to silence and degrade messenger RNA (mRNA). Clinical studies indicate that 33% of patients with GWB autoantibodies have a motor/sensory neuropathy and/or ataxia. Preliminary data show that GWB are highly expressed in the central nervous system, particularly in astrocytes. Characterizing the protein and RNA components of GWB is key to elucidating their function in astrocyte and astrocytoma cells.

First, a detailed immunoprecipiation (IP)-Western blot (WB) protocol was developed to addresses challenges in isolating low abundance protein GW182 and GWB-associated proteins. This protocol provides a biochemical approach for detecting GW182 and associated proteins in biological samples facilitating the elucidation of the diverse functions of GWB.

Second, astrocytoma GWB exhibit complex heterogeneity with combinations of LSm4 and XRN1 as well as Ago2 and Dicer, key proteins involved in mRNA degradation and RNA interference respectively. GWB subsets contained the mRNA transport and stabilization proteins SYNCRIP, hnRNPA1 and FMRP, not previously described as part of the GWB complex. Astrocytoma GWB-IP suggested that Dicer, hDcp, LSm4, XRN1, SYNCRIP and FMRP form a multiprotein complex and are involved in a number of regulatory mRNA pathways.

Third, GWB/RISC mRNA and miRNA components were profiled by microarray analysis of astrocytoma cells and astrocytes. MiRNAs were highly enriched in astrocyte

RISC compared to astrocytoma RISC, astrocytoma and astrocyte cells each contained unique RISC miRNA profiles as compared to their respective cellular miRNA profiles, miR-195, 10b, 29b, 19b, 34a and 455-3p levels were increased and the miR-181b level was decreased in astrocytoma RISC as compared to astrocyte RISC, and the RISC contained decreased levels of mRNAs in astrocyte and astrocytoma cells. Biological pathway analysis of RISC mRNA suggests that ultimately GWB play a pivotal role in malignancy.

In future, it is important to move beyond characterizing the GWB components of resting cells, but determine the functional response of GWB when subjected to physiologically relevant stimuli. Clinically, there is much to learn about other GWB autoantigens, other diseases associated with GWB autoantibodies and the genetic basis for GWB autoimmunity.

Thesis Publications

The following publications have been used for the main context of Chapters 1 – 5:

Moser JJ and Fritzler MJ. Cytoplasmic ribonucleoprotein (RNP) bodies and their relationship to GW/P bodies. International Journal of Biochemistry and Cell Biology, 2010 Jun;42(6):828-43. PMID: 19944184.

Moser JJ, Chan EKL, Fritzler MJ. Detection of components of GW Bodies by immunoprecipitation and western blot analysis. Nature Protocols, 2009 Apr 16; 4(5):674-685. PMID: 19373232.

Moser JJ, Eystathioy T, Chan EKL, Fritzler MJ. Markers of mRNA stabilization and degradation, and RNAi within astrocytoma GW bodies. Journal of Neuroscience Research, 2007 Jul 30; 85(16): 3619-3631. PMID: 17663465.

Moser JJ and Fritzler MJ. The MicroRNA and MessengerRNA Profile of the RNA-Induced Silencing Complex in Human Primary Astrocyte and Astrocytoma Cells. *Submitted to PLoS ONE May 04, 2010.*

Collaborators and Co-authors

The authors of the listed publications, Marvin J. Fritzler and I would like to recognize the contribution of the following co-author and collaborator:

Dr. Edward K.L. Chan, PhD (University of Florida, Gainesville, FL, USA) for his advice and fruitful discussion of all things GWB.

Acknowledgements

I would like to acknowledge and express my deepest gratitude to my supervisor and mentor, Dr. Marvin Fritzler for his never-ending support and advice throughout my research program. Thank you for challenging me to reach the professional goals I have set for myself. Your knowledge, wisdom and vast experience in objectively assessing a given situation and providing alternative interventions and/or conceptualizations will forever be etched into my memory. To my committee members, Dr. JB Rattner for his friendship, patience, advice and collaboration, Dr. Zochodne for his expertise in clinical neurology and Dr. Colicos for his neuroscience and live cell imaging advice. All of you have played an important role in furthering my research experience. I consider it an honour and privilege to have worked with you.

I also acknowledge the Canadian Institute for Health Research (CIHR) and the Alberta Heritage Foundation for Medical Research who provided my funding through a Doctoral Research Award in the Area of Clinical Research and a Full-Time Studentship Award, respectively. Many thanks to the Medical Science graduate department for multiple Medical Science Academic Productivity Awards over the years and to the Faculty of Graduate Studies for the Dean's Research Excellence Award.

Dedication

To Verna Moser, my mom and best friend.

Thank-you for your prayers, steadfast love and commitment.

Without your guiding wisdom and support none of this would have been possible.

Table of Contents

List of Tables

List of Figures

List of Symbols, Abbreviations and Nomenclature

Abbreviation	Full Name
Ago2	Argonaute 2
AREs	AU-rich elements
ATP	adenosine triposphate
Ca^{2+}	calcium
cDNA	complementary DNA
CNS	central nervous system
CPEB	cytoplasmic polyadenylation element-binding protein
Ct	cycle threshold
cyPrP	cytoplasmic prion protein
DAPI	4',6-diamidino-2-phenylindole
$_{dd}H_2O$	double distilled water
DIC	differential interference contrast
dlP-bodies	dendritic P-body like structures
DMP	dimethyl pimelimidate dihydrochloride
DNA	deoxyribonucleic acid
dsRNA	double-stranded RNA
eIF	eukaryotic translation initiation factor
FMRP	fragile X mental retardation protein
G	glycine
GFAP	glial fibrillary acidic protein
GFP	green fluorescent protein
GWB	glycine- and tryptophan-rich cytoplasmic processing bodies
hAgo2	human Argonaute 2
hnRNPs	heterogeneous nuclear ribonucleoproteins
Hsp	heat-shock protein
HuR	Hu antigen R
IB	immunoblot
IIF	indirect immunofluorescence
IP	immuoprecipitation
IPA	Ingenuity Pathway Analysis
LSB	Laemmli sample buffer
LTD	long term depression
LTP	long term potentiation
miRNA, miR	microRNA
mRNA	messenger RNA
NHS	normal human serum
NMDA	N-methyl-D-aspartic acid
PBC	primary biliary cirrhosis
P-bodies	processing bodies

PBS	phosphate buffered saline
pre-miRNA	precursor-miRNA
PrP	prion protein
PSDs	postsynaptic densities
PVDF	polyvinylidene fluoride
Q	glutamine
qkRT-PCR	quantitative kinetic reverse transcription polymerase chain reaction
RA	rheumatoid arthritis
RISC	RNA induced silencing complex
RNA	ribonucleic acid
RNAi	RNA interference
RNP	ribonucleoprotein
RRM	RNA recognition motif
RT	room temperature
SDS-PAGE	sodium dodecyl sulphate – polyacrylamide gel electrophoresis
siRNA	small interfering RNA
SjS	Sjögren's syndrome
SLE	systemic lupus erythematosus
snRNPs	small nuclear ribonucleoproteins
SSc	systemic sclerosis
SYNCRIP	synaptotagmin-binding, cytoplasmic RNA-interacting protein
TAM	temporal asymmetric mitochondrial RNA processing
TIA	T-cell intracellular antigen
TNR	trinucleotide repeat
TNRC6A	trinucleotide repeat containing 6A
UTR	untranslated region
W	tryptophan
WB	Western blot

Epigraph

The search for truth is in one way hard and in another easy. For it is evident that no one can master it fully nor miss it wholly. But each adds a little to our knowledge of Nature, and from all the facts assembled there arises a certain grandeur.

-Aristotle

Chapter One: **Introduction***

*Parts of this chapter have been published and used with permission:

- Moser JJ and Fritzler MJ. Cytoplasmic ribonucleoprotein (RNP) bodies and their relationship to GW/P bodies. International Journal of Biochemistry and Cell Biology 2010 Jun;42(6):828-43. PMID: 19944184
- Moser JJ, Eystathioy T, Chan EKL, Fritzler MJ. Markers of mRNA stabilization and degradation, and RNAi within astrocytoma GW bodies. Journal of Neuroscience Research 85 (16): 3619-3631, 2007. PMID: 17663465

Parts of this chapter have been submitted for publication:

- Moser JJ and Fritzler MJ. The MicroRNA and MessengerRNA Profile of the RNA-Induced Silencing Complex in Human Primary Astrocyte and Astrocytoma Cells (submitted May 4, 2010).

1.1 Brief history of the use of autoantibodies to discover novel cellular proteins and cellular compartments

Historically, human autoantibodies directed to nuclear and cytoplasmic antigens have aided clinicians in the diagnosis of many autoimmune diseases and, for cell and molecular biologists, have been remarkably powerful tools to discover and understand the structure, composition and function of novel macromolecules and cellular compartments (Tan, 1991;Fritzler, 1996). These include small nuclear ribonucleoproteins (snRNPs) and components of the spliceosome, kinetochores, nucleoli, the Golgi complex and endosomes, to name only a few (reviewed in (Stinton et al., 2004)). Some of the target autoantigens such as Sm, U1-RNP, SS-A/Ro, SS-B/La, Hu, and Nova bind to specific RNAs, which then associate with other proteins to form macromolecular complexes that perform a variety of functions (Musunuru and Darnell, 2001;Mansfield and Keene, 2009). At the clinical interface, autoantibodies directed to snRNP components of Sm and U1-RNP, as well as SS-A/Ro and SS-B/La, have been used as powerful tools to make an earlier and more accurate diagnosis and to elucidate the immune aberrations and pathogenesis of autoimmune diseases such as systemic lupus erythematosus (SLE), systemic sclerosis (SSc) and Sjögren's syndrome (SjS) (Perl, 2009;Rosen and Casciola-Rosen, 2009).

1.2 Discovery of GW bodies and the GW182 protein

Distinct cytoplasmic foci were initially reported in 1997 when Bashkirov and colleagues examined the cellular localization of mXRN1p in mouse E10 cells by indirect immunofluorescence (IIF) (Bashkirov et al., 1997). Related cytoplasmic foci were

rediscovered five years later when a human autoimmune serum from a patient with ataxia and polyneuropathy was used to immunoscreen a HeLa expression complementary deoxyribonucleic acid (cDNA) library that led to the discovery of the novel phosphoprotein named GW182 (Figure 1.1).

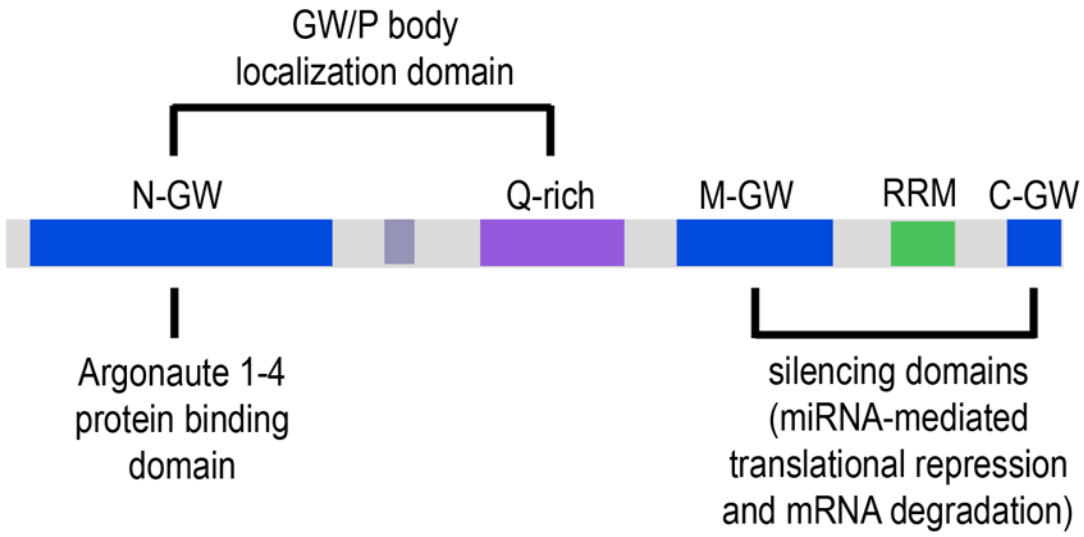

Figure 1.1: The GW182 protein.

GW182 belongs to a family of proteins that are characterized by a glutamine-rich (Q-rich) domain, a C-terminal RNA-recognition motif (RRM) and three blocks of glycine–tryptophan (GW) repeats at the N-terminal, middle (M) and C-terminal domains of the protein. It is currently thought that the N-GW and Q-rich domains participate in targeting the GW182 protein to GW/P bodies (Behm-Ansmant et al., 2006;Eulalio et al., 2009a;Lazzaretti et al., 2009). Argonaute proteins (1-4) bind to the N-GW region of GW182 (Behm-Ansmant et al., 2006;Lazzaretti et al., 2009). Both the M-GW and the C-GW regions of the GW182 protein have been implicated in silencing of microRNA-targeted messenger RNA (mRNA) (Lazzaretti et al., 2009).

GW182 is located in distinct cytoplasmic foci, named GW bodies, that contain key 5'→ 3' messenger RNA (mRNA) degradation proteins hDcp and LSm4 (Eystathioy et al., 2002a;Eystathioy et al., 2003c) (Figure 1.2A). Accordingly, GW bodies are thought to be closely related or identical to processing bodies (P-bodies) that are involved in mRNA storage and decay in *S. cerevisiae* (Sheth and Parker, 2003;Eulalio et al.,

2007). Due to the inherent structural similarity of GW bodies and P-bodies in mammalian cells, we have elected to refer to these structures using the GW/P body nomenclature.

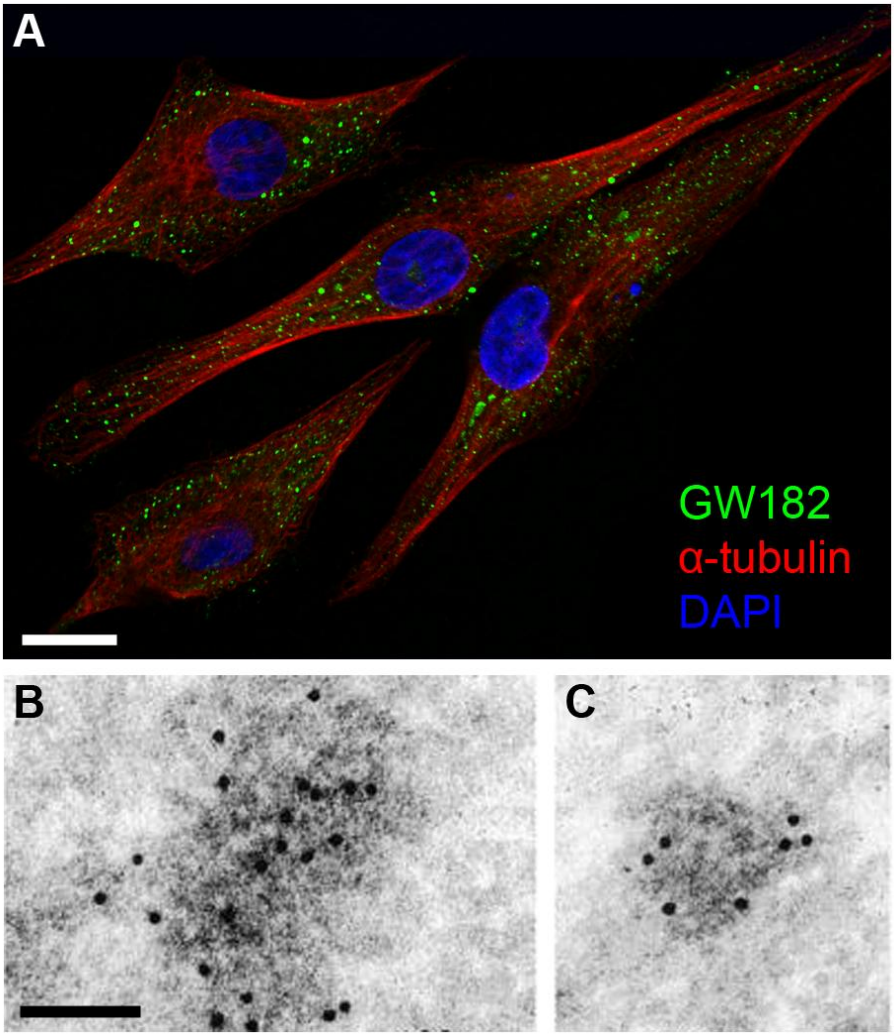

Figure 1.2: GW/P bodies.

(A) GW/P bodies visualized by indirect immunofluorescence (IIF) in human U-87 astrocytoma cells as marked by anti-GW182 (green) in relation to microtubules as marked by anti-α-tubulin (red). Nuclei are stained with DAPI. Scale bar = 15 μm. Used with permission (Moser and Fritzler, 2010): Figure 1.1 A-C. (B) and (C) Immunogold electron microscopic analysis of GW182 localization to 300 nm and 100 nm electron-dense GW/P bodies in human HeLa cells, respectively. Scale bar = 100 nm. Figure 1.2 B-C reproduced with permission (Eystathioy et al., 2002a): © 2002 with permission from Elsevier.

GW/P bodies are distinct from other cytoplasmic organelles such as endosomes, lysosomes, the Golgi complex or peroxisomes (Eystathioy et al., 2002a). When examined by anti-GW182 immunogold electron microscopy, it was noted that these electron-dense structures are 100-300 nm in diameter and do not have a limiting membrane (Figure 1.2 B,C) (Eystathioy et al., 2002a;Yang et al., 2004). A recent ultrastructural study has further elucidated the fine structure of GW/P bodies in unstressed control and arsenite-stressed conditions as marked by GWB component Rck/p54 (Souquere et al., 2009). Under control conditions, GW/P bodies are round, electron dense bodies with a diameter of up to 300 nm where anti-Rck/p54 labeled gold particles clustered on 10-15 nm fibril strands (Souquere et al., 2009). When stressed, the ultrastructure of GW/P bodies was unchanged, but an increased number of gold particles were detected on the fibril strands (Souquere et al., 2009).

GW/P body components have subsequently been identified in both lower and higher eukaryotic cells such as *S. cerevisiae, D. melanogaster, C. elegans* and mammals (reviewed in (Parker and Sheth, 2007;Jakymiw et al., 2007;Eulalio et al., 2009d)). Since, to date, there is no homologue of the GW182 protein identified in yeast, it is inappropriate to refer to yeast P bodies as GW/P bodies. Nevertheless, GW/P bodies have been studied in numerous human cells including, but not limited to, HeLa cells (Eystathioy et al., 2002a;Jakymiw et al., 2005;Moser et al., 2009), normal and malignant breast cells (Luft, 2005), astrocytes and astrocytoma cells (Moser et al., 2007), and skin cells (Zee et al., 2008). GW/P bodies are thought to be ubiquitous but they are variably expressed in cells and tissues of different origins; vary in size and number in proliferating and malignant cells (Luft, 2005;Moser et al., 2007) and in different phases of the cell

cycle (Yang et al., 2004); in stress responses (Anderson and Kedersha, 2009); mRNA decay inhibition (Andrei et al., 2005;Cougot et al., 2004;Sheth and Parker, 2003); stalled translational initiation (Brengues et al., 2005;Sheth and Parker, 2003;Teixeira et al., 2005) and during transcription inhibition and deadenylation or translational elongation of mRNA (Cougot et al., 2004;Sheth and Parker, 2003).

1.3 GW/P body dynamics and function

There are likely additional protein components of GW/P bodies yet to be identified, but components of GW/P bodies determined by methods such as IIF and Western blot analysis include mRNA (Liu et al., 2005b;Brengues et al., 2005;Eystathioy et al., 2002a), microRNA (miRNA) (Lian et al., 2006;Pauley et al., 2006), 5'→ 3' mRNA degradation pathway proteins (Andrei et al., 2005;Bashkirov et al., 1997;Cougot et al., 2004;Eystathioy et al., 2003c;Fenger-Gron et al., 2005;Ingelfinger et al., 2002;Rehwinkel et al., 2005;Sheth and Parker, 2003;van Dijk et al., 2002), proteins involved in the RNA silencing pathway (Jakymiw et al., 2005;Liu et al., 2005a;Liu et al., 2005b;Pillai et al., 2005;Rehwinkel et al., 2005;Sen and Blau, 2005;Baillat and Shiekhattar, 2009;Lazzaretti et al., 2009;Zipprich et al., 2009), and proteins involved in mRNA stabilization, transport, and processing (Moser et al., 2007) (for reviews that list GW/P body components in multiple species see (Eulalio et al., 2007;Jakymiw et al., 2007;Parker and Sheth, 2007;Eulalio et al., 2009d)).

1.3.1 GW/P body intracellular and intercellular dynamics

GW/P bodies move dynamically in a number of ways: passively within a confined cytoplasmic region where interactions with mRNA transcripts may be based on random encounters rather than on an active or directed mechanism; bidirectionally along microtubules to facilitate interactions with mRNA transcripts; actively along the nuclear periphery where interactions could occur with the nuclear pore complex and exported mRNAs (Aizer et al., 2008). Aizer *et al.* also reported that GW/P bodies move in channel-like regions between mitochondria where, after disrupting the microtubule network with nocodazole, the areas of movement and diffusion were reduced (Aizer et al., 2008). Besides intracellular cytoplasmic movement, there is recent evidence that GW/P body components, GW182 and a nascent fraction of miRNA-loaded Ago2, move into an intercellular endosome-lysosome-multivesicular body pathway as 50-100 nm microvesicles referred to as extracellular exosomes (Gibbings et al., 2009;Lee et al., 2009). These microvesicles are particularly enriched in GW182 and contain inactive forms of mRNA and miRNA that may be transferred between cells and remain functional in a new cellular environment (Gibbings et al., 2009). These and other recent observations highlight the importance of extracellular exosomal miRNA and GW/P body components for use as diagnostic biomarkers of a number of diseases (Simpson et al., 2009;Rabinowits et al., 2009;McLellan, 2009).

1.3.2 Messenger RNA (mRNA) regulation through RNA interference (RNAi), mRNA processing and degradation

RNA interference (RNAi) is a key pathway involved in the post-transcriptional silencing of >50% of all mRNAs in a variety of organisms (Friedman et al., 2009). RNAi begins in the nucleus where miRNA genes are transcribed by RNA polymerase II into primary transcripts (pri-miRNA) that are then cleaved by the Drosha-DGCR8 complex into precursor miRNAs (pre-miRNA) (Rana, 2007) (Figure 1.3). Pre-miRNA are rapidly processed into miRNA duplexes of 18-22 nucleotides in length by Dicer, an RNase III specific endonuclease (Meister and Tuschl, 2004) (Figure 1.3). RNAi can also be mediated by exogenous dsRNA that is rapidly processed by Dicer into small interfering (siRNA) duplexes of similar length (Meister and Tuschl, 2004). These small RNA duplexes (miRNA and siRNA) are then incorporated into the RNA-induced silencing complex (RISC) where the passenger RNA strand is dissociated by cleavage, degradation or a bypass mechanism (Matranga et al., 2005) by interacting with Argonaute 2 (Ago2), one of four Ago proteins (Liu et al., 2004;Ares and Proudfoot, 2005) (Figure 1.3). The RISC then recruits one or more heteromeric protein complexes (e.g. GW182 and rck/p54) to associate with the mRNA leading to the formation of the ribonucleoprotein (RNP) structure known as GW/P bodies (Figure 1.3). Depending on the degree of complementarity between the guide-strand miRNA or siRNA and its target mRNA, this augmented RISC then initiates post-transcriptional inhibition of gene expression through cleavage or translational repression (Jakymiw et al., 2007;Eulalio et al., 2009d). Importantly, each miRNA is predicted to regulate hundreds of different target mRNAs while a single mRNA has the potential to be regulated by dozens of different miRNAs.

The 5'→ 3' degradation of targeted mRNA by XRN1 exonuclease is initiated after the poly(A) tail is shortened by the deadenylase CCR4:NOT complex and removal of the 5' cap by decapping factors that include the LSm1-7 ring and the Dcp 1/2 complex (Eystathioy et al., 2003c;Rehwinkel et al., 2005;Behm-Ansmant et al., 2006) (Figure 1.3).

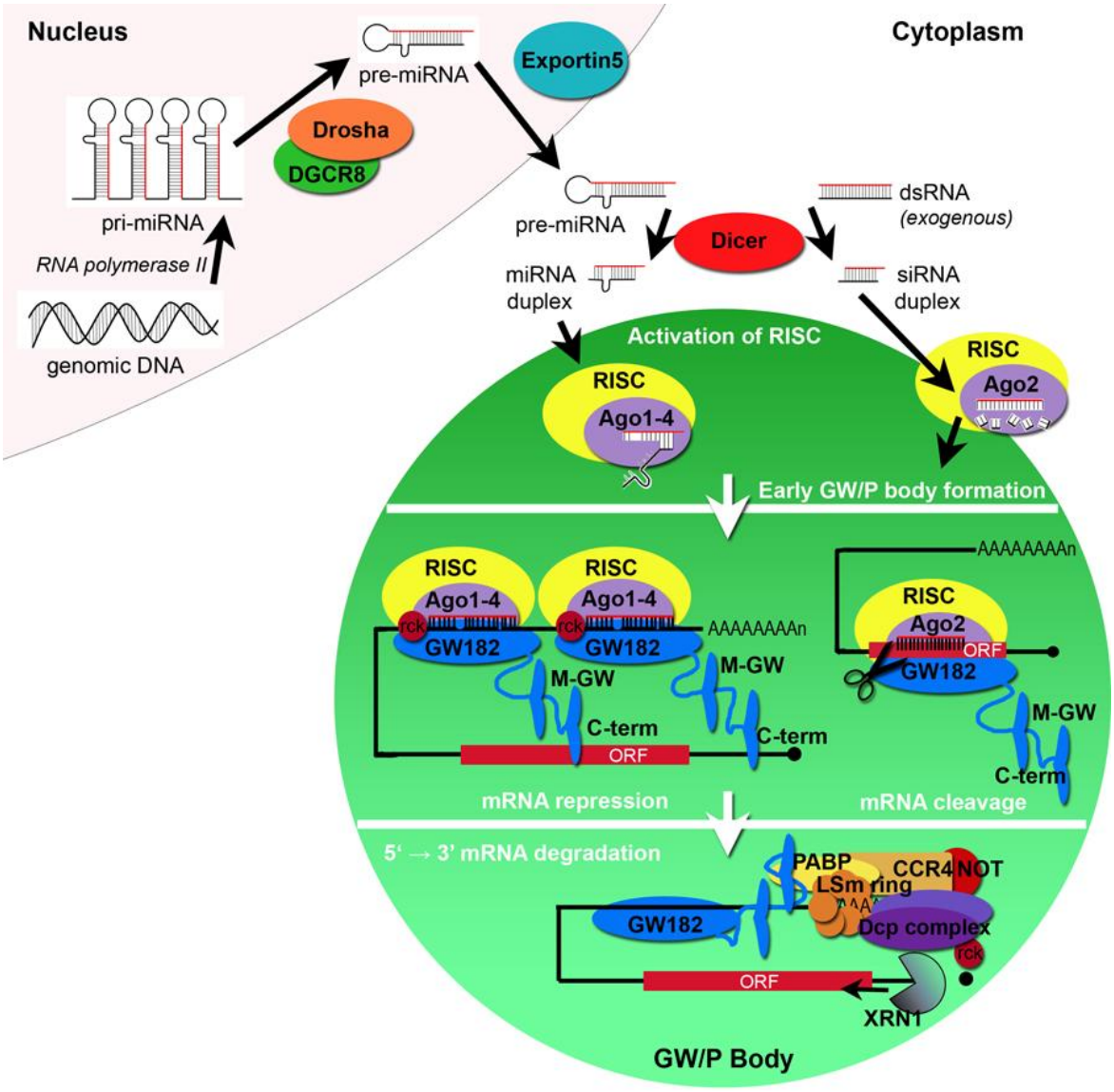

Figure 1.3: A model linking RNAi and GW/P body assembly and function. See text for description.

While some evidence suggests a central role for GW/P bodies in RNAi, other studies have shown that the process of active RNAi can occur in the absence of visible GW/P bodies (Chu and Rana, 2006;Rehwinkel et al., 2005;Lazzaretti et al., 2009). In addition, it has been observed that GW/P bodies exist in the absence of active RISC, as in Dicer knockout cells (Leung et al., 2006). Although often overlooked, there is compelling evidence that GW182 is a requisite component of GW/P bodies. For example, after knockdown of GW182 by a cognate siRNA, GW/P bodies became inconspicuous by conventional microscopy (Yang et al., 2004) (reviewed in (Jakymiw et al., 2007;Eulalio et al., 2009d)). Furthermore, GW182 is a key co-factor of Ago2 which plays an essential role in siRNA and miRNA-mediated gene silencing (Jakymiw et al., 2005;Liu et al., 2005a;Meister et al., 2005;Rehwinkel et al., 2005;Behm-Ansmant et al., 2006;Chu and Rana, 2006;Eulalio et al., 2008;Eulalio et al., 2009b;Eulalio et al., 2009c;Eulalio et al., 2009a;Eulalio et al., 2009d) as evidenced by the C-terminal domain of GW182 being essential for miRNA function (Eulalio et al., 2009a), the contribution of the RRM domain of GW182 to miRNA-mediated silencing of mRNA (Eulalio et al., 2009c) and the essential binding of the C-terminal domain of hAgo2 to the GW-rich regions of GW182 to mediate silencing (Lian et al., 2009).

On balance, GW/P bodies assembled in the absence of GW182 under arsenite-induced stress conditions (Serman et al., 2007), where Rck/p54 helicase, rather than GW182, was suggested to be the requisite component of GW/P bodies. In addition, RNAi depletion of proteins such as eIF4E transporter, LSm1, Rck/p54, CCR4 (Andrei et al., 2005), LSm4 (Kedersha et al., 2005), Ge-1 (Yu et al., 2005), RAP55 (Yang et al., 2006), CPEB1 (Serman et al., 2007) and PatL1 (Scheller et al., 2007) was attended by the

disappearance of GW/P bodies suggesting that these proteins are also requisite components of GW/P bodies. Recently, heat-shock protein (Hsp) 90 was found to be a critical modulator of Argonaute function as evidenced by the observation that Hsp90 activity was required for efficient targeting of human Ago2 (hAgo2) to GW/P bodies (Pare et al., 2009). This study also showed that miRNA-dependent translational repression and siRNA-directed cleavage functions of hAgo2 are dependent upon the activity of Hsp90 (Pare et al., 2009). Taken together, these findings suggested that GW/P body assembly and stability are governed by the activity of the Hsp90 chaperone, which may be dependent upon adenosine triphosphate (ATP) that was previously shown to stimulate RISC activity (Gregory et al., 2005).

In miRNA-mediated post-transcriptional silencing of mRNA, the 3'UTR (untranslated region) of mRNA may serve as the docking site for various RNA-binding proteins and miRNA ribonucleoproteins that regulate mRNA stability, mRNA localization, and translational efficiency. In cycling/proliferating cells (S/G_2), such as cancer cells, miRNAs are generally thought to repress mRNA translation (Vasudevan et al., 2008). To date, miRNA have been shown to have an effect on the development of many cancers (He et al., 2005;O'Donnell et al., 2005;Lu et al., 2005;He et al., 2007b) and it is now understood that greater than half of the annotated human miRNA genes are located in chromosomal regions frequently displaying amplification, deletion, or translocation in human cancers (Calin et al., 2004). In addition, miRNAs are aberrantly expressed in a wide variety of human cancers, including but not limited to those originating in ovarian, breast, lung, gastrointestinal and brain tissues where they are thought to play important roles by regulating the expression of various oncogenes and

tumour suppressors (Lu et al., 2005;Lee and Dutta, 2009;Calin and Croce, 2006;Iorio et al., 2005;Yanaihara et al., 2006;Iorio et al., 2007;Wang et al., 2008). When miRNAs are downregulated, they can act as tumour suppressors if they target tumour suppressor mRNA (Griffis et al., 2007). When overexpressed, miRNAs can act as oncogenes (referred to as oncomirs) if their target is within the promoter region of an oncogenic mRNA (Volinia et al., 2006;He et al., 2005;Chan et al., 2005) possibly through dysregulation of the cell cycle leading to the formation of tumors.

1.4 Other cytoplasmic ribonucleoprotein (RNP) bodies and their relationship to GW/P bodies

Relevant mRNA silencing and degrading factors are partitioned to restricted cytoplasmic GW/P body microdomains thus effecting post-transcriptional regulation and the prevention of accidental degradation of functional mRNA. Although much attention has focused on GW/P bodies, other cytoplasmic RNP bodies, which have highly specialized functions, share some structural characteristics with (Table 1.1.) and interact or co-localize with components of GW/P bodies (Table 1.2). These include neuronal transport RNP granules, stress granules, RNP-rich cytoplasmic germline granules or chromatoid bodies, sponge bodies, cytoplasmic prion protein-induced RNP granules, U bodies and TAM bodies (Moser and Fritzler, 2010). Of relevance to my study of GW/P bodies in astrocyte and astrocytoma cells, neuronal transport RNP granules are discussed in greater detail.

Table 1.1: Structural characteristics of RNP-rich cytoplasmic bodies.

Cytoplasmic Body	Cytoplasmic Foci	Size (nm)	Quantity (foci/cell)	Membrane-Bound	Associated with Ribosomes	Movement	Microtubule-dependent	Contain	
								mRNA	miRNA
GW/P body (P body in yeast)	+	100 – 300	3-4§ 3-8¤ >30*	–	–	+	+	+	+
Neuronal transport RNP granule	+	150 – 1000	n/a§ 10-15¤ >20*	–	+ (small 40S and large 60S)	+	+	+	+
Stress granule	+	100 – 2000	1-5§ ND¤ >20*	–	+ (small 40S only)	– (change shape)	+ (formation)	+	+
Chromatoid body	+	200 – 900	n/a§ ND¤ 2-10*	–	–	+	+	+	+
Sponge body	+	500 – 3000	ND§ 10-20¤ ND*	–	–	+	ND	+	ND
cyPrP-induced RNP granule	+	4000 – 5000	ND§ ND¤ 1*	– (vimentin cage)	ND	ND	+	+	+
U body	+	200 – 400	ND§ 5-15¤ ND*	–	ND	ND	ND	+	ND

+ = positive/yes, – = negative/no, ND = no data, n/a = not applicable
The approximate number of foci/cell is indicated by § in S. cerevisiae, ¤ in D. melanogaster cells and * in mammalian cells.
For a detailed review of all structural characteristics and original references see (Moser and Fritzler, 2010).

Table 1.2: Common GW/P body proteins found in other RNP-rich cytoplasmic bodies.

	Protein	RNP-rich cytoplasmic bodies						
		GW/P body	Neuronal transport RNP granule	Stress granule	Chromatoid body	Sponge body	cyPrP-RNP granule	U body
RNA interference	Dicer	+/–	+	ND	+	ND	+	ND
	Ago2/EIF2C2	+	+	+	+	ND	ND	ND
	GW182/ TNRC6A/ AIN-1	+	+	–	+	ND	ND	ND
mRNA degradation	CCR4	+	ND	–	ND	ND	ND	ND
	Dcp1	+	+	–	+	+	+	+/–
	Dcp2	+	ND	–	+	+	ND	ND
	Sm proteins (LSm1-7)	+	ND	–	+	+	ND	+
	RAP55/ LSm14A	+	ND	+	ND	ND	ND	ND
	XRN1	+	+/-	+	+	ND	ND	ND
	Ge-1/Hedls/ RCD8	+	ND	–	ND	ND	ND	ND
	Rck/p54/ Dhh1/DDX6/ Me31B	+	+	+	+	ND	+	+/–
RNA stabilization, processing, transport	HuR	+/–	ND	+	+	ND	ND	ND
	FMRP	+	+	+	ND	ND	ND	ND
	SYNCRIP/ hnRNPQ/ NSAP1	+	+	+	ND	ND	ND	ND
	Staufen	+/–	+	+	ND	ND	ND	ND
	hnRNPs	+	+	+	+	ND	ND	ND
	CPEB	+	+	+	+	ND	ND	ND

+ = localize to foci, +/– = partially localize to foci and other places in cell, – = no localization to foci, ND = no data.
For a detailed review of all structural characteristics and original references see (Moser and Fritzler, 2010).

1.5 Neuronal Transport Ribonucleoprotein Granules

Neuronal transport RNPs are broadly identified by the presence of two highly conserved proteins: the double-stranded RNA-binding protein, Staufen (Barbee et al., 2006;Kiebler and Bassell, 2006;Thomas et al., 2005) and fragile X mental retardation protein (FMRP) (Barbee et al., 2006;Eddy, 1975;Mazroui et al., 2002), both of which have been identified by IIF (often including fluorescence-labelled cDNA constructs) and Western blot (WB). Neuronal transport RNPs are also known as neuronal RNA granules, RNA granules, RNA particles, dendritic P-body like structures (dlP-bodies), FMRP granules and Staufen granules, but for this thesis they will be referred to as neuronal transport RNP granules. Akin to GW/P bodies these granules are cytoplasmic, non-membrane bound 150 – 1000 nm foci that store translationally repressed mRNAs (reviewed in (Krichevsky and Kosik, 2001)). Unlike GW/P bodies, neuronal transport RNP granules contain ribosomal RNA (40S and 60S) and to date they have been primarily studied in mammalian and *D. melanogaster* neurons (reviewed in (Sossin and DesGroseillers, 2006;Hillebrand et al., 2007)) (Table 1.1; Figure 1.4).

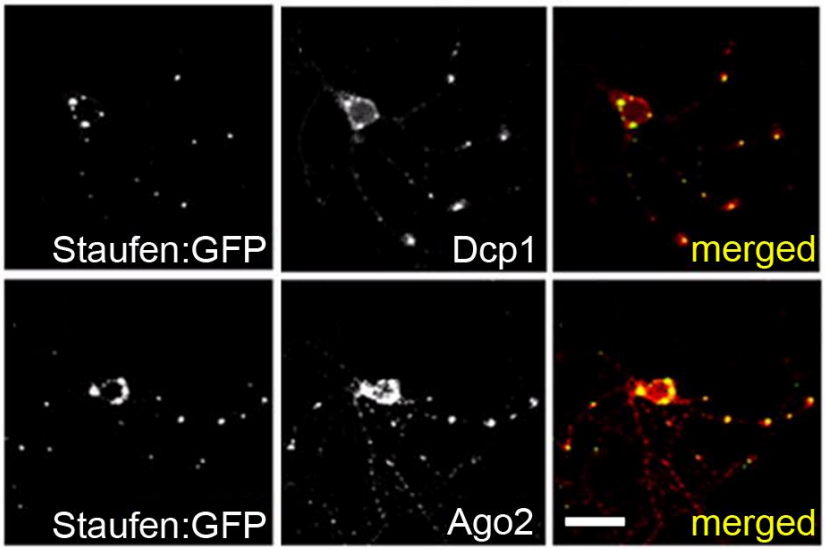

Figure 1.4: Neuronal transport RNP granules in *D. melanogaster* neurons as detected by Staufen:GFP expression colocalize to GW/P bodies as marked by antibodies to Dcp1a and Ago2. Scale bar = 10μm. Reprinted from Neuron (Barbee et al., 2006): Figures 2B-D,2Q-S © 2002 with permission from Elsevier.

Transport of mRNA to subcellular domains is essential for establishing cellular polarity (St Johnston, 2005). In highly polarized cells, such as neurons, the dendritic localization of mRNAs and their subsequent translation at synapses is thought to contribute to remodelling of synapses and the subsequent establishment of long term memory (St Johnston, 2005;Sutton and Schuman, 2006). In mammalian cells, there are two distinct phases of neuroplasticity: an early phase (~ 1–3 h) that is independent of new protein synthesis and a late phase (lasting >8 h) that is dependent on new protein synthesis in dendrites (Sutton and Schuman, 2006). Recently, the molecular mechanisms underlying new protein synthesis have focused on local dendritic regulation of mRNA translation. In neurons, local mRNA translation is important for the regulation of synaptic plasticity as well as development and growth of axons and dendrites (Hillebrand et al.,

2007). To ensure that the appropriate mRNA will be available for translation upon a specific stimulus, neurons have developed elaborate systems for delivering RNPs into the distant reaches of their cytoplasm, which include the movement of neuronal transport RNPs along the microtubule cytoskeleton by the kinesin protein KIF5 (Hirokawa, 2006;Kiebler and Bassell, 2006). It is likely that the composition of neuronal transport RNPs at a given time determines whether specific mRNAs are transported to a certain location (i.e. synapse), translated locally (i.e. at the post-synaptic density (PSD)), or targeted for storage and/or degradation to GW/P bodies. Indeed, our findings show that GW/P bodies marked by antibodies to GW182 localize to post-synaptic densities in rat hippocampal neurons marked by antibodies to PSD-95 (Figure 1.5).

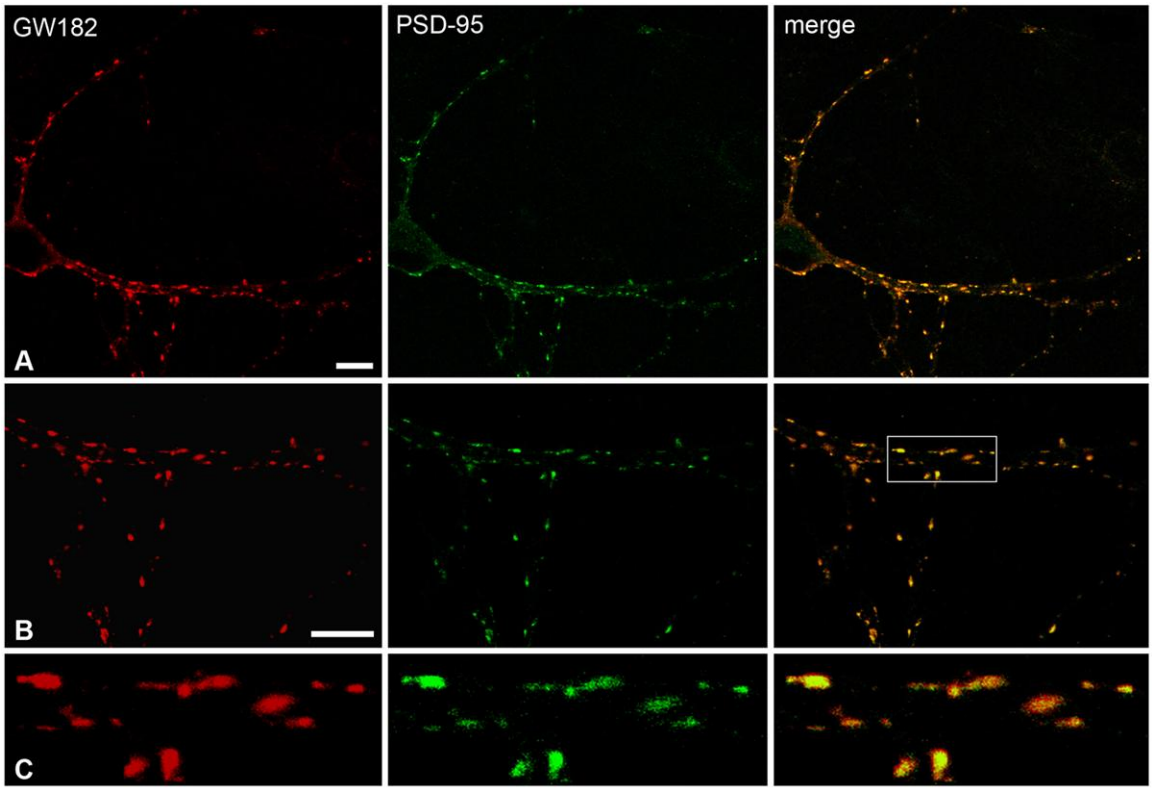

Figure 1.5: GW182 localizes to post-synaptic densities (PSDs).

(A) IIF analysis of GW/P bodies as marked by anti-GW182 antibody (red) shows that GW/P bodies localize to postsynaptic densities (PSDs) in rat hippocampal neuronal dendrites (merge, yellow) as marked by anti-PSD-95 (green). Scale bar = 10 μm. (B) Enlarged GW/P bodies, PSDs and merged image from panel A. Scale bar = 10 μm. (C) Enlarged images from panel B. (Moser and Fritzler, 2010)

These observations suggest that mRNA or miRNA targeted to dendrites may be stored and/or silenced in GW/P bodies until an appropriate signal directs the mRNA for local translation or degradation.

Recently, neuronal transport RNPs have been shown to be structurally and functionally similar to GW/P bodies with respect to protein components such as GW182/TNRC6A, Ago2/EIF2C2, Rck/p54/Dhh1/DDX6/Me31B, FMRP, Staufen, SYNCRIP/hnRNPQ/NSAP1, hnRNPs, CPEB, mRNA and miRNA (Anderson and

Kedersha, 2006;Zeitelhofer et al., 2008;Cougot et al., 2008) (Table 1.2; Figure 1.5). In astrocytes and astrocytoma cells, these neuronal transport RNP components were only present in subsets of GW/P bodies (Moser et al., 2007) (Chapter Four). Further, miRNA-mediated regulation of mRNA presumably in the GW/P body microdomain is important in the controlled regulation of neuronal development and plasticity (Ashraf and Kunes, 2006;Schratt et al., 2006).

MiRNAs and protein components of GW/P bodies have been observed in neurons and astrocytes, however, it remains to be determined which physiologically relevant signals activate Dicer to process precursor-miRNAs (pre-miRNA) into miRNAs in these excitable cells. This has been elucidated, in part, by two studies that focused attention on the somatodendritic compartment of neurons in the adult mouse brain (Lugli et al., 2005;Fierro-Monti et al., 2006) where Dicer and Ago2 were localized to dendritic spines and enriched in PSDs. In a separate study, GW182 was found to localize in close proximity to PSDs (Cougot et al., 2008) whereas we found that GW182 colocalized directly to PSDs (Figure 1.5). In addition, Dicer and Ago2 were biochemically associated with FMRP macromolecular complexes in PSDs (Lugli et al., 2005). This cellular localization placed PSDs in contact with intracellular ionic fluxes, such as calcium (Ca^{2+}) influx, and second messenger cascades generated by neurotransmitters binding to ligand-gated Ca^{2+} channels and, accordingly, provide a suitable microenvironment for neurotransmitter-mediated Ca^{2+} influx and subsequent activation of signaling proteins. Lugli *et al.* showed that Dicer was inactive when localized to PSDs (Lugli et al., 2005), but upon Ca^{2+} influx, NMDA (N-methyl-D-aspartic acid) stimulation or exogenous treatment with the protease calpain, it together with Ago2 was released into

the cytosol and became enzymatically activated (Lugli et al., 2005). The calpain specific protease inhibitor, calpeptin, was observed to reverse the effects of calpain even in the presence of Ca^{2+} indicating that Dicer mediated RNAse III activation was calpain-dependent (Lugli et al., 2005). Lugli *et al.* (2008) went on to examine the expression of miRNAs and pre-miRNA in synaptic fractions of the adult mouse forebrain and found that pre-miRNAs were predominantly associated with PSDs whereas miRNAs were enriched in soluble synaptic fractions (Lugli et al., 2008). The observation that Dicer only interacted with pre-miRNA (Lugli et al., 2008) suggested that Dicer dissociated from mature miRNA.

Taken together, these observations suggested that synaptic stimulation mediated by Ca^{2+} induced calpain activation released pre-miRNA, Dicer, FMRP and Ago2 from PSDs into the cytosol where activated Dicer cleaved pre-miRNA into mature miRNA. These data also suggested that mature miRNA in association with Ago2 and GW182 are capable of regulating target mRNA perhaps within GW/P body components that may be present in the soluble components of synaptic fractions. Future studies into the physiological cues that regulate GW/P bodies and their interactions with neuronal transport RNP granules will be useful to understand their role in cell signaling pathways.

Many authors have reported that neuronal transport RNPs colocalize with GW/P bodies. Zeitelhofer *et al.* (2008) observed that they are distinct compartments because only 3-4% of the structures were colocalized and were not transported in the same particles in the dendrites of mammalian neurons (Zeitelhofer et al., 2008). Using time-lapse video microscopy, 50% of GW/P-bodies and transport RNPs transiently interacted, however, the authors emphasized that the nature and purpose of this interaction is

presently unknown (Zeitelhofer et al., 2008). After synaptic stimulation with glutamate, approximately 60% of GW/P bodies disassembled, which implied that the mRNAs stored in GW/P bodies were translated upon stimulation (Zeitelhofer et al., 2008). These data support the possibility that mRNAs localized to dendrites might be stored in GW/P bodies and are then released and translated when synapses are activated. Clearly, further studies that focus on the relationship between neuronal transport RNPs and GW/P bodies (and their corresponding mRNAs and miRNAs) in neurons under physiologically relevant stimuli, such as long term potentiation (LTP) or long term depression (LTD), are still required.

1.6 Rationale

1.6.1 Why Study GW/P Bodies in Astrocyte and Astrocytoma Cells?

In 2006, clinical studies of patient serum with autoantibodies to GW/P bodies showed that approximately 33% of the patients had ataxia and/or motor and sensory neuropathy (Eystathioy et al., 2003b;Bhanji et al., 2007). Ataxia is a non-specific clinical symptom consisting of the gross lack of coordination of muscle movements that may be due to the dysfunction of the cerebellum that coordinates movement. Motor and sensory neuropathies involve damage to the peripheral nervous system. The clinical symptoms for motor neuropathy involve muscle weakness, cramps, spasms and a loss of balance and coordination. Clinical sensory neuropathic symptoms include tingling, numbness, and pain. This initial clinical finding that one third of patients with autoantibodies to GW/P body components had these neurological symptoms suggested that an analysis of GW182 and GW/P body-associated mRNA, miRNA and proteins and their relationship

to GW/P body structure and function should be studied in cells of the mammalian nervous system as an approach to understanding why the specific autoantibodies arise in these patients and the role of GWB in neural cells.

GW/P body-like RNP granules had been described in *D. melanogaster* neurons (Barbee et al., 2006), yet there were no published studies prior to the start of this thesis research that had described the presence or function of GW/P bodies in cells of the mammalian central nervous system (CNS). Therefore, the patterns of GW/P body expression pattern in various cells of the mammalian CNS, including neurons, oligodendrocytes, astrocytes and stem cells were needed to determine which of these cells should be the focus of my studies. As such, a preliminary IIF study of saggital sections of cryopreserved normal mouse brain was examined using the index anti-GWB human serum 18033. Neurons were marked by mouse anti-neurofilament 200 antibody (Figure 1.6), oligodendrocytes by mouse anti-CNPase antibody (Figure 1.7), astrocytes by chicken anti-GFAP antibody (Figure 1.8) and stem cells by chicken anti-nestin antibody (Figure 1.9). Secondary antibody staining alone (with no primary antibody) did not show background stain (data not shown). Figures 1.6 to 1.9 illustrate the GW/P body staining in the mouse cerebellum only, but it was also observed that GW/P bodies were highly expressed in the mouse cerebral cortex and hippocampus (data not shown).

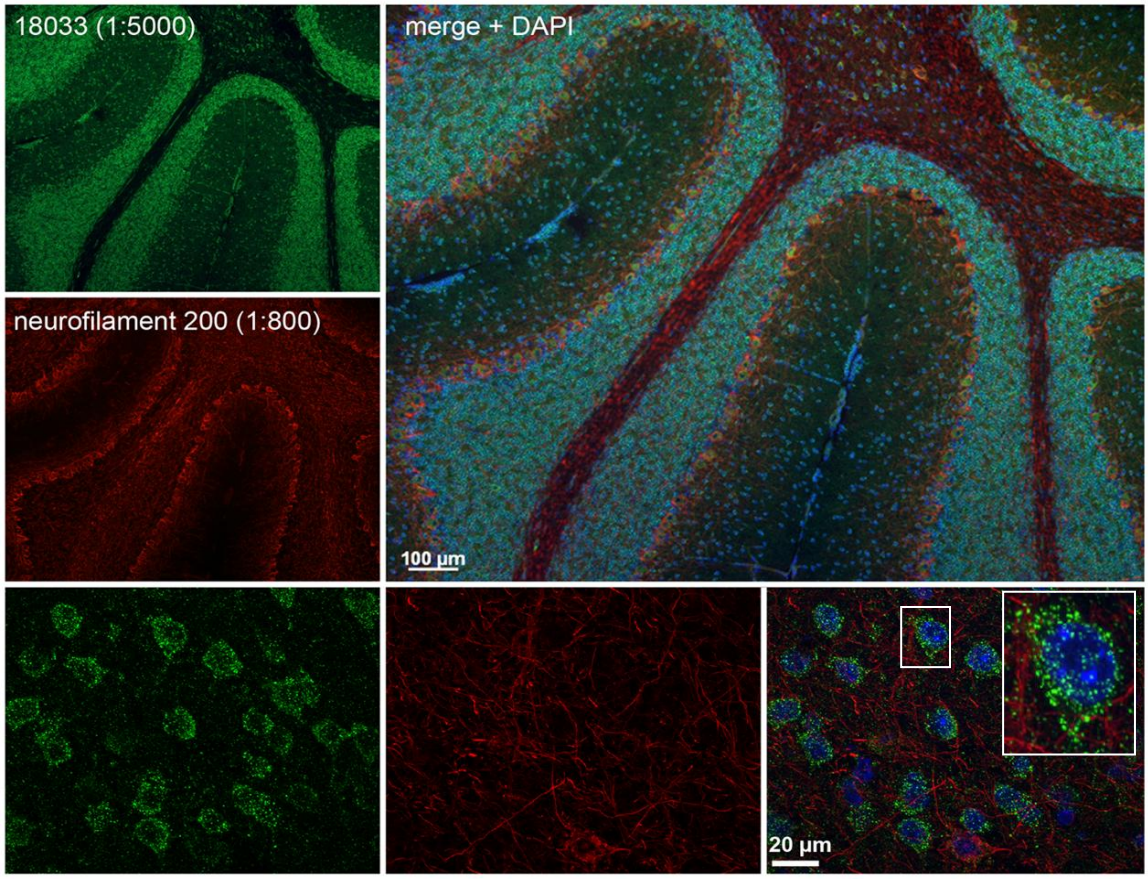

Figure 1.6: GW/P body expression relative to neurons as marked by mouse anti-neurofilament 200 antibody in the cerebellum of the mouse brain. GW/P bodies are marked by the index human serum 18033 (1:5000; green). Neurons are marked by mouse anti-neurofilament200 antibody (1:800, red). Nuclei are counterstained by DAPI (blue). Images in the top panel were taken with a 10x objective (100 µm scale bar) to show tissue morphology and in the bottom panel with a 60x objective (20 µm scale bar) to show the cytoplasmic GW/P body staining. The inset box shows GWB staining in a single cell.

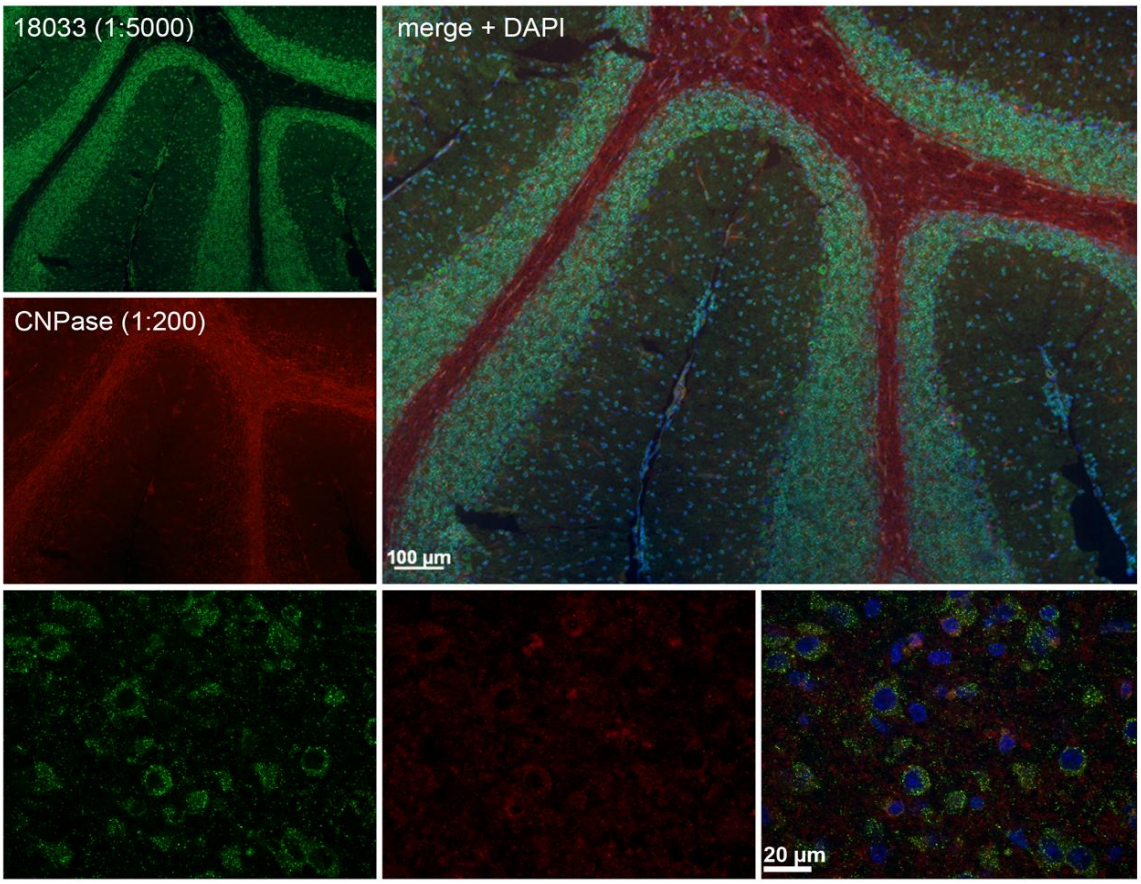

Figure 1.7: GW/P body expression relative to oligodendrocytes as marked by mouse anti-CNPase antibody in the cerebellum of the mouse brain. GW/P bodies are marked by the index human serum 18033 (1:5000; green). Oligodendrocytes are marked by mouse anti-CNPase antibody (1:200, red). Nuclei are counterstained by DAPI (blue). Images in the top panel were taken with a 10x objective (100 µm scale bar) to show tissue morphology and in the bottom panel with a 60x objective (20 µm scale bar) to show the cytoplasmic GW/P body staining.

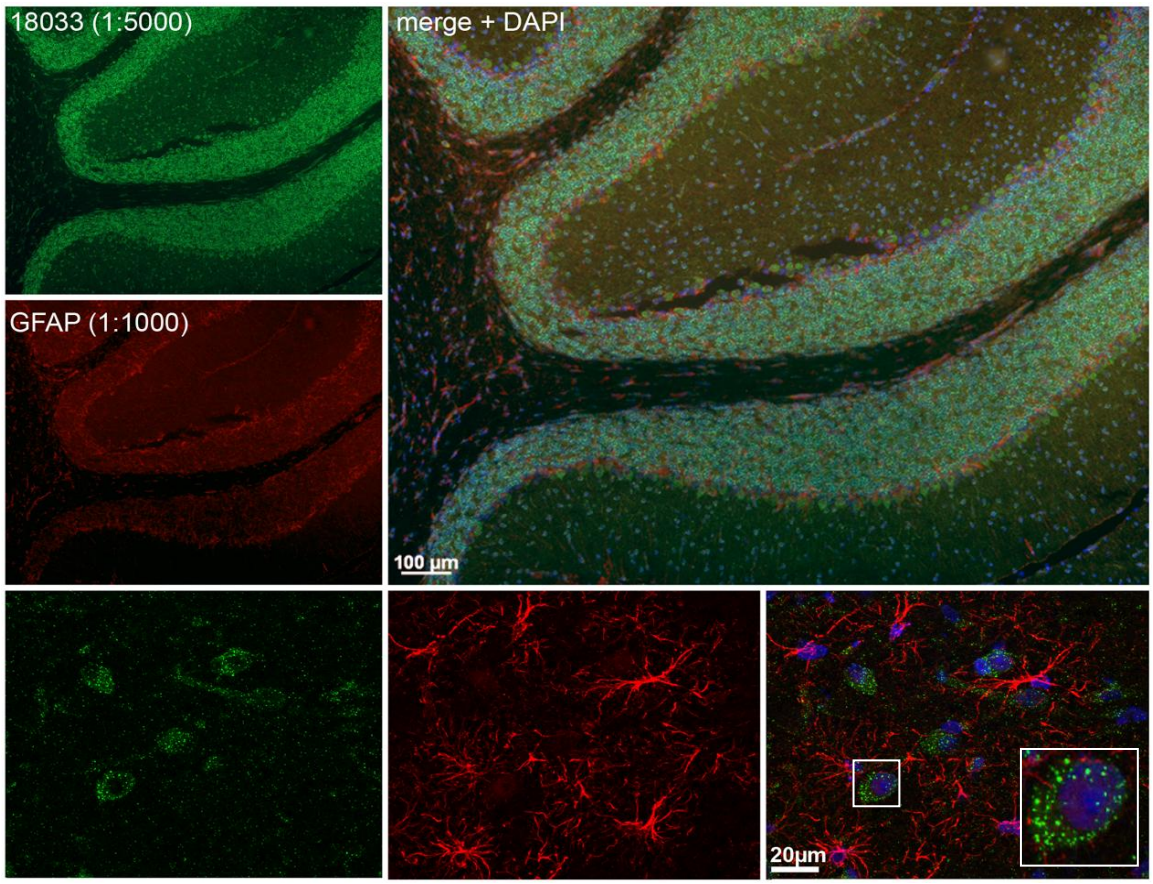

Figure 1.8: GW/P body expression relative to astrocytes as marked by chicken anti-GFAP antibody in the cerebellum of the mouse brain. GW/P bodies are marked by the index human serum 18033 (1:5000; green). Astrocytes are marked by chicken anti-GFAP antibody (1:1000, red). This specific GFAP antibody marks the finely branching astrocyte processes and does not detect the astrocyte cell body. Nuclei are counterstained by DAPI (blue Images in the top panel were taken with a 10x objective (100 µm scale bar) to show tissue morphology and in the bottom panel with a 60x objective (20 µm scale bar) to show the cytoplasmic GW/P body staining. The inset box shows GWB staining in a single cell.

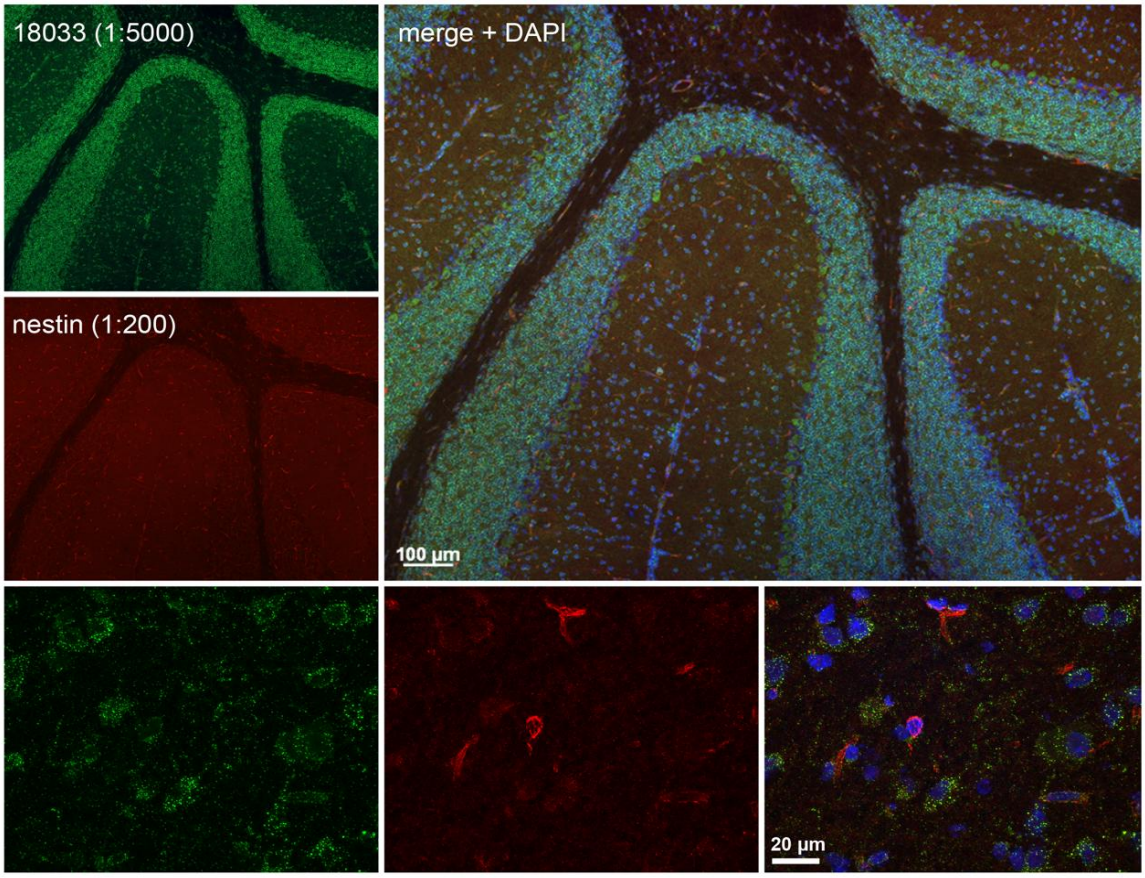

Figure 1.9: GW/P body expression relative to stem cells as marked by chicken anti-nestin antibody in the cerebellum of the mouse brain. GW/P bodies are marked by the index human serum 18033 (1:5000; green). Neurons are marked by chicken anti-nestin antibody (1:200, red). Nuclei are counterstained by DAPI (blue). Images in the top panel were taken with a 10x objective (100 µm scale bar) to show tissue morphology and in the bottom panel with a 60x objective (20 µm scale bar) to show the cytoplasmic GW/P body staining.

Examination of the GW/P body staining relative to the cell-specific markers showed that GW/P bodies did not appear to be present in oligodendrocytes (Figure 1.7) or localized specifically within stem cells (Figure 1.9). However GW/P bodies were highly expressed in astrocytes (Figure 1.8) and to a lesser extent in neurons (Figure 1.6). This preliminary study showed that GW/P bodies are highly expressed in astrocytes, suggesting that this would be a fertile area of investigation. Primary astrocytes isolated

from the human cerebral cortex and a malignant counterpart, U-87 astrocytoma cells, were commercially available for purchase and these were selected for the majority of the studies described in this thesis. Of importance, GW/P bodies had a similar expression pattern in cultured human astrocytes (Figure 1.10) as they did in mouse astrocytes (Figure 1.8) and in cultured astrocytes isolated from the mouse hippocampus (Chapter Four, Figures 4.1 and 4.4).

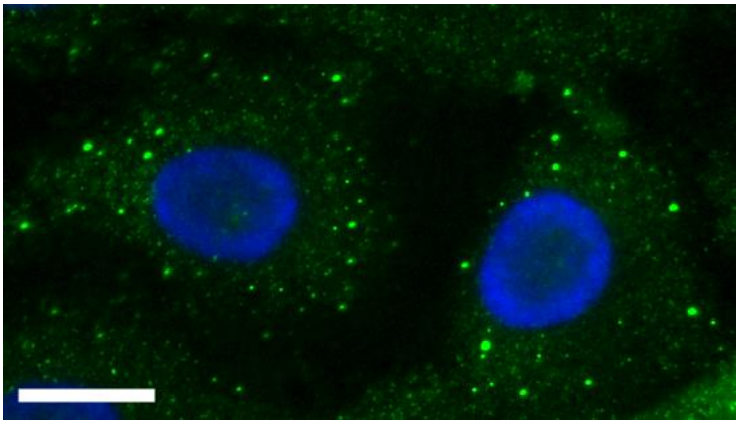

Figure 1.10: GW/P body expression (human serum 18033, 1:5000, green) in cultured human astrocytes (ScienCell Research Laboratories, Carlsbad, CA). Nuclei were counterstained with DAPI (blue). Scale bar = 15µm.

1.6.2 Astrocytes and Astrocytomas

The CNS comprises a network of approximately 10^{12} neural cells and the vast majority (~90%) of these cells are astrocytes (Nedergaard et al., 2003) where astrocytes outnumber neurons by approximately 10:1 and are estimated to occupy 25-50% of brain volume. Malignant CNS tumours represent only about 2% of all cancers but account for a disproportionate rate of morbidity and mortality, with more than 40,000 malignant and benign cases diagnosed annually in the United States as of 2007 (Buckner et al., 2007).

Of these cases, approximately half were benign, but were still fatal as a result of progressive growth in the closed space of the skull (Buckner et al., 2007). Meningiomas are the most common benign brain tumour, and astrocytomas, including glioblastoma multiforme, are the most common malignant brain tumours (Buckner et al., 2007). Unfortunately, despite initial disease treatments with radiation, chemotherapy and surgery, the mortality rate is very high with aggressive malignant astrocytoma brain tumours. This is because astrocytoma tumour cells invade the surrounding brain tissue and are very difficult to be completely surgically resected. Therapy is further complicated by the fact that most astrocytoma cells are at least partially resistant to radiation and chemotherapy (Buckner et al., 2007). Thus, current treatments for astrocytomas generally are not curative but they do prolong life.

In the normal brain, astrocytes were thought for many years to have primarily a supporting role for neurons, however many studies within the last decade showed that astrocytes play crucial roles in the CNS in organizing the structural architecture of the brain as well as its communication pathways, activation, thresholds and plasticity (Nedergaard et al., 2003;Newman, 2003;Schipke and Kettenmann, 2004;Volterra and Meldolesi, 2005). As such, astrocytes are thought to be important for neuronal survival and function, contribute to the formation and preservation of a secure blood-brain barrier and control ionic and osmotic homeostasis (Amiry-Moghaddam and Ottersen, 2003). Astrocytes have also been implicated in the development and plasticity of the central nervous system by modifying the growth of axons and dendrites and regulating synapse formation (Helmuth, 2001). Of possible relevance to anti-GWB responses that formed the impetus for this thesis research, astrocytes also play a central role in the control of the

innate immune response and surveillance in the CNS in infectious diseases and also after brain injury and in autoimmune and neurodegenerative disorders of the CNS (Farina et al., 2007;Griffiths et al., 2009). The multiple functions of astrocytes likely require highly integrated and controlled networks of mRNA processing and transport within astrocyte cells suggesting that GW/P bodies may play a role in mediating the transport, silencing or degradation of mRNA involved in these functions in astrocytes and astrocytoma cells. In astrocytes, stabilization and transport proteins (i.e. Hu antigen R (HuR), FMRP, heterogeneous nuclear ribonucleoproteins (hnRNPs), and Staufen often associate with GW/P bodies (Barbee et al., 2006;Moser et al., 2007) (Chapter Four) while possibly awaiting a signal to initiate mRNA degradation, repression or release of translational inhibition.

1.7 Summary

As our understanding of cell and molecular biology advances, it has become clear that the cellular cytoplasmic milieu is more complex and highly partitioned than previously thought. In addition to being the location of a variety of membrane bound organelles, the cytoplasm contains a number of non-membranous RNP bodies that house specific mRNAs at various stages of post-transcriptional processing. GW/P bodies and their roles in RNA stabilization, transport, translational repression and/or degradation have emerged from this list as key players in the modulation of mRNA expression. Evidence to date also indicates that GW/P bodies transiently interact with other RNP bodies in a molecular 'dance' moving protein, mRNA and miRNA from one body to another (Figure 1.11), and in the case of extracellular exosomes, possibly from one cell to another (Gibbings et al.,

2009). It is obvious from protein colocalization studies that GW/P bodies are heterogeneous in protein composition and at any given time a subset of GW/P bodies may contain protein cargo that is different from another subset of GW/P bodies. The complete proteome of GW/P bodies and other RNP bodies have not yet been elucidated and, therefore, other functions of these important bodies remains to be discovered.

Given the evidence that other RNP bodies such as neuronal transport RNP granules and stress granules share similar components to GW/P bodies, it is entirely possible that they interact with GW/P bodies to allow their cargo mRNA to become associated with the RNAi or decapping machinery (Figure 1.11). Regulation of molecular signals or physiologically relevant cues that direct interactions of RNP bodies with GW/P bodies has yet to be elucidated. Furthermore, it would be important to determine if these cues alter or affect GW/P body protein composition and thereby their function. These questions are essential to understanding GW/P body assembly, function, their interactions with other RNP bodies, disassembly and ultimately are key to understanding the role of these structures in cellular processes such as the regulation of mRNA expression.

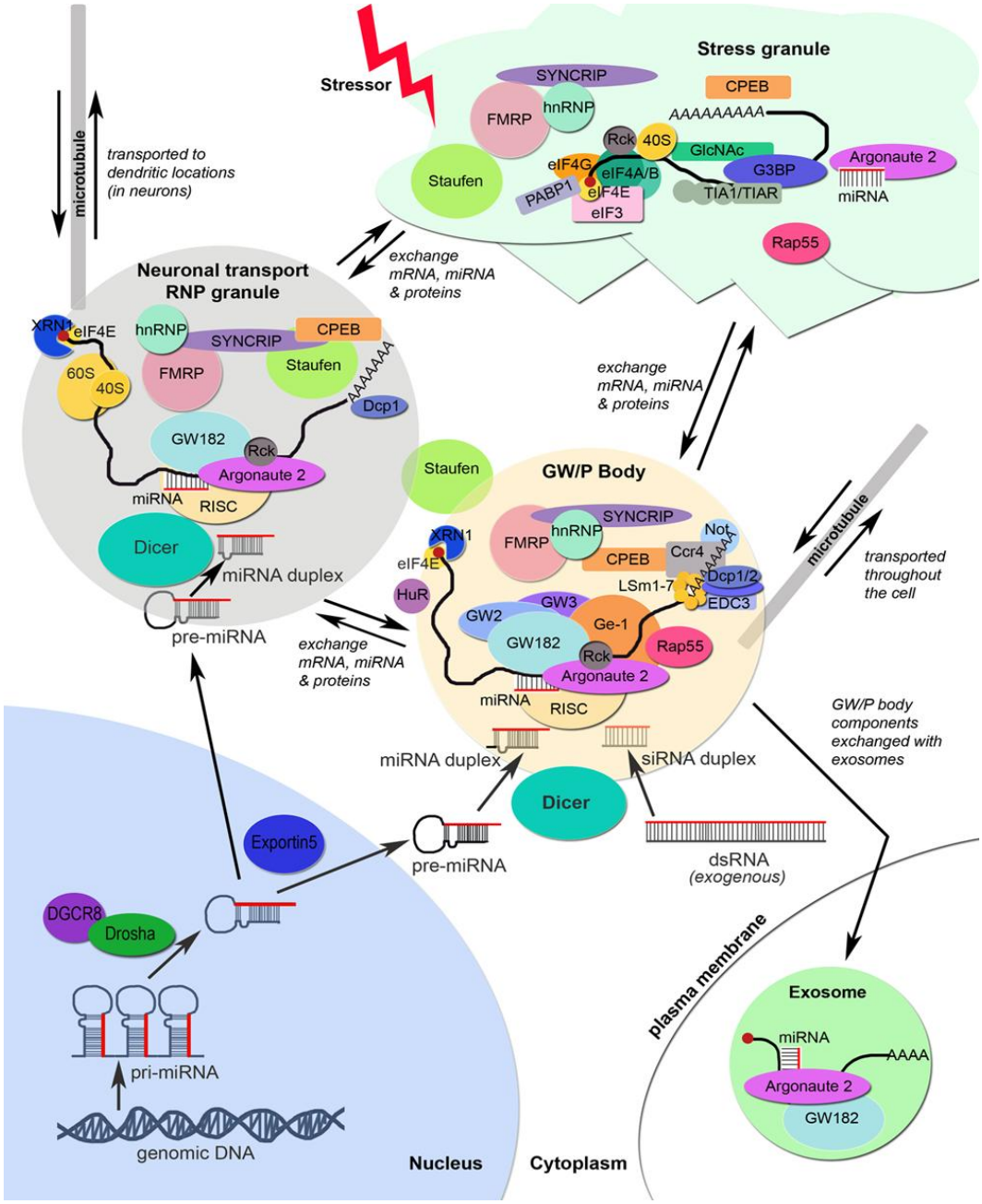

Figure 1.11: Conceptual model of a generalized mammalian cell showing the relationships between GW/P bodies, stress granules and neuronal transport RNP granules and their various protein and RNA components.

GW/P body components GW182 and nascent amounts of Ago2, mRNA and miRNA have recently been shown to be excreted from living cells into extracellular exosomes. (Moser and Fritzler, 2010)

1.8 Objectives and Hypotheses

There were four main **objectives** for this dissertation:

1) To investigate the presence and localization of GW/P bodies in cultured primary mouse astrocytes and human U-87 astrocytoma cells using immunocytochemistry and colocalization analysis.
2) To investigate if proteins involved in mRNA degradation, RNAi and mRNA transport, localization and stabilization of mRNAs colocalize to GW/P bodies in primary mouse astrocytes and human astrocytoma cells.
3) Optimize and establish an immunoprecipitation-Western Blot (IP-WB) protocol that specifically determines the natural ligands of GW/P bodies. Using this IP/WB protocol, determine which of the proteins in objective #2 are natural ligands of GW182.
4) Identify the global cellular and GW/P body/RISC-specific miRNA and mRNA profiles of primary human astrocytes and human astrocytoma cell culture to gain insight into the functional role of GW/P bodies and determine if this role differs in normal astrocytes compared to astrocytoma cells.

The specific **hypotheses** included:

1) GW/P bodies are more highly expressed in astrocytoma cells than in primary astrocytes.
2) Proteins involved in mRNA degradation, RNAi and mRNA transport and stabilization colocalize to a subset of GW/P bodies in astrocytes and astrocytoma cells showing that there is significant heterogeneity of GW/P bodies in astrocytes and astrocytoma cells. These proteins immunoprecipitated with antibodies to GW/P body components in astrocytoma cells.
3) The GW/P body/RISC-specific miRNA profile will differ between human astrocytes and astrocytoma cells. MiRNAs involved in the repression of mRNAs involved in cancer progression pathways will have an increased expression level in astrocytoma cells compared to astrocytes.
4) The GW/P body/RISC-specific mRNA profile will be similar in human astrocytes and astrocytoma cells; however the mRNAs involved in cancer progression pathways will have an increased expression in astrocytoma GW/P bodies/RISC compared to astrocyte GW/P bodies/RISC.

The subsequent chapters in this dissertation are organized as follows:

- Chapter Two provides detailed materials and methods of the studies in the following chapters.
- Chapter Three describes the detection of GW182-associated components of GW/P bodies using an optimized IP-WB protocol.
- Chapter Four describes the first characterization of GW/P bodies in human astrocytoma cells and mouse astrocytes and their heterogeneous protein composition.
- Chapter Five reveals RISC-specific miRNA and mRNA fold changes between human astrocytoma cells and primary astrocytes as compared to the global cellular miRNA and mRNA profile in these two cell types.
- Chapter Six contains the conclusions, limitations of the research approach and a proposal for future studies.

Chapter Two: **Materials and Methods**

2.1 Cells

As discussed in the Introduction, the focus for this thesis research was human astrocyte and astrocytoma cells.

2.1.1 Primary human astrocytes

Primary human cerebral cortex astrocyte cells (used between passages 4-6, cat# 1800, ScienCell Research Laboratories, Carlsbad, CA) were cultured under 5% CO_2 in astrocyte medium containing 2% fetal bovine serum, 1% astrocyte growth supplement and 1% penicillin/streptomycin (ScienCell Research Laboratories).

2.1.2 U-87 human astrocytoma/glioblastoma cells

Human U-87 astrocytoma cells (used between passages 15-24, cat# HTB-14, American Type Culture Collection (ATCC), Rockville, MD) were cultured in DMEM F12 + 1% L-glutamine (2 mM) (Cambrex, Walkersville, MD) supplemented with 10% fetal bovine serum (Gibco, Burlington, ON), 1% penicillin-streptomycin (Gibco), 1% sodium pyruvate (1 mM) (Gibco) and 1% non-essential amino acids (0.1 mM) (Gibco) at 37°C and 5% CO_2.

2.1.3 Mouse hippocampal cells

Hippocampal cell cultures were prepared by Dr. Sanja Selak (Cajal Institute, Madrid, Spain) from P0 C57 mice for use in some of the studies described in Chapter Four. The procedures for housing, handling and sacrificing mice followed guidelines of the European Commission (86/609/CEE) and the Canadian Council on Animal Care.

Hippocampi were dissected in ice-cold HEPES-buffered salt solution (HBSS) medium and digested with DNase (5µg/ml) and trypsin (0.125%) for 30 minutes at 37°C. The tissue was dissociated with a flame-polished Pasteur pipette. After centrifugation (300*g* for 5 minutes), cells were plated on poly-L-lysine coated coverslips (BD Falcon, Mississauga, ON) pre-treated with laminin (10 µg/ml; Sigma) and cultured at 37°C and 5% CO_2 in DMEM (Gibco, Burlington, ON) supplemented with 10% fetal bovine serum (Gibco) and 1% penicillin-streptomycin (Gibco). The medium was replaced after 3 hours with Neurobasal/B27 medium (Gibco) supplemented with L-glutamine (2 mM) (Gibco), 10% fetal bovine serum (Gibco) and 1% penicillin-streptomycin (Gibco). Cells were maintained by replacing 1/3 of the medium per week and used for experiments between 14 and 18 days *in vitro*. Dr. Sanja Selak provided the hippocampal cells fixed on coverslips (see section 2.3) ready for IIF analysis.

2.2 Antibodies

Mouse monoclonal antibodies to recombinant GW182 (2D6, 4B6) (Eystathioy et al., 2003a) and human anti-GWB serum 18033 was obtained from the serum bank at the Mitogen Advanced Diagnostics Laboratory (University of Calgary, Calgary, AB). Chicken anti-LSm4, mouse monoclonal to Dicer and rabbit anti-HuR antibodies were purchased from Abcam Incorporated (Cambridge, MA). Mouse monoclonal 4F9 to recombinant hAgo2 was a gift from Dr. Edward K.L. Chan (Department of Oral Biology, University of Florida, Gainesville, FL) and used as previously described (Ikeda et al., 2006). Rabbit anti-XRN1 antibody was purchased from Bethyl Laboratories (Montgomery, TX) and rabbit anti-hDcp was provided by Dr. Bertrand Séraphin (CNRS

Centre de Génétique Moléculaire, Gif-sur-Yvette, France). Rabbit anti-SYNCRIP antibody was a gift from Dr. Akihiro Mizutani (Department of Basic Medical Science, University of Tokyo, Japan) and human anti-hnRNPA1 antibody was a gift from Dr. Günter Steiner (Medical University of Vienna, Vienna, Austria). Rabbit anti-Staufen was purchased from Sigma-Aldrich Co. (St. Louis, MO) and mouse monoclonal antibody to fragile X mental retardation protein (FMRP) was purchased from Chemicon (Temecula, CA). The neuron cell marker, rabbit anti-neuron specific beta III tubulin and the astrocyte cell marker mouse GF5 monoclonal anti-glial fibrillary acidic protein (GFAP, catalogue # ab10062) were purchased from Abcam. The staining pattern produced by GF5 GFAP monoclonal antibody on fixed rat glial cells is shown on their website: http://www.abcam.com/index.html?pageconfig=datasheet&intAbID=10062.

The antibodies used for staining of mouse brain sections in Chapter One were chicken anti-GFAP astrocyte marker (Abcam), mouse anti-CNPase oligodendrocyte marker (Abcam), chicken anti-nestin stem cell marker (Abcam) and mouse anti-neurofilament 200 (a kind gift from Dr. Douglas Zochodne, University of Calgary, Calgary, AB).

2.3 Indirect Immunofluorescence (IIF)

Cells were plated on poly-L-lysine coated coverslips (BD Falcon) for approximately 24 hours at 37°C, fixed for 10 min in 4% paraformaldehyde/10% sucrose and then permeabilized for 2 min with 0.2% Triton X-100. Mouse brain (cryopreserved in OCT and stored at -80°C) was prepared as 9 µm sections that were fixed for 10 min in 4%

paraformaldehyde/10% sucrose and then permeabilized for 2 min with 0.2% Triton X-100.

The fixed cells were then incubated in a blocking buffer containing 10% normal goat serum (Antibodies Incorporated, Davis, CA) and 2% bovine serum albumin (Sigma-Aldrich) to minimize non-specific binding of the antibodies. For colocalization studies in Chapter Four, cells were incubated with either human anti-GWB 18033 serum (1/5000) or the monoclonal antibodies to recombinant GW182 and then stained with either chicken anti-LSm4, rabbit anti-XRN1, mouse anti-Ago2, mouse anti-Dicer, rabbit anti-SYNCRIP, human anti-hnRNPA1, rabbit anti-Staufen, mouse anti-FMRP, or rabbit anti-HuR at their appropriate working dilutions. After washing with phosphate buffered saline (PBS), cells were incubated in a dark chamber with the corresponding secondary goat fluorochrome-conjugated antibodies. Unless otherwise stated, the fluorochromes were Alexa Fluor (AF) 488 (green) and 568 (red) secondary antibodies purchased from Invitrogen (Burlington, ON). After washing with PBS, the cell nuclei were counterstained with 4',6-diamidino-2-phenylindole (DAPI), mounted in Vectashield (Vector Laboratories, Burlingame, CA) and examined by IIF using a 63x objective on a Leica DM RXA2 microscope with a EXFOS Xcite-120 light source and Chroma HQ filter sets (Chroma Technology Corp) fitted with a Roper (Princeton Instruments) cooled scientific CCD camera (Microscopy and Imaging Facility, Faculty of Medicine, University of Calgary, Calgary, AB). Multiple stacks were obtained and analyzed per image set, and AutoDeblur software (version 9.3, AutoQuant Imaging, Inc.) was used to collapse the stacks into final images. Digital images were prepared using Imaris (version 4.1) and figures were compiled in Adobe PhotoShop (version 7.0). Appropriate IIF

controls with no or only one primary antibody or both secondary antibodies alone or in combination were included in each experimental set to assess non-specific background staining and to ensure that there was negligible bleed-through of fluorochromes between microscope filter sets.

2.4 Quantitation of GW/P bodies

GW/P body colocalization with the various protein markers used in IIF were manually quantitated using the counting module in ImageJ software (National Institutes for Health, NIH) to enumerate overlapping foci. The calculated percentages were averaged from a homogeneous population of 3 to 10 astrocytes observed over 3 independent experiments and over 9 to 12 astrocytoma cells observed from 6 independent experiments with each cell containing on average 100 foci. Statistical significance of overlap was calculated using the Chi squared (χ^2) test. Error bars represent standard deviation from the mean percentages.

2.5 Cell Lysates

2.5.1 Cytoplasmic Lysate

U-87 cells were cultured as outlined above, harvested, pooled, and pelleted by centrifugation at 196*g* for 5 minutes and washed several times with sterile PBS. The cell pellets were resuspended, mixed in an equal pellet volume of PBS containing Complete EDTA-Free Protease Inhibitor (Roche, Mannheim, Germany), and then lysed by sonication in a water bath for two 80 second bursts. Finally, the viscous lysates were sheared by passing them through a syringe fitted with a 21G 1.5-inch needle and

centrifuged in a tabletop microfuge at 16,000*g* for 10 min. The supernatant was collected and stored at -20°C or -70°C for short term or long term use, respectively. The amount of protein in each sample was quantitated using a NanoVue spectrophotometer (GE Healthcare Life Sciences, Baie d'Urfe, QC). A typical U-87 cell extract had a protein concentration of approximately 12 mg/ml.

2.5.2 Ribonucleoprotein (RNP) Lysate Preparation

Primary astrocytes and U-87 astrocytoma cells were cultured as described above in multiple 150cm^2 tissue culture flasks, harvested, washed in sterile RNase-free ice-cold PBS (Ambion, Streetsville, ON) pooled and pelleted by centrifugation at 196*g* for 5 min at 4°C as previously described in detail (Moser et al., 2009). PBS was aspirated from the cell pellets and 1 equal volume of freshly prepared RNase-free ice-cold polysome lysis buffer (10 mM HEPES pH 7.0, 100 mM KCl, 5 mM $MgCl_2$, 25 mM EDTA pH 8.0, 0.5% IGEPAL, complete EDTA-free protease inhibitors, 2 mM DTT, 50 U/ml RNase OUT, 50 U/ml Superase IN) was added to the cell pellets (Baroni et al., 2008). Whole cell RNP lysates were vortexed, set on ice for 3 minutes and then transferred to -80°C until use. To isolate the cellular RNP proteins, the lysates were thawed on ice, sheared by passing them through a syringe fitted with a 21G 1.5-inch needle and centrifuged in a tabletop microfuge at 16,000*g* for 10 min at 4°C (Moser et al., 2009;Moser et al., 2007). The supernatant was removed, transferred to a new centrifuge tube and re-centrifuged at 16,000*g* for 10 min at 4°C to facilitate removal of the lipid layer overlying the supernatant. The protein concentration in the cellular RNP lysate was quantitated using a NanoVue spectrophotometer (GE Healthcare Life Sciences) and stored at -80°C. The

protein concentration of the cytoplasmic RNP lysates in representative samples was in the range of 11-13 mg/ml for primary astrocytes and 10-12 mg/ml for U-87 astrocytoma.

2.6 Coupling Antibodies to Protein Sepharose Beads

To prepare the coupling reaction, 150µl of normal human serum (NHS), 150µl of human anti-GWB (18033) or 500 µl of mouse monoclonal antibody (golgin 97 control or anti-GW182 4B6 clone) was added to 2ml of a 10% suspension of protein A-Sepharose beads or protein G-Sepharose beads, respectively, in PBS containing protease inhibitors (Amersham Biosciences, Uppsala, Sweden). The reaction was allowed to proceed for 2 hours at room temperature (RT) on a rolling mixer; the beads were then washed twice with 5ml of sodium borate buffer (0.2 M sodium borate, pH 9.0) and then resuspended in fresh 20mM dimethyl pimeliminade dihydrochloride (DMP) solution (Sigma-Aldrich). The beads were placed on a rolling mixer for 1 hour at RT, pelleted by centrifugation at 196*g* and the supernatant was discarded. The coupling reaction was stopped when the beads were washed twice in 1ml of 0.2M ethanolamine (pH 8.0). The beads were resuspended in 2 ml of ethanolamine, incubated at RT for 2 hours on a rolling mixer, washed twice with 2 ml sterile PBS and then stored at 4°C in 1 ml of PBS containing protease inhibitor.

2.7 Immunoprecipitation (IP) – Western Blot (WB)

Prior to IP, the U-87 cell lysate extracts were pre-cleared by adding an equal volume of 10% protein-A-Sepharose beads to the cell lysate followed by incubation for 5 min at RT on a rotator. After incubation, the unbound cell lysate was aspirated from the beads and

used for the IP reaction. IP reactions were prepared by combining 100µl of the 40% suspension of antibody-coupled protein-A-Sepharose beads (NHS or 18033 serum as outlined above), 500µl NET2F buffer (50mM Tris-HCl, pH 7.4, 150mM NaCl or 500mM NaCl, 2mM EDTA, pH 8.0), and 200µl of U-87 cell extract and incubated for 2 hours at 4°C on a rotator. After incubation, the Sepharose beads were washed 5 times in 1ml NET2F buffer (containing either 150mM or 500mM NaCl).

The cytoplasmic protein preparations were resolved in either 6.5% or 10% sodium dodecyl sulphate – polyacrylamide gel, electrophoretically transferred to nitrocellulose membranes (Bio-Rad Laboratories, Hercules, CA) and then processed for WB analysis. Nitrocellulose membranes were blocked for 1 hour in 5% non-fat milk (Lucerne) in PBS-T (0.05% Tween-20) and overlayed with the primary antibody at the appropriate dilution for 1 hour at RT. Following washing with PBS-T for a total of 30 min, horseradish peroxidase (HRP)-conjugated antibodies, either goat anti-human (diluted 1:20,000; Sigma, St. Louis, MO), goat anti-rabbit (diluted 1:20,000; Jackson ImmunoResearch, West Grove, PA) or goat anti-mouse (diluted 1:2000; Santa Cruz Biotechnology, Santa Cruz, CA) were overlayed on the appropriate strips for 1 hour at RT. Strips were then washed with PBS-T and subsequent identification of bound antibody was detected using the Amersham enhanced chemiluminescence (ECL) kit (GE Healthcare). Reactive proteins were visualized by exposure and recording on Amersham Hyperfilm ECL scientific imaging film (GE Healthcare).

2.8 RISC RNA Immunoprecipitation (RISC-RIP)

Human anti-GWB serum (18033), was used as the source of antibodies that were covalently coupled to protein A-Sepharose beads as previously described in detail (Moser et al., 2007;Moser et al., 2009;Li et al., 2008). We had previously shown that 18033 immunoprecipitated both GW182 and hAgo2 proteins (Moser et al., 2009). Prior to IP, 150µl of the antibody-coupled protein A-Sepharose beads for each IP reaction was washed five times with NT2 buffer (50 mM Tris-HCl pH 7.4, 150 mM NaCl, 1 mM $MgCl_2$, 0.05% IGEPAL) at RT. Washed antibody-coupled beads were resuspended in 1000µl of freshly prepared ice-cold NET2F buffer (850 µl NT2 buffer, 10 µl 0.1M DTT, 30 µl 0.5M EDTA pH 8.0, 50 µl of 50mg/ml ultrapure bovine serum albumin, 5 µl RNase OUT, 5 µl Superase IN) and mixed by inversion. Immunoprecipitation of the RISC-RNP complexes was accomplished by adding 200µl of the cellular RNP lysates to the antibody-coupled beads in NET2F buffer. IP reactions were incubated overnight at 4°C on a rotator. After incubation, the beads were centrifuged at 82*g* for 30 seconds at 4°C, the supernatant removed and the RISC-RNP complex-antibody-beads washed six times in 1 ml of ice-cold NT2 buffer. RISC-RNP complexes were dissociated from the antibody-beads by SDS-TE heat denaturation by resuspension of the washed beads in 100µl NET2F buffer and 100 µl of SDS-TE buffer (20 mM Tris-HCl pH 7.5, 2 mM EDTA pH 8.0, 2% SDS) and incubation at 55°C for 30 min with occasional mixing (Baroni et al., 2008). Total RNA enriched in small RNAs was isolated from the RISC-RNP complex using the mirVana kit (Ambion) according to the procedures outlined in the manufacturer's protocol. RNA samples were stored at -80°C until required for analysis by miRNA and gene expression microarrays. The total RNA concentration of the

RISC-RNP complex was 0.108 µg/µl for primary astrocytes and 0.318 µg/µl for U-87 astrocytoma.

2.9 µParaflo miRNA Microarray

Microarray assays of global miRNA and RISC-immunoprecipitated miRNA in primary human astrocytes and U-87 astrocytoma cells was outsourced to LC Sciences (Houston, TX). To isolate global miRNA, total RNA was isolated from primary human astrocytes (ScienCell) and U-87 astrocytoma cells (ATCC) using the mirVana kit (Ambion). The global total RNA concentration of representative preparations was 4.10 µg/µl for primary astrocytes and 2.49 µg/µl for U-87 astrocytoma cells. RISC-specific total RNA was isolated as described above and RNA integrity was assessed with an Agilent Bioanalyzer 2100 (Foster City, CA). The microarray assay was performed using samples containing 5 µg total RNA that was fractionated using a YM-100 Microcon centrifugal filter (Millipore, Billerica, MA) to isolate small RNAs (< 300 nt). Small RNAs were 3'-extended with a poly(A) tail using poly(A) polymerase. An oligonucleotide tag was then ligated to the poly(A) tail for later fluorescent dye staining with Cy5.

Hybridizations were performed overnight on a µParaflo microfluidic chip using a micro-circulation pump (Atactic Technologies, Houston, TX) (Zhu et al., 2007). Each detection probe on the microfluidic chip consisted of a chemically modified nucleotide coding segment complementary to 6211 target human miRNAs (Sanger miRBase version 11, http://microrna.sanger.ac.uk/sequences/) or control RNAs (array hybridization controls and single-base mismatch targets), and a polyethylene glycol spacer segment to extend the coding segment away from the substrate. The detection probes were

synthesized *in situ* using photogenerated reagent chemistry and were replicated seven times within each microarray chip (Gao et al., 2004). The hybridization melting temperatures of the probes were balanced by chemical modifications of the detection probes. Hybridization was performed at 34°C using 100 µL of 6xSSPE buffer (0.90 M NaCl, 60 mM Na_2HPO_4, 6 mM EDTA pH 6.8) containing 25% formamide. After washing, the hybridized fluorescent Cy5 signals were detected with a laser scanner (GenePix 4000B, Molecular Devices, Sunnyvale, CA) and digitized by Array-Pro image analysis software (Media Cybernetics, Bethesda, MA).

Data were further processed by subtracting the background followed by signal normalization with a LOWESS (locally weighted regression) filter (Bolstad et al., 2003). For a miRNA transcript to be classified as reliably detectable, it had to satisfy the following criteria: overall signal intensity >3× background standard deviation, spot coefficient of variation <0.5, and >50% of the repeated probes had signal intensities above detection level. The data were log2 transformed and the p-values of the t-test were calculated. Differentially detected miRNA signals with a p value of less than 0.01 were considered significant ($p<0.01$). Heat maps were generated for the differentially expressed miRNAs with $p<0.01$.

2.10 Gene Expression Microarray

Gene expression microarray analyses of global mRNA and RISC-immunoprecipitated mRNA in primary human astrocytes and U-87 astrocytoma cells were also outsourced to LC Sciences who were partnered with an Affymetrix Authorized Service Provider, SeqWright DNA Technology Services (Houston, TX). Global and RISC-RNP enriched

total RNA were isolated as described above and RNA integrity was assessed by an Agilent Bioanalyzer 2100 (Foster City, CA). Affymetrix's GeneChip IVT Express kit was used for cDNA synthesis and *in vitro* transcription. The gene expression microarray assay was performed using a 5 µg total RNA sample on an Affymetrix Human Genome U133A 2.0 Array which analyzes the expression level of 18,400 transcripts and variants, including 14,500 well-characterized human genes (Affymetrix, Santa Clara, CA). All procedures and analyses were performed according to the protocol outlined in detail in the GeneChip® Expression Analysis Technical Manual (Affymetrix, http://www.affymetrix.com/support/downloads/manuals/expression_analysis_technical_manual.pdf). Multi-chip expression intensity normalization was performed for all 4 samples on gene expression chips using the robust multichip average (RMA) algorithm (Irizarry et al., 2003), which consisted of three steps: background correction, quantile normalization (each performed at the individual probe level), and robust linear model fit using log-transformed intensities (at the probe set level). RMA normalization was used not only because multiple chips were compared, but also because RMA methods allow for better detection of low-abundance genes, which include many genes of interest, such as transcription factors, and signalling proteins. The overall selection criteria for presence used genes with expression values larger than a threshold 3.5 in more than 50% of samples.

2.11 Data Availability

The miRNA and mRNA microarray data generated by this study have been deposited and are available in the NCBI Gene Expression Omnibus (GEO) as series accession identifier GSE21514.

2.12 Functional Network Analysis

Functional profiling was performed by employing the computational gene network prediction tool Ingenuity Pathway Analysis version 8.5 (IPA, Ingenuity Systems; http://www.ingenuity.com) on all significantly expressed ($p<0.01$) miRNAs with log2 fold change greater than or equal to 2 and mRNAs with a log2 fold change greater than or equal to 2.5. For biological pathway connections in U-87 astrocytoma RISC, miRNAs with a log2 fold change greater than or equal to 3 and mRNAs with a log2 fold change greater than or equal to 2 were used. IPA maps the uploaded microarray datasets into a global molecular network developed from a literature-supported Ingenuity Pathways Knowledge Base, and then generated networks that represent the molecular relationships between the miRNAs and mRNAs. Canonical pathways were selected and overlayed onto the biological pathway based on known biological significance from the most highly overlapping pathways. MRNAs and miRNAs without connections to other molecules or pathways were removed from the final figure. The biological functions significantly associated with the genes in the networks are provided by the Ingenuity Pathways Knowledge Base and scored employing Fischer's exact test with a $p<0.01$.

2.13 cDNA Synthesis and Quantitative Kinetic Reverse Transcription Polymerase Chain Reaction (qkRT-PCR)

Global and RISC-RNP-enriched total RNA was extracted and quantitated as described above. Poly-A tailing of the miRNA in the total RNA sample and cDNA synthesis was performed using the NCode VILO miRNA cDNA synthesis kit (Invitrogen, Burlington, ON) according to the manufacturer's instructions. In brief, 1 µg of total RNA was added to 4 µl of 5X Reaction Mix and 2 µl of 10X SuperScript Enzyme mix up to a total volume of 20 µl. Reactions were mixed by pipeting and incubated at 37°C for 60 min. The reactions were terminated at 95°C for 5 min and stored at -20°C until use in the qkRT-PCR reaction. The cDNA was diluted with nuclease free water to give a DNA concentration of ~375 ng/µl and qkRT-PCR reactions performed using the EXPRESS SYBR GreenER Universal qkRT-PCR kit (Invitrogen). Each 20 µl qkRT-PCR reaction contained 10 µl of EXPRESS SYBR GreenER qkRT-PCR SuperMix Universal, 0.4 µl of 10 µM miRNA-specific forward primer or 10 µM mRNA-specific forward primer (listed in Table 2.1), 0.4 µl of 10 µM Universal reverse qkRT-PCR primer or 10 µM mRNA-specific reverse primer (listed in Table 2.1), 1 µl of 1:10,000 diluted fluorescein calibration dye and 1 µl of diluted cDNA up to a final volume of 20 µl with nuclease-free water.

Table 2.1: Forward and reverse primers used for validation of gene expression and miRNA expression by qkRT-PCR analysis.

Primer	Forward Probe Sequence (5'→3')	Reverse Probe Sequence (5'→3')
β-actin	CTGGAACGGTGAAGGTGACA	AAGGGACTTCCTGTAACAATGCA
RAB12	GAAGTGCCAAGGGGATCATA	TGGCACTTGCTTCACAGAAC
ITCH	GTAGCCTCACCATGAAATCACA	CGATAACTGTAAGGGGTTGCTT
GW182 (TNRC6A)	AGTGGGAGTTCTGGCATCAAT	CAGGCTCACAAGTTTCCTGAAG
hAgo2 (eIF2C2)	CGTCCTTCCCACTACCACG	CCAGAGGTATGGCTTCCTTCA
GW2 (TNRC6B)	AGGAAATTGGAGGAATGTGAGTG	GGATGTCTGACCTACTGTGCT
MAP1B	AAGCTGAGAGGTCCCTTATGT	CTTCGTCTTCGATTAGCTCCAG
CEP350	AGAACGGAATATACGGAGCTGT	TTAGTCGTAACGCTTTTGGATCA
SNRPA1	TGCTACGTTAGACCAGTTTGATG	CCCTCACCTATACGGCATATTCT
RNU6B	TGACACGCAAATTCGTGAAG	Universal qkRT-PCR primer*
hsa-miR-29b	TAGCACCATTTGAAATCAGTGTT	Universal qkRT-PCR primer*
hsa-miR-29c	TAGCACCATTTGAAATCGGTTA	Universal qkRT-PCR primer*
hsa-miR-195	GATAGCAGCACAGAAATATTGGC	Universal qkRT-PCR primer*
hsa-miR-10b	TACCCTGTAGAACCGAATTTGTG	Universal qkRT-PCR primer*
hsa-miR-20b	CAAAGTGCTCATAGTGCAGGTAG	Universal qkRT-PCR primer*
hsa-miR-181b	TCATTGCTGTCGGTGGGT	Universal qkRT-PCR primer*
hsa-miR-1280	CACCGCTGCCACCCA	Universal qkRT-PCR primer*
hsa-miR-1826	TCGACACTTCGAACGCAATA	Universal qkRT-PCR primer*
hsa-miR-432	TGGAGTAGGTCATTGGGTGG	Universal qkRT-PCR primer*
hsa-miR-19b	GCAAATCCATGCAAAACTGA	Universal qkRT-PCR primer*
hsa-miR-455-3p	GCAGTCCATGGGCATATACAC	Universal qkRT-PCR primer*
hsa-miR-27b	TTCACAGTGGCTAAGTTCTGC	Universal qkRT-PCR primer*

*Source: EXPRESS SYBR GreenER Universal qkRT-PCR kit (Invitrogen).

The qkRT-PCR reactions were performed in triplicate with a BioRad MyiQ Single Color Real-Time PCR detection system iCycler programmed as follows: 1 cycle at 50°C for 2 min for uracil DNA glycosylase incubation; 1 cycle at 95°C for 2 min; 40 cycles of 95°C for 15 seconds and 60°C for 1 min, followed by a melt curve analysis at 95°C for 1 min

and 60°C for 1min and 10sec. The cycle threshold (Ct) values, corresponding to the PCR cycle numbers at which fluorescence emission reaches a threshold above baseline emission, were determined and the mRNA and miRNA levels was calculated using the comparative $2^{-\Delta\Delta Ct}$ method. A comparison of the relative mean fold increase in gene expression between two housekeeping genes, beta-actin and 80S RNA was examined to determine the most stable housekeeping gene. Due to smaller standard deviations between the $2^{-\Delta\Delta Ct}$ over 3 independent experiments, the beta-actin gene was used as the reference marker for gene expression normalization. For analysis of miRNA by qkRT-PCR, RNU44 and RNU6B controls were examined to determine the most stable small RNA endogenous control. Due to smaller standard deviations between the $2^{-\Delta\Delta Ct}$ values over 3 independent experiments, RNU6B was used as the reference marker for miRNA expression normalization.

Chapter Three: **Detection of GW182-associated components of GW/P Bodies using an optimized IP-WB protocol***

* This work has been published and used with permission: Moser JJ, Chan EKL, Fritzler MJ. Optimization of immunoprecipitation-western blot analysis in detecting GW182-associated components of GW/P bodies. Nature Protocols 2009;4(5):674-85. PMID: 19373232

3.1 Introduction

Characterizing the components of GW/P bodies is key to elucidating RNA interference and messenger RNA processing pathways. However, many laboratories have had significant difficulties identifying GW182 and related GWB proteins by conventional Western blot (WB), a challenge that may be attributed to a number of features that include their molecular mass, relatively low abundance and/or incompletely understood unique physicochemical properties such as the high density hydrophobic glycine(G)/tryptophan(W) domains (Eystathioy et al., 2002a). Prior to examining the biochemical interactions between GW182 and other messenger ribonucleoprotein (mRNP) components, indirect immunofluorescence and colocalization studies are commonly used as a first step to determine whether a protein of interest is located in spatial proximity to GW182/GWB.

Optimized protocols needed to be developed to addresses the challenges in isolating an apparently low abundance protein GW182 and GWB-associated proteins. These protocols were built on previous reports (Moser et al., 2007;Li et al., 2008) that used polyclonal sera containing autoantibodies to GW/P body components by utilizing commercially available monoclonal antibodies to GW182 that were covalently coupled to Protein A or G sepharose beads and then used to immunoprecipitate GW182 and associated proteins from cell extracts. Immunoprecipitates were separated by SDS-PAGE (sodium dodecyl sulphate–polyacrylamide gel electrophoresis), transferred to nitrocellulose membranes and probed by Western blot with antibodies directed to proteins of interest. This protocol provides a biochemical approach for detecting GW182 and associated proteins in biological samples and thus facilitates the elucidation of the

diverse functions of GWB. It is expected that this protocol can be adapted to the detection of other RNA binding complexes.

This chapter is focused on GW182 and the optimized biochemical protocol that was developed to aid in identifying the diverse functions of GWB but as discussed later, it can be adapted or suitably modified to study a variety of cellular components such as neuronal granules, RNA granules, mRNP and other RNA binding protein complexes. As a brief overview, this protocol first immunoprecipitates (IP) the protein complex of interest from the cellular milieu using GWB antibodies covalently coupled to Protein A or G sepharose beads, followed by WB to detect proteins of interest associated with the cognate protein complex of interest (Figure 3.1). First, an antibody demonstrating high specificity for the low abundance target (i.e. GW182) is coupled to a solid phase matrix (Protein A or G sepharose beads) that then binds protein(s) of interest and adsorbs the protein complex from the cell lysates. Other proteins not bound to the antibody-Protein A or G bead support are washed away and the proteins of interest are eluted from the antibody-coupled beads and separated by SDS-PAGE. This is followed by WB to determine the identity of proteins that are associated with the protein of interest. An important advantage of combined IP-WB reactions over WB alone is their potential to deliver not only the target protein but also other macromolecules that interact with the target protein. The IP-WB protocol previously published by our group (Moser et al., 2007;Li et al., 2008) that used human polyclonal sera to detect other proteins associated with RISC, P-bodies and mRNA granules has been modified by adopting the use of monoclonal antibodies raised against GW182 and other key components of GWB (reviewed in (Jakymiw et al., 2007)). Although monoclonal antibodies are probes of

choice, they may have limitations in biochemical techniques that can be attributed to low affinity, polyreactivity (particularly IgM antibodies), low concentrations in commercially available preparations and reactivity to restricted epitopes that may be inaccessible when proteins retain their tertiary structures.

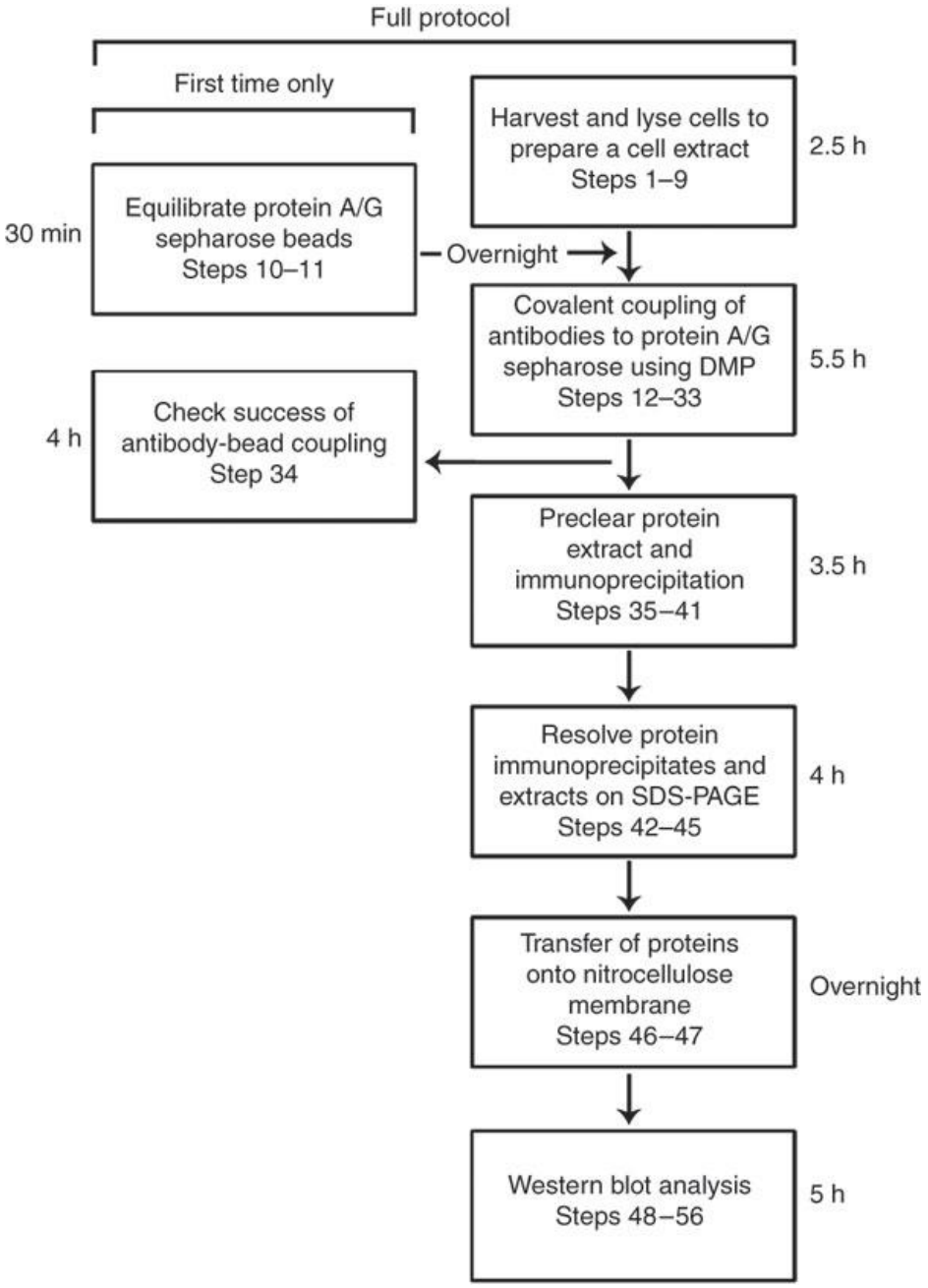

Figure 3.1: Summary of the steps involved and the approximate time required in detecting GW182 and associated proteins that are components of GWB. Note that the steps shown in the boxes on the left are required only the first time if sufficient reagent is prepared for future experiments.

3.2 Experimental Design

3.2.1 Sample type and preparation

This method was first published using U-87 astrocytoma cells (Moser et al., 2007) and more recently HeLa cells (Li et al., 2008) but it can be applied to other cell types according to the user's preference. Protein isolated from tissues may be examined using the methodology outlined in this protocol but has not been examined by the authors. Cell morphology, growth patterns and resulting cell density are well known to differ between cell lines. For example, when examining the difference between HeLa cells and U-87 astrocytoma cells, it is obvious that the latter cells have long, widely spread projections that are remarkably different from the much more compact phenotype seen in HeLa cell cultures. This type of growth pattern typical of astrocytoma cells requires incrementally more U-87 cells to obtain the same amount of protein harvested from HeLa cells. It is very important to appreciate that a relatively large amount of protein (~40 μg/lane) is recommended to IP the GW182 associated proteins or other low abundance proteins. Cell lysis in this protocol is achieved by mechanical methods without the addition of salts or detergents. From experience, mechanical methods for the detection of GW182 are superior to the use of lytic or chaotropic agents. Addition of lysis buffers containing detergents and salts may interfere with native protein conformation, protein-protein interactions and the binding of proteins to antibodies in the subsequent IP. Both lysis approaches must be tested and optimized for particular cells and tissues that may be used in other studies. Comparison of lysis methods are made following IP and WB steps and the choice ultimately rests with the investigator.

3.2.2 Choice of antibodies for IP and WB

First, an important consideration is the choice of antibodies used to IP the protein complex of interest. The chosen antibodies should have proven specificity and minimal cross-reactivity or non-specific binding. Human serum 18033 was initially used to IP GW182 (Moser et al., 2007;Li et al., 2008), but the results have recently been improved with the use of the commercially available mouse monoclonal 4B6 antibody. Human 18033 serum is polyclonal, recognizes multiple GWB-associated proteins such as GW182, Ago2 and Rap55, and efficiently IP GWB-associated proteins and detects GW182 by WB (Figure 3.2).

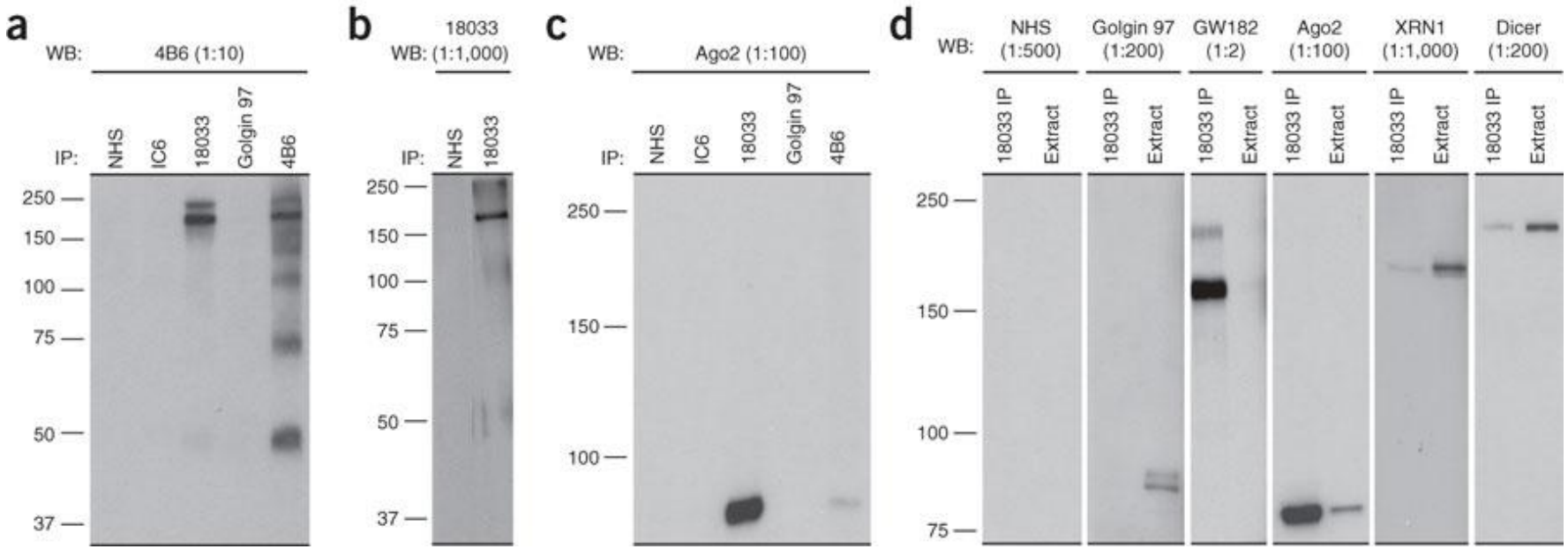

Figure 3.2: Antibodies to GW182-immunoprecipitated Ago2, Dicer and XRN1 proteins from HeLa cell extracts as examined by WB analysis. GW182 and associated proteins were immunoprecipitated using human sera 18033 containing antibodies to GW182 coupled with Protein A sepharose beads and by mouse anti-GW182 monoclonal 4B6 coupled to Protein G sepharose beads. Normal human serum (NHS), IC6 human serum and mouse monoclonal antibody to golgin 97 were used as IP controls. Immunopreciptates were carried out with buffer that did not contain detergent. Proteins (40 µg) were resolved on a 10% SDS-PAGE gel and were detected with a 4B6 monoclonal antibody (a) or 18033 human anti-GWB serum (b). Immunopreciptates were carried out with buffer that contained 0.3% NP-40 detergent. Proteins (40 µg) were resolved on a 6.5% SDS-PAGE gel and were detected using a mouse anti-Ago2 monoclonal 4F9 antibody (c). Protein (40 µg) from whole cell extracts or 18033 immunoprecipitates carried out using 0.3% NP-40 buffer were separated on a 6.5% SDS-PAGE gel and probed with NHS or antibodies to golgin 97, GW182, Ago2, XRN1 or Dicer. (d) Mouse monoclonal antibody to Dicer and rabbit anti-XRN1 antibody were purchased from Abcam Inc. (cat. no. ab14601) and Bethyl Laboratories (cat. no. A300-443A), respectively. Mouse monoclonal 4F9 to recombinant hAgo2 was obtained (Ikeda et al., 2006).

Mouse monoclonal 4B6 was generated by immunization with recombinant GW182 (Eystathioy et al., 2003a) and it can be used to IP GW182 from the cytoplasmic protein milieu and to detect GW182 by WB (Figure 3.2, panel a and c). Since cross-reactivity tends to be more common when polyclonal antibodies are used or when low avidity IgM monoclonal antibodies are used, it is very important to select antibodies of the highest specificity and affinity for the protein in question. Hence, it is important to test the specificity and binding characteristics of different antibodies in a pilot IP analysis to validate their efficiency and usefulness. For WB analysis, antibodies should be proven acceptable for WB applications, be specific for the protein of interest and their dilution must be optimized to achieve a result that produces low background reactions.

3.2.3 Control antibodies

Control antibodies must be chosen for IP and WB that do not cross react with the proteins of interest (i.e. GW182) but are specific for their cognate antigen. For example, mouse monoclonal golgin-97 (CDF4) antibody is specific to the Golgi complex golgin 97 protein (Figure 3.2, panel d, extract lane, protein band at ~97kDa) but does not bind to GW182 or associate with GWB complex proteins (Figure 3.2, panel d, 18033 IP lane) in WB analysis. Another example is IC6 human serum which contains antibodies that recognize the Ge-1/Hedls protein (Figure 3.2, panels a and c). Normal human serum (NHS) or sera with an unrelated autoantibody should be used as another control (Figure 3.2, IP and WB applications). To account for non-specific binding of the Protein A or G sepharose beads, another control to be considered are IPs in the absence of cell lysate extracts (i.e. no protein, PBS only) or extracts that do not contain the protein targets of

interest. However, the two latter controls are not necessary when the cell lysates are pre-cleared by incubation with the beads. Pre-clearing of the cell lysate normally removes non-specific, high affinity proteins that bind to Protein A or G prior to IP reactions. In addition, a whole cell extract can be included in a parallel SDS-PAGE lane to examine the baseline expression of a particular protein without IP and to check if the antibody is an appropriate reagent for WB. For example, XRN1 and Dicer are two proteins that are enriched in the whole cell extract as compared to the GW182 IP; however, Ago2 and GW182 are enriched in the GW182 IP as compared to the whole cell extract (Figure 3.2, panel d).

3.2.4 Optimization of IP conditions

This protocol uses dimethyl pimelimidate dihydrochloride (DMP) to covalently link Protein A sepharose beads to human IgG antibodies and Protein G sepharose beads to mouse IgG antibodies. Protein A and G Sepharose preparations have the cognate immunoglobulin binding proteins already immobilized on insoluble beads. The A and G proteins immobilized on the sepharose beads bind to the Fc domain of antibodies. Only the Fc antibody region is bound to sepharose, thus the Fab antibody region is available for antigen binding. Depending on the species from which the primary antibody is derived, the appropriate beads for antibody IP must be chosen by the user. In general, human IgGs bind to both Protein A and G, whereas mouse IgGs show variable binding properties (mouse IgG1 binds very poorly to Protein A, whereas IgG2a and 2b bind to both with equal specificity). Hence, for mouse antibodies Protein G is the preferred ligand. The option of covalently coupling the antibody to the beads rests with the user but

if the antibodies are not covalently linked to a solid phase bead matrix, boiling the IP sample in 2x Laemmli sample buffer (LSB) will result in the co-elution of the antibody along with the target protein(s) (Figure 3.3).

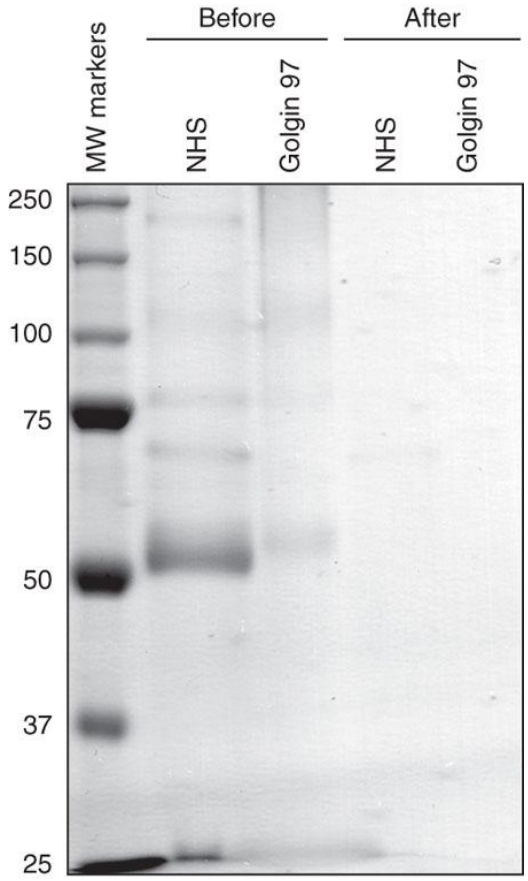

Figure 3.3: Example of successful covalent coupling of antibodies to sepharose beads.

The 'Before' conjugation samples and 'After' conjugation samples (NHS-Protein A, golgin 97-Protein G) were resolved on 10% SDS-PAGE and stained with the Colloidal Blue Staining Kit. The antibody light (25-kDa) and heavy (50-kDa) chains are visible on the gel in the 'Before' samples, but not in the 'After' samples, indicating that covalently coupled antibodies remained bound to the beads after boiling in 2 xLSB.

If co-elution of antibody fragments with the antigen results in bands interfering with detection of any co-precipitated proteins on SDS-PAGE, the antibody should be cross-linked to the beads. Although cross-linking is not entirely efficient and a small amount of IgG may be eluted from the beads inevitably, this method does improve the quality of WB results.

The IP buffer should be chosen after considerable planning and can be modified to increase or decrease stringency. Options include increasing salt concentrations to reduce ionic interactions (ranges between 150 mM NaCl up to 1000 mM NaCl; 150 mM NaCl used in this protocol) and/or adding one or more detergents such as NP-40 or Triton X-100 to increase protein solubility and unfold proteins. The effectiveness of IP buffers to wash away non-specific binding proteins will become evident after WB if extra protein bands appear in the IP lane and are similar to what is observed in the whole cell extract.

3.2.5 SDS-PAGE considerations

Detection and resolution of GW182 and TNGW1 (a recently characterized longer isoform of GW182 (Li et al., 2008)) depends upon the resolving power of the SDS-PAGE gel at high molecular masses (i.e. 182 kDa and 210 kDa respectively). In these situations, a 6.5% (vol/vol) SDS-PAGE gel is recommended, but if 30-100 kDa proteins are of interest a 10% (vol/vol) SDS-PAGE gel may be desirable. See Reagent Setup for varying percentage resolving gel components and 5% (vol/vol) stacking gel components. Once proteins from SDS-PAGE are transferred onto nitrocellulose or polyvinylidene fluoride membranes, a Ponceau S stain is used as a rapid and reversible stain to ensure

transfer of proteins from the SDS gel before WB (Figure 3.4). Ponceau S stain is easily reversed by washing the membrane in $_{dd}$H2O.

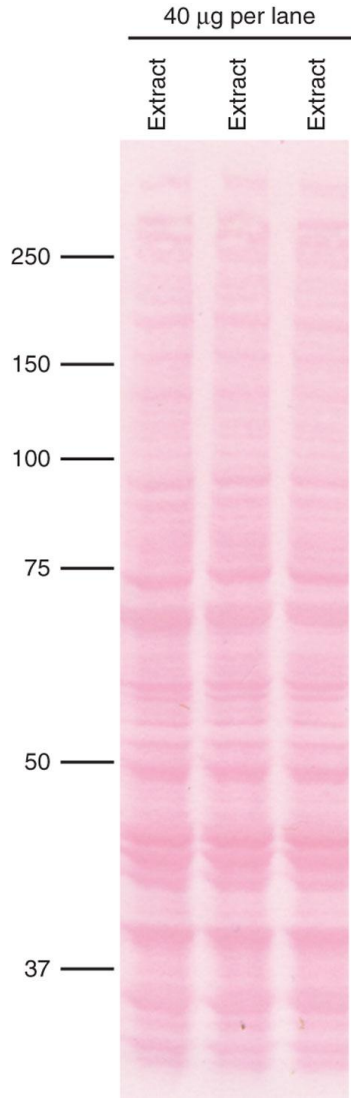

Figure 3.4: Example of a Ponceau S-stained nitrocellulose membrane containing 40µg of protein per lane from a HeLa cell lysate extract.

The membrane was stained for 1 min with Ponceau S and destained with quick washes in ddH_2O until proteins bands became pink and the background became white. Numbers are protein size in kDa.

3.2.6 Membrane choice and transfer

Nitrocellulose membranes are used in this protocol but polyvinylidene fluoride (PVDF) membranes may be used although they have not been extensively tested by the authors. Wet transfers at 22-25V (overnight, 4°C) have worked best for transfer of proteins from SDS-PAGE (6.5%, 10%, or 12% (vol/vol) gel), although semi-dry transfer has also been used with some success (unpublished data).

3.3 Detailed Materials and Methods

3.3.1 Reagents

- Cells of choice approximately $1x10^9$ - 10^{11} cells (~20 T-150cm^2 U-87 cell flasks to yield 12 mg ml^{-1} protein and ~10 T-150cm^2 HeLa cell flasks to yield 20 mg ml^{-1} protein)
- Phosphate Buffered Saline (PBS), pH 7.4 diluted from 10xPBS pH 7.4 sterile, RNase, DNase and Protease free as tested by supplier (Ambion, http://www.ambion.com, cat. no.AM9625)
- Complete Mini EDTA-free Protease Inhibitor Cocktail Tablets (Roche, https://www.roche-applied-science.com, cat. no.04693159001)
- BCA Protein Assay Reagent kit (Pierce, http://www.piercenet.com, cat. no.23227)
- Protein A Sepharose CL-4B beads (Amersham/GE Healthcare, http://www1.gelifesciences.com, cat. no.17-0780-01)
- Protein G Sepharose 4 Fast Flow beads (Amersham/GE Healthcare, cat. no.17-0618-01)

- Primary antibodies of choice to detect GWB or the RISC complex, for example:
    - Mouse GW182 (4B6) Monoclonal Antibody (Santa Cruz Biotechnology Inc., http://www.scbt.com, cat. no.sc-56314). 4B6 mouse monoclonal antibody has proved to be the best available monoclonal antibody for IP and WB applications. Mouse GW182 (2D6) monoclonal antibody (Santa Cruz Biotechnology Inc., cat. no.sc-56313) may also be used in IP and WB applications however is a weaker antibody. Human 18033 serum (or equivalent) containing autoantibodies directed to GWB (Mitogen Advanced Diagnostics Laboratory, limited supply available on request to Dr. M. Fritzler: fritzler@ucalgary.ca).
- Primary antibodies for controls include:
    - Mouse anti-human golgin-97 (Golgi) Monoclonal Antibody, Clone CDF4 (Molecular Probes/Invitrogen, http://products.invitrogen.com, cat. no.A21270)
    - Normal human serum (NHS; Mitogen Advanced Diagnostics Laboratory)
- Ethanolamine (Sigma, http://www.sigmaaldrich.com, cat. no.E9508). This chemical is corrosive and toxic and is harmful if inhaled or in contact with skin. Toxic if ingested. Wear gloves, lab coat, safety glasses and keep the bottle pointed away from user when transferring liquid.
- Sodium Tetraborate or Borax Anhydrous, pH 9.0 (Sigma, cat. no.71996). This chemical is harmful with possible risk of impaired fertility and of harm to an unborn child. Wear suitable protective clothing and gloves.

- Dimethyl Pimelimidate Dihydrochloride (DMP; Sigma, cat. no.D8388). This chemical is irritating to the skin and contact with skin and eyes should be avoided by wearing suitable protective clothing and gloves.
- Colloidal Blue Staining Kit (Invitrogen, cat. no.LC6025)
- Tris-HCl (Trizma; Sigma, cat. no.T-3253)
- Tris-base (Bio-Rad, http://www.bio-rad.com, cat. no.161-0719)
- Sodium chloride (NaCl; VWR, http://www.vwrcanlab.com, cat. no.CA-EM7760)
- 0.5M ethylenediaminetetraacetic acid, pH 8.0 (EDTA; Gibco/Invitrogen, http://products.invitrogen.com, cat. no.15575-020)
- NP-40 detergent (Sigma, cat. no.N-6507)
- 2x Laemmli sample buffer (2xLSB, see Reagent Setup)
- Glycerol (VWR, cat. no.CA-EM4750)
- bromophenol blue (VWR, cat. no.CA-EM2830)
- 2-mercaptoethanol (Bio-Rad, cat. no.161-0710)**.** Use with caution as this chemical is toxic in contact with skin, harmful if swallowed, causes burns and is combustible. Wear protective gloves/protective clothing/eye protection/face protection. Keep away from heat/sparks/open flames/hot surfaces. Handle in a fume hood.
- Ammonium Persulfate (APS; Sigma, cat. no.A-1433). Note this chemical is harmful if swallowed and irritating to the eyes/respiratory system/skin. Wear suitable protective clothing and gloves and avoid contact with combustible materials as this may cause a fire.

- 40% Acrylamide (wt/vol) (Bio-Rad, cat. no.161-0140). Note that acrylamide is a suspected human carcinogen, severe neurotoxin, and causes irritation of the eyes, skin (is readily absorbed), and respiratory tract. Wear gloves, lab coat, safety lab goggles and keep the bottle pointed away from user when transferring liquid.
- 2% Bis-acryl (wt/vol) (Bio-Rad, cat. no.161-0142)
- Sodium dodecyl sulfate (SDS; Bio-Rad, cat. no.161-0302). This chemical is highly flammable, harmful in contact with skin and irritant to the respiratory tract and eyes. Wear suitable protective clothing, gloves and a mask covering the mouth and nose.
- double distilled water ($_{dd}H_2O$)
- N, N, N', N' – Tetra-methyl-ethylenediamine (TEMED; Bio-Rad, cat. no.161-0800). This chemical is corrosive, highly flammable and harmful by inhalation. Suitable protective clothing, gloves and eye/face protection must be worn.
- Running Buffer (see Reagent Setup)
- Protein molecular weight markers of choice
- Nitrocellulose membrane (recommend 0.45µm pore size; Bio-Rad, cat. no.162-0115)
- Transfer buffer (see Reagent Setup)
- Ponceau S stain (see Reagent Setup)
- Skim milk powder
- Phosphate Buffered Saline with 0.05% (vol/vol) Tween (Sigma; cat. no.P1379) (PBST), pH 7.4

- Secondary antibodies of choice conjugated to horse radish peroxidase (HRP) for enhanced chemiluminescence (ECL) visualization, for example:
    - goat anti-mouse IgG-HRP (Santa Cruz Biotechnology Inc., cat. no.sc-2005)
    - goat anti-human IgG-HRP (Sigma, cat. no.A8667)
- Enhanced chemiluminescence (ECL) Western Blotting Detection Reagents (Amersham/GE Healthcare, cat. no.RPN2106)

3.3.2 Equipment

- Cell scrapers (40cm, VWR, cat. no.CA15621-015)
- 120V Ultrasonic water bath sonicator/cleaner (VWR, cat. no.98000-328)
- 3 ml syringe fitted with a 21G 1½ inch needle (BD, http://www.bd.com, cat. no.305274)
- 1.5 ml micro-centrifuge tubes (VWR, cat. no.20170-355)
- 15 ml and 50 ml conical polystyrene centrifuge tubes (BD Falcon, VWR, cat. no.CA21008-930 and CA21008-938)
- Refrigerated microcentrifuge of choice for 1.5ml/2.0ml microtubes (VWR, cat. no. 13916-836)
- Nanodrop 1000 (Thermo Scientific, cat. no.ND-1000) or NanoVue spectrophotometer (GE Healthcare Life Sciences, Baie d'Urfe, QC, cat. no. 28-9569-62)

- Accumet Basic AB15 pH meter (Fisher Scientific, https://www1.fishersci.com/wps/portal/CMSTATIC?href=index.jsp&store=Scientific&segment=scientificStandard, cat. no.13-636-AB15V)
- Nutating mixer (VWR, cat. no.82007-202)
- Microtube rotator (VWR, cat. no.13916-822)
- Rocking platform shaker (VWR, cat. no.40000-300)
- centrifuge of choice for 15ml centrifuge tubes (VWR, cat. no. 82017-654)
- Protein running gel apparatus of choice (SE 260 Mini-Vertical Unit, Amersham/GE Healthcare, cat. no.80-6149-35)
- Power pack of choice (EPS 301, Amersham/GE Healthcare, cat. no.18-1130-01)
- Wet transfer apparatus of choice (TE 22 Mini Tank Transfer Unit, Amersham/GE Healthcare, cat. no.80-6204-26)
- Film of choice (recommend either Kodak BioMax MR Film, VWR, cat. no.IB-IB8701302 or Amersham Hyperfilm ECL, VWR, cat. no.CA95017-659L)
- Automated film developer or dip trays/tanks with fixer and developing reagents (reagents supplied by Christie Group Ltd., http://www.christiegrp.com/english/index.html, cat.no.V-306A, V-306B, V-307).

3.3.3 Reagent Setup

- **PBS with protease inhibitor**

Combine 1 Complete Mini EDTA-free Protease Inhibitor Cocktail Tablet per 10 ml of sterile PBS. Mix until tablet dissolved. This solution is stable for 12 weeks when stored at -20°C.

- **10% (wt/vol) Protein A Sepharose bead slurry**

Wash 0.75 g of Protein A beads 2 times with 10 ml of sterile PBS . Equilibrate Protein A beads in 25 ml of sterile PBS containing protease inhibitor. Allow the beads to swell overnight at 4 °C. Store at 4°C for 1 year with the addition of 0.05% (wt/vol) sodium azide.

- **10% (wt/vol) Protein G Sepharose bead slurry**

Transfer 5 ml of beads stored in 70% (vol/vol) ethanol to a 50 ml centrifuge tube and wash a total of 5 times with 20 ml of sterile PBS to remove all traces of ethanol. Rinse out the supply bottle with 5 ml of sterile PBS to collect remaining beads and add to the 50 ml centrifuge tube. Prepare a 10% (wt/vol) Protein G sepharose slurry by adding 25ml of sterile PBS containing protease inhibitor to the washed Protein G beads. Allow the beads to swell overnight at 4 °C. Store at 4°C for 1 year with the addition of 0.05% (wt/vol) sodium azide.

- **0.2 M Ethanolamine, pH 8.0**

Dilute 2.44 ml ethanolamine up to 200 ml with autoclaved double distilled water ($_{dd}H_2O$). Adjust pH to 8.0 using glacial acetic acid. Store at room temperature (RT) for a maximum of 2 years. RT can range from 17°C-24°C. A fume hood is used

when the pH is adjusted with hydrochloric acid as this acid will vaporize upon addition to ethanolamine. Hydrochloric acid vapors irritate the nose and respiratory tract. Recommend adjusting pH with acetic acid instead.

- **0.2 M Sodium Borate Buffer (SBB), pH 9.0**

Mix 20.12 g of sodium tetraborate anhydrous in 500 ml of autoclaved $_{dd}H_2O$. Adjust pH to 9.0. Filter-sterilize and store at RT for a maximum of 2 years. Anhydrous sodium tetraborate is difficult to dissolve until at optimal pH of 9.0.

- **20 mM DMP**

Add 26 mg of DMP powder to 5 ml of 0.2 M SBB pH 9.0. This must be made immediately before use because of its instability in solution (hydrolyzes at neutral pH).

- **1M Tris-HCl, pH 7.4**

Mix 132.2g Tris HCl and 19.4g Tris base into 500ml of $_{dd}H_2O$ and adjust pH to 7.4 if necessary. Bring up to a final volume of 1L with $_{dd}H_2O$. Store at RT for a maximum of 2 years.

- **NET2F IP buffer**

50mM Tris-HCl, pH 7.4, 150mM NaCl, 2mM EDTA, pH 8.0. For greater stringency add 0.3% (vol/vol) NP-40 detergent and/or 0.3% (vol/vol) Triton X-100 and/or adjust to 500mM NaCl. Filter-sterilize and store at 4°C for a maximum of 1 year.

- **2x LSB**

25% (vol/vol) glycerol, 2% (wt/vol) SDS, 250mM Tris-HCl pH6.8, 0.1% (wt/vol) bromophenol blue up to desired volume with $_{dd}H_2O$. Without reducing agent can be stored up to 1 year at RT. Prior to adding to protein samples, add 50µl of reducing

agent 2-mercaptoethanol per 950µl of 2xLSB for a final concentration of 5% (vol/vol) 2-mercaptoethanol. Alternatively, dithiothreitol (DTT) may be used at a final concentration of 350mM (54mg ml^{-1}). With the addition of reducing agent can be stored for up to 3 months at -20°C.

- **1M Tris-HCl pH 8.7**

Mix 30.0g Tris-HCl and 98.0g Tris base into 500ml of $_{dd}H_2O$ and adjust pH to 8.7 if necessary. Bring up to a final volume of 1L with $_{dd}H_2O$. Store at RT for a maximum of 2 years.

- **1M Tris-HCl pH 6.9**

Dissolve 121.1g Tris-HCl in 500ml $_{dd}H_2O$ to dissolve, adjust pH to 6.9 using HCl, bring volume up to 1L with $_{dd}H_2O$. Store at RT for a maximum of 2 years.

- **10% (wt/vol) APS**

Dissolve 0.1g APS in 1 ml of $_{dd}H_2O$ and mix by vortexing. This is best if stored at 4°C and used within 7 days.

- **10% (wt/vol) SDS**

Dissolve 5.0g SDS powder in 30ml of $_{dd}H_2O$ over warm hot plate and take volume to 50ml using $_{dd}H_2O$. Store at RT for a maximum of 1 year. SDS is highly flammable, harmful in contact with skin and irritant to the respiratory tract and eyes. Wear a nose and mouth face mask to avoid oral and nasal contact with powder. Do not autoclave and do not adjust pH.

- **5x Stock Running Buffer** (dilute 200ml of 5x stock Running buffer into 800ml $_{dd}H_2O$ to make working 1x Running buffer)

Mix 45g Tris base, 282g glycine and 15g SDS up to 3L of $_{dd}H_2O$. Store at 4°C. Prepared 1x Running Buffer is best if used within 1 week **but** do not adjust pH.

- **SDS-PAGE Resolving Gels and 5% Stacking Gel** (for 2 mini gels)

Materials	**6.5% Resolving**	**10% Resolving**	**12.5% Resolving**	**15% Resolving**	**5% Stacking**
40% (wt/vol) acrylamide	3.1 ml	4.8 ml	6.0 ml	7.1 ml	1.2 ml
2% (wt/vol) bis-acryl	1.7 ml	2.7 ml	3.4 ml	4.0 ml	0.7 ml
1 M Tris, pH 8.7	7.5 ml	7.5 ml	7.5 ml	7.5 ml	-
1 M Tris, pH 6.9	-	-	-	-	1.5 ml
10% (wt/vol) SDS	200 µl	200 µl	200 µl	200 µl	125 µl
ddH_2O	7.4 ml	4.7 ml	2.8 ml	1.0 ml	8.9 ml
10% (wt/vol) APS	100 µl	100 µl	100 µl	100 µl	63 µl
TEMED	10 µl	10 µl	10 µl	10 µl	13 µl

Mix the top 5 reagents in a 50ml centrifuge tube or Erlenmeyer flask to obtain the gel percentage of choice. The components of the 5% stacking gel are combined in another 50ml centrifuge tube or Erlenmeyer flask. Add 10% (wt/vol) APS and TEMED to the other reagents immediately prior to pouring the gel liquid into the gel apparatus. After pouring the resolving gel, layer the top with water saturated butanol or water. Leave the gel to solidify for 45 min to 1 h. If using water saturated butanol, rinse the gel surface with $_{dd}H_2O$ five times. Add 10% (wt/vol) APS and TEMED to stacking gel mixture and pour on top of the resolving gel. Position combs and let gel solidify for 45 min to 1 h.

- **Transfer Buffer**

Combine 23.2g Tris base, 11.6g glycine, 1.48g SDS and 800ml of methanol in $_{dd}H_2O$ up to 4L. Store at RT for a maximum of 3 months.

- **Ponceau S stain**

Prepare 0.5% (wt/vol) Ponceau Red and 1% (vol/vol) glacial acetic acid in $_{dd}H_2O$. May be reused several times. Store at RT indefinitely.

- **5% (wt/vol) skim milk in PBST**

Dissolve 5.0 g of skim milk powder in 100 ml of PBST. Use immediately or store at 4°C for up to 2 days.

- **Stripping buffer**

Prepare 2% (wt/vol) SDS, 62.5mM Tris, pH 6.7 and 100 mM, 2-mercaptoethanol in PBST in the fume hood. Store at RT for a maximum of 1 year without the addition of 2-mercaptoethanol. Use immediately after the addition of 2-mercaptoethanol.

3.4 Procedure

3.4.1 Overview

Steps 1 - 9: preparing cell lysates

Steps 10 - 11: equilibrating sepharose beads

Steps 12 - 34: covalent coupling of antibodies to Protein A or G using DMP

Steps 35 - 41: preclearing protein extracts and immunoprecipitation

Steps 42 - 47: resolving GW182 and control immunoprecipitates on SDS-PAGE and wet transfer to nitrocellulose membrane

Steps 48 - 56: detecting GW182, other RISC components or mRNA degradation proteins by WB analysis

3.4.2 Detailed Procedure

Cell lysate preparation

1. Harvested approximately $1x10^9$ cells from the appropriate number of T-150cm^2 tissue culture flasks by discarding growth medium and adding 10ml of ice-cold sterile PBS (protease-free tested by supplier) to each flask. Scraped the cells with a cell scraper to detach the cells from the flask and transfered to two pre-chilled 50ml tubes on ice.
2. Centrifuged for 3 min at 196*g*, 4 ^oC.
3. Discarded supernatant and added 5ml of ice-cold sterile protease-free PBS to each 50 ml tube. Resuspended the pellets and pooled into one 15 ml tube.
4. Repeated step 2 and washed with an additional 5 ml aliquot of ice-cold sterile protease-free PBS.
5. Repeated step 2 and discarded the supernatant. Added an equal pellet volume of ice-cold sterile protease-free PBS with protease inhibitor (~850µl) to the cell pellet, resuspended the cells and placed on ice.
6. Sonicated the cells in the water bath sonicator for 80 seconds, vortexed and placed cells on ice. Repeated after 1 min.
7. Sheared the viscous lysate by passing 4 times through a syringe fitted with a 21G 1½ needle. Transferred the lysate to a 1.5ml microfuge tube.

8 Centrifuged the lysate in a tabletop microfuge for 10 min at 16,000*g*, 4 °C. Collected the supernatant into a new 1.5ml microfuge tube and placed on ice.

9 Quantitated the concentration of protein extract in the sample using the Nanodrop 1000 or NanoVue spectrophotometer. The concentration of the protein extracted was typically 12-15 μg μl^{-1}.

■ **PAUSE POINT** Stored lysate at -20°C or -70°C for short term (up to 1 week) or long term (up to 1 year) use, respectively.

Equilibration of sepharose beads

10 Prepared a 10% (wt/vol) Protein A sepharose slurry by washing 0.75 g of Protein A beads 2 times with 10 ml of sterile PBS with protease inhibitor. Equilibrated Protein A beads in 25 ml of sterile PBS containing protease inhibitor. Allowed the beads to swell overnight at 4 °C to prepare for Day 2.

11 Protein G sepharose beads were supplied in ethanol. Transferred 5 ml of beads stored in 70% (vol/vol) ethanol to a 50 ml centrifuge tube. Centrifuged the beads at 196*g* for 5 min and discarded the supernatant. Washed a total of 5 times with 20 ml of sterile PBS to remove all traces of ethanol. Prepared a 10% (wt/vol) Protein G sepharose slurry by adding 25ml of sterile PBS containing protease inhibitor to the washed Protein G beads. Allowed the beads to swell overnight at 4 °C to prepare for Day 2.

Covalent Coupling of Antibodies to Protein A or G using DMP

12 Transferred 2ml of the 10% (wt/vol) suspension of Protein A sepharose beads into two 15 ml centrifuge tubes. Added 150µl of normal human serum (NHS control) to the bead slurry in one tube and 150µl of the human serum 18033 to the other tube.

13 Transferred 2 ml of 10% (wt/vol) suspension of Protein G sepharose beads into two 15 ml centrifuge tubes. Added 500 µl of mouse monoclonal golgin 97/CDF4 antibody control to the bead slurry in one tube and 500 µl of mouse monoclonal 4B6 antibody to the other tube.

14 Allowed the antibodies to bind to the beads (from steps 12 and 13) at RT for 2 h on a rolling (nutating) mixer.

15 Added 5 ml of SBB to each antibody bound bead slurry.

16 Centrifuged for 1 min at low speed (196*g*) to pellet the beads, discarded the supernatant.

17 Washed the beads once using 5ml of SBB, centrifuged as in step 16 and discarded the supernatant.

18 To determine if the coupling procedure was successful, resuspended the beads (approximately 200 µl packed bead volume) in 200 µl of SBB to achieve a 50% bead suspension. Removed a 10 µl aliquot of beads and labelled as "Before Sample". Added 10 µl of 2x LSB to this aliquot, mixed and stored at -20 °C until the coupling procedure was complete.

19 Centrifuged the remaining 50% bead suspension as in step 16 and discarded the supernatant.

20 Dissolved solid DMP in SBB and added 5ml to each 15ml tube of beads. DMP was prepared in SBB immediately before use because of its instability in solution.

21 Mixed the beads by placing 15 ml tubes on a rolling (nutating) mixer for 1 h at RT.

22 Centrifuged for 1 min at 196*g* to pellet the beads and discarded the supernatant.

23 Added 1 ml of 0.2 M ethanolamine, pH 8.0 and mixed gently.

24 Repeated Step 22.

25 Repeated Steps 23 and 24.

26 Added 5 ml of ethanolamine and incubated at RT for 2 h on a rolling (nutating) mixer.

27 Centrifuged for 1 min at 196*g* to pellet the beads and discarded the supernatant.

28 Added 2 ml of sterile PBS, mixed gently.

29 Centrifuged for 1 min at 196*g* and discarded the supernatant.

30 Repeated Steps 28 and 29.

31 Resuspended the beads (approximately 200 µl packed bead volume) in 200 µl of sterile PBS to achieve a 50% bead suspension. Removed a 10 µl aliquot of beads and labelled as "After Sample". Added 10 µl of 2x LSB to this aliquot, mixed and stored at -20 °C.

32 Using the remaining 50% bead solution repeated step 29.

33 Added 1 ml of sterile PBS with protease inhibitor to each 15 ml tube to achieve a 20% suspension of beads.

■ **PAUSE POINT** Stored beads at 4 °C for up to 1 year. For long term storage added 0.05% (wt/vol) sodium azide to prevent bacterial contamination. After storage in

sodium azide, the beads were washed three times with sterile PBS and resuspended in sterile PBS with protease inhibitor prior to use.

34 Checked the success of the antibody coupling to the beads by analyzing the "Before" and "After" samples on 10% SDS-PAGE (see Reagent Setup). Boiled the samples at 95°C for 5 min and loaded carefully into wells along with a protein ladder of interest. Separated the proteins with 120V until the blue bands migrated to the bottom of the gel. Stained the gel with Colloidal Blue Staining Kit as per the manufacturer's instructions and left in $_{dd}H_2O$ overnight to destain the background (see Figure 3.3 for an example of successful covalent coupling of antibodies to sepharose beads).

Pre-clearing protein extracts and immunoprecipitation

35 Thawed the protein extract from Day 1 on ice and divided into two 1.5ml microcentrifuge tubes (200 µl to each tube). Labelled tubes "Protein A extract" and "Protein G extract". Saved ~50 µl of protein extract to use as a "no IP extract control" on Day 4. Protein extracts have a protein concentration of approximately 12 µg μl^{-1}, therefore each tube of 400 µl contained 2400 µg of protein.

36 To pre-clear the extract added 50 µl of 10% Protein A sepharose beads in sterile PBS with protease inhibitors (prepared in Step 10) to "Protein A extract" and 50 µl of 10% Protein G sepharose beads in sterile PBS with protease inhibitors (prepared in Step 11) to "Protein G extract". Incubated on a rotator for 30 min up to 1 h, 4 °C. Alternatively, incubated on a rotator at RT for 5 to 10 min.

37 Centrifuged for 1 min at 82*g* with a microcentrifuge and removed the pre-cleared extract into a clean 1.5 ml tube to use for immunoprecipitation (IP).

38 For IP combined 100 µl of the 20% suspension of antibody-coupled Protein A or G Sepharose beads (prepared in Step 33; NHS, 18033, golgin 97 and 4B6) with 500µl NET2F buffer of choice and 200 µl of pre-cleared protein extract from step 37 (approximately 1200 µg) and incubated for 2 h at 4 °C on a rotator. While waiting for the IP incubation, prepared protein SDS-PAGE gels for Step 42.

39 Centrifuged for 1 min at 82*g* to collect the beads and discarded the supernatant.

40 Washed the beads with 1 ml of ice cold NET2F by rotating the tubes for 5 min, 4°C. Centrifuged for 1 min at 82*g* to collect the beads and discarded the supernatant. Washed the beads a total of five times. If using a NET2F buffer with a high salt concentration (i.e., 500 mM), washed four times with the same NET2F buffer and washed an additional two times with a NET2F buffer that contained a lower salt concentration (i.e., 150 mM). IPs that are carried out and washed with higher salt concentrations will alter the expected protein migration.

41 After the last wash, pelleted the beads by centrifugation at 82*g* and discarded the supernatant. Added an equal volume of 2x LSB to the bead volume (~20-25 µl).

■ **PAUSE POINT** Stored IPs with 2x LSB at -20 °C overnight or proceeded right away to SDS-PAGE described on Day 4. Pre-prepared gels could be stored overnight at 4°C wrapped in moist paper towel and saran wrap.

Resolving GW182 and control immunoprecipitates on SDS-PAGE and wet transfer to nitrocellulose membrane

42 Prepared the gel percentage of choice during the 2 h IP incubation in Step 38, set up electrophoresis apparatus and filled with cold Running Buffer.

43 Based on the protein concentration of the extract determined in Step 9 diluted the "no IP extract control" (from Step 35) with PBS to load between 30-40 µg of protein into gel wells beside the IP samples from Step 41. Added an equal volume of 2x LSB.

44 Boiled the "no IP extract control" and the four IP samples for 5 min at 95 °C and loaded carefully into wells along with a protein ladder of choice.

45 Inserted electrodes into power supply and set the gel to run at 120V (increase to 150V after 15 min) at RT or 4 °C for desired time. If interested in examining high molecular weight proteins such as GW182 and TNGW1, run the 6.5% gel for at least 3 h until the 75 kDa ladder band is at the bottom of the gel.

46 While the protein samples were resolving, set up the wet transfer according to the manufacturer's for overnight transfer. Removed the gels from the electrophoresis apparatus carefully and placed in a dish with Transfer buffer.

47 Transferred the proteins from the SDS-PAGE gel onto a nitrocellulose membrane at 25 V in a wet transfer apparatus overnight (approximately 14 to 18 h) at 4°C.

Detecting GW182, other RISC components or mRNA degradation proteins by Western blot (WB) analysis

48 Removed the membrane from the overnight wet transfer and washed briefly in $_{dd}H_2O$. Stained membranes briefly (~1 min) with Ponceau S stain on a rocking platform shaker and destained with quick washes with $_{dd}H_2O$ until proteins bands were pink and the background was nearly white. Dried the membrane at RT on filter paper. Labelled the membrane as needed.

■ **PAUSE POINT** Stored the membrane at -20 °C until required between 2 sheets of filter paper and wrapped in tin foil OR proceeded directly with WB.

49 Blocked the nitrocellulose membrane for 1 h at RT in 5% (wt/vol) non-fat milk in PBST.

50 Overlayed the membrane with the primary antibody of choice at the appropriate dilution in 5% (wt/vol) milk/PBST for 1 h at RT. Recommended dilutions for WB using the same antibodies used in the IP included 4B6 (1:2 up to 1:10), 18033 (1:1000), NHS (1:500) and golgin 97 (1:200).

51 Washed the membrane with PBST three times, 10 min each on a rocking platform shaker.

52 Overlayed the membrane with secondary horseradish peroxidase (HRP)-conjugated antibodies of choice at their appropriate dilution in 5% (wt/vol) milk/PBST for 1 h at RT. Although this may vary from laboratory to laboratory, suggested dilutions for secondary HRP antibodies (see Reagents) are goat anti-human (1:20,000) and goat anti-mouse (1:2000).

53 Repeated Step 51.

54 Detected bound antibody using ECL reagents (mixed in a 1:1 ratio) for 1 min. Removed excess ECL reagent and placed in film cassette.

55 In the dark room, exposed the film to the membrane for the desired length of time (start at 1 min up to a maximum of 15 min depending upon the type of film used). Developed in an automated film developer or in developing reagents (fixer and developer).

56 To re-use membranes, washed them with three changes of PBST for 10 min each. Stripped antibodies from antigens using stripping buffer (see Reagent Setup) for 45 min at 50 °C to allow re-probing using different antibodies in further WB analysis. Washed three times for 10 min with PBST and stored in fresh PBST at 4 °C.

3.4.3 Troubleshooting

Troubleshooting issues are found in Table 3.1.

Table 3.1 Troubleshooting table.

Step	Problem	Possible reason(s)	Suggested solution(s)
9	No protein detected by BCA protein assay or Nanodrop after the cell lysis procedure	Cell lysis conditions are not strong enough to disrupt the cells	Use a lysis buffer that includes a detergent. Detergents may include 0.5% Triton X-100 or 0.3–0.5% NP-40
34 and 55	Heavy (50 kDa) and light (25 kDa) chains appear in gel stained with Colloidal Blue (Step 34) and on WB (Step 55) after coupling with DMP	Cross-linking of antibody to Protein A or G was not effective	Verify that the pH of DMP is between 8 and 9 before and after addition to beads as cross-linking efficiency is greatly reduced outside this pH range
			Ensure that DMP is prepared in SBB immediately before use because of its instability in solution
48	Protein did not transfer from gel to membrane	Transfer not set up with gel and membrane positioned correctly	Proteins are negatively charged. Ensure correct gel–nitrocellulose orientation in the transfer cassette to allow migration of proteins from gel to nitrocellulose
		Voltage or time not sufficient for proteins to transfer	Increase the voltage from 25 to 30 V overnight (14 h) and increase the voltage in the morning to 70 V for an additional 30 min to ensure that high molecular weight proteins have transferred. Transfer efficiency can be monitored by examining the molecular weight standard
		Transfer method may have to be changed	If using a wet transfer method, switch to a semidry transfer method or vice versa
		Membrane type may have to be changed	Switch from nitrocellulose membranes to PVDF membranes or vice versa
55	Protein(s) are not immunoprecipitated from the cell lysate	Antibody does not immunoprecipitate the protein of interest	Antibody may not work for IP
			Obtain an antibody that has been shown to immunoprecipitate the protein of interest

Step	Problem	Possible reason(s)	Suggested solution(s)
		Interactions between antibodies and proteins were disrupted during IP or wash steps	Use a less stringent IP buffer, i.e., with less salt, less detergent or less EDTA
	Nonspecific proteins are immunoprecipitated from the total cell extract after the IP step	Antibodies bound nonspecifically to other proteins	Decrease the concentration of the primary antibody used. Alternatively, use a different antibody, perhaps a monoclonal antibody. Under certain conditions, a monoclonal antibody may bind a variety of epitopes on unrelated targets that bear similar linear or conformational domains
		IP and wash steps did not disrupt nonspecific interactions	Increase the stringency of the IP buffer, i.e., add more salt and gradually increase the number of detergents. Increase the number of wash steps or prolong washes
	Protein bands are too dark on WB	Secondary antibodies may have expired or not stored correctly	Purchase new secondary antibodies
		Secondary antibodies may be too concentrated	Dilute the secondary antibody
		Film may be overexposed	Expose film for less time. Usually, exposures are optimal between 1 and 10 min. However, WBs with human antibodies usually require less exposure (<1 min)
	Protein bands are too light on WB	Secondary antibodies may have expired or not stored correctly	Purchase new secondary antibodies
		Secondary antibodies are not concentrated enough	Decrease the dilution of the antibody
		Film may be underexposed	Expose film for more time. Some WBs may require exposure times of up to 10 min

3.5 Results

The yield of protein depended upon the volume of lysis buffer, cell type used and the growth pattern of the cell line. In general, approximately $1x10^9$ to $1x10^{11}$ cells were harvested to yield 12 – 20 μg of protein. Prior to IP, the success of the coupling procedure was examined by resolving "Before" coupling and "After" coupling antibody-bead samples in 10% SDS-PAGE (Figure 3.3). As expected, the antibody light and heavy chains were visible on the gel in the "Before" sample, but not in the "After" sample as the covalently coupled antibodies remain bound to the beads after boiling in 2x LSB (Figure 3.3).

If the protein of interest is associated with GWB, optimal results would appear as clean, sharp bands in the 4B6 and 18033 IP lanes with no bands present in the golgin 97, NHS and IC6 IP control lanes. Cell lysate extracts with no IP served as a control to ensure that the antibody recognizing the protein of interest was working properly by WB analysis (Figure 3.2, panel d, extract lanes). Figure 3.2 shows a variety of typical IP-WBs to examine the proteins associated with GWB. Panel a showed the detection of the 182 kDa GW182 by WB with monoclonal antibody 4B6 in the 18033 and 4B6 IPs but not in the control IPs (NHS, IC6, and golgin 97). This showed that commercially available 4B6 can be used effectively to IP GW182 and detect it by WB. The additional lower molecular weight bands observed with the 4B6 IP (Figure 3.2, panel a) were unexplained but may be related to the observation that the epitope bound by 4B6 (Eystathioy et al., 2003a) is not an epitope bound by human sera tested to date (Eystathioy et al., 2003b). Panel b showed the detection of GW182 at 182 kDa by WB with 18033 serum (contains autoantibodies directed to GWB components GW182,

hAgo2 and Ge-1) in the 18033 IP but not in the control NHS IP. This confirmed that 18033 anti-serum contains GW182 antibodies. Panel c showed the detection of hAgo2 (the catalytic effector protein of the RISC) at ~95 kDa by WB analysis in GW182 IPs (18033 and 4B6) but not in the control IPs (NHS, IC6, golgin 97). This confirmed previous observations that hAgo2 is associated with GW182 (Jakymiw et al., 2005;Liu et al., 2005a;Liu et al., 2005b;Pillai et al., 2005;Rehwinkel et al., 2005;Sen and Blau, 2005;Eulalio et al., 2008). The apparent enrichment of hAgo2 in the 18033 IP lane as compared to the 4B6 IP lane is due to the high titre of hAgo2 antibodies in the 18033 serum. Panel d showed that GWB contain proteins GW182, hAgo2, XRN1 (exonuclease involved in 5'→3' mRNA degradation) and Dicer (double-stranded RNA-specific endonuclease involved in RNAi). GW182 and hAgo2 were enriched in the 18033 IP as compared to the cellular extract (4B6 and hAgo2 WB) whereas XRN1 and Dicer were enriched in the cellular extract as compared to the 18033 IPs (XRN1 and Dicer WB). As expected, control golgin 97 (97 kDa) was present in the cellular extract but not in the 18033 IP. As indicated, control NHS was not expected to react with 18033 IP or the cellular extract. All cell extracts contained 40 μg of protein. Panels a and b were run on 10% SDS-PAGE gels and Panels c and d were run on 6.5% SDS-PAGE gels to show that a lower percentage gel increases the separation of high molecular weight proteins. Images in Figure 3.2 were compiled in Adobe PhotoShop (version 7.0) and were the result of four separate experiments. IP buffer for Panels a and b contained no detergent and for Panels c and d contained 0.3% NP-40 detergent. Antibodies used are as described in Moser *et al.* (Moser et al., 2007).

3.6 Discussion

The optimized IP-WB protocol described in this study differed from previously published reports (Moser et al., 2007;Li et al., 2008) that used 18033 human serum as the antibody of choice for the IP of GW182 and GWB-associated proteins. Instead, a mouse monoclonal antibody generated to recombinant GW182 protein (4B6 clone) was shown to be an effective and specific antibody for the immunoprecipitation of GW182-specific binding proteins (Figure 3.2). Although the 4B6 antibody was specific for GW182 and gave good results in Figure 3.2, but our results show that it was not necessarily as powerful a probe as the human 18033 serum which contains a high titre of GW182 antibodies. A key problem that remains with the mouse monoclonal 4B6 antibody is its intrinsic low titre of GW182 antibody. Given these limitations, this protocol was the first detailed method specifically optimized for the biochemical probe of GW182 and GWB-associated protein complex. As such, it built upon the knowledge gained from previous studies (Moser et al., 2007;Li et al., 2008) in astrocytoma cells and HeLa cells and discussed key considerations, optimizing techniques and troubleshooting advice that would aid other scientists in their research of GW/P bodies.

Of importance, this protocol could likely be adapted and modified to detect other RNA binding proteins and mRNA complexes that can lead to a further understanding of the role of GWB components in RNA interference (Jakymiw et al., 2007), mRNA stabilization and transport (Moser et al., 2007;Eulalio et al., 2007) and cell stress responses (Kedersha et al., 2005). These analyses include quantitative reverse-transcription polymerase chain reaction (qkRT-PCR) that examine interactions of RNA binding proteins with their cognate mRNAs (Zeng et al., 2006), or cDNA arrays that

examine large scale RNA binding protein mRNAs (Tenenbaum et al., 2000). In addition, this protocol has been adapted to identify mRNAs and miRNAs associated with GW182 in miRNA microarrays as when total RNA was extracted from IPs and analyzed in a protocol that employed a monoclonal Ago2 antibody to identify the associated miRNAs by qkRT-PCR (Ikeda et al., 2006). This protocol has also been used to IP the total RNA associated with the RISC using the 18033 serum for subsequent gene expression and miRNA microarray analysis (Chapter Five).

Chapter Four: **Markers of mRNA stabilization and degradation, and RNAi within astrocytoma and astrocyte GW bodies***

* This work has been published and used with permission: Moser JJ, Eystathioy T, Chan EKL, Fritzler MJ. Markers of mRNA stabilization and degradation, and RNAi within astrocytoma GW bodies. Journal of Neuroscience Research 85 (16): 3619-3631, 2007. PMID: 17663465

4.1 Introduction

GW bodies (GWB) are unique cytoplasmic structures that contain the mRNA binding protein GW182 and other proteins involved in mRNA processing pathways. The rationale for this study arose from clinical studies which indicated that 33% of patients with GWB autoantibodies have a motor/sensory neuropathy and/or ataxia. Since GWB were shown to be involved in mRNA processing in HeLa and several other tissue culture cells, it was expected that an elucidation of the protein constituents of GWB in astrocytoma cells would shed light on the function of GWB within astrocytes and perhaps provide clues to the pathogenesis of the neurological diseases associated with autoantibodies directed to these structures.

Our indirect immunofluorescence (IIF) studies of mouse astrocytes and human U-87 glioblastoma/astrocytoma cells produced four key observations: 1) GWB are present in astrocyte/astrocytoma cell bodies and cytoplasmic projections, 2) astrocyte/astrocytoma GWB contain proteins involved in 5'$\rightarrow$3' mRNA degradation and RNAi, 3) the miRNA processing enzyme, Dicer is localized in close proximity to GWB in astrocytoma cells, and 4) astrocyte/astrocytoma GWB contain varying percentages of the mRNA binding/stabilization/transport proteins SYNCRIP, hnRNPA1, Staufen, FMRP and HuR. By quantitation of GWB overlap with other foci, we found that astrocytoma GWB exhibit complex heterogeneity with combinations of LSm4 and XRN1 as well as Ago2 and Dicer, key proteins involved in mRNA degradation and RNA interference respectively. GWB subsets contained the mRNA transport and stabilization proteins SYNCRIP, hnRNPA1 and FMRP, not previously described as part of the GWB complex. Using the optimized Immunoprecipitation (IP)-Western blot (WB) protocol in

Chapter Three and the exact IP-WB method as outlined in Chapter Two, IP of astrocytoma GWB suggested that Dicer, hDcp, LSm4, XRN1, SYNCRIP and FMRP form a multiprotein complex. GWB are likely involved in a number of regulatory mRNA pathways in astrocytes and astrocytoma cells.

4.2 Results

4.2.1 GWB are present in the cell body and cytoplasmic projections of astrocytes and astrocytoma cells

Mouse hippocampal cell culture contained mixed populations of both neurons and macroglia (astrocytes and oligodendrocytes), however the phenotypic differences between astrocytes and neurons was readily apparent from the phase-contrast image (Figure 4.1A). These cellular phenotypes were confirmed by IIF staining using cell type specific markers: GFAP to mark astrocytes (Figure 4.1B) and neuron specific β-III tubulin to mark neurons (Figure 4.1 C). Primary mouse astrocytes marked by GFAP were found to contain GWB as identified by staining with human anti-GWB serum (Figure 4.1D).

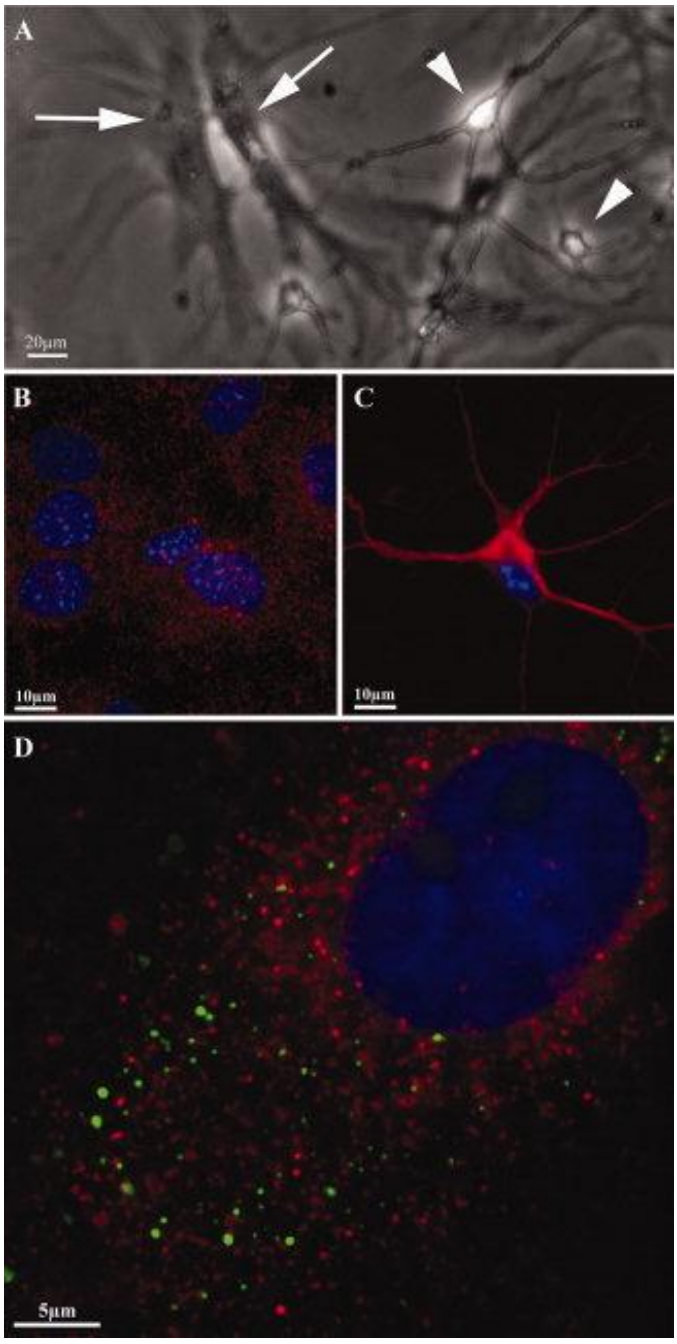

Figure 4.1: IIF analysis of mouse hippocampal cell culture between 14 and 18 days *in vitro* shows that GWB are present in astrocytes. A phase-contrast image of primary mouse hippocampal cell culture shows the distinct morphological differences between astrocytes (arrow) and neurons (arrowheads) (panel A). These apparent cell phenotypes were confirmed by IIF staining using mouse anti-glial fibrillary acidic protein (GFAP; 1/200; red) to mark astrocytes (panel B) and rabbit anti-neuron specific beta III tubulin (1/400; red) to mark neurons (panel C). To confirm that GWB were present in primary astrocytes, double IIF staining of GWB using human anti-GWB serum (green) is shown in an astrocyte as marked by GFAP (red) (panel D).

Human U-87 glioblastoma/astrocytoma cells were used as a model system for this study and were confirmed to have an astrocyte phenotype using the astrocyte marker, GFAP (data not shown) (Korzhevskii et al., 2005). U-87 glioblastoma/astrocytoma cellular morphology was captured by differential interference contrast (DIC) microscopy (Figure 4.2A), while GWB immunofluorescence staining of the same cells showed that GWB were located in the astrocytoma cell bodies and along the cytoplasmic projections (Figure 4.2B). GWB were localized to regions of the cells where cytoplasmic processes interact (Figure 4.2 C-E) and closer examination showed that GWB of varying size were distributed along the length of cell processes (Figure 4.2B, F). GWB were marked by either human polyclonal serum or mouse monoclonal anti-GW182 antibodies, thus both human and murine reagents were considered effective markers for GWB in astrocytes and astrocytoma cells (Figure 4.2 C-F). Moderate, but not complete, colocalization was observed between the mouse monoclonal antibodies to GW182 and the human polyclonal antibodies to GWB. This is explained by previous studies showing that human GWB polyclonal antibodies are polyspecific and react with a number of GWB protein components such as GW182 (Eystathioy et al., 2003a), GW2 (unpublished data) (Meister et al., 2005), Ago2 (Jakymiw et al., 2006), and Ge-1/Hedls (Bloch et al., 2006;Fenger-Gron et al., 2005;Yu et al., 2005).

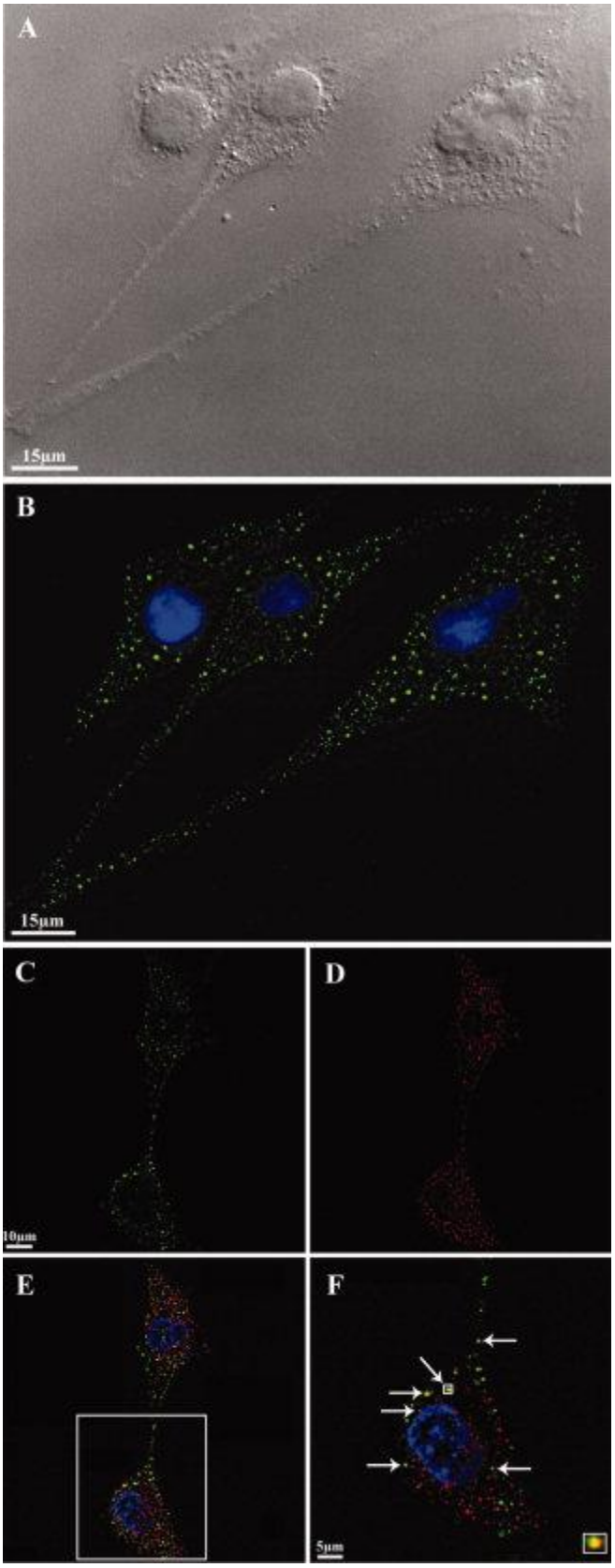

Figure 4.2: IIF analysis of human U-87 glioblastoma/astrocytoma cells shows that both human and murine antibodies are effective markers for GWB.

U-87 cellular morphology was shown by differential interference contrast (DIC; A). IIF staining of the same cells in A showed that GWB (green) are located in the astrocytoma cell bodies and along the cytoplasmic projections (B; nuclei stained with DAPI). GWB were marked by human GWB polyclonal serum (green; C) and mouse monoclonal anti-GW182 antibodies (red; D). The nuclei were stained with DAPI and the images merged (E). F focuses on GWB in the cell body and along a single cytoplasmic projection, where overlap is indicated by arrows. The inset box located at bottom right in F illustrates the colocalization between the human and the mouse anti-GWB antibodies.

4.2.2 Subset of astrocytoma GWB contain proteins involved in 5'→3' mRNA degradation and RNA interference

To examine whether human astrocytoma GWB contain proteins involved in mRNA degradation and RNAi, IIF colocalization studies were performed with antibodies to LSm4 and XRN1, proteins that are involved in mRNA degradation, and to Ago2 and Dicer, proteins involved in the RNAi pathway (Figure 4.3). Colocalization of GWB with these markers was observed in the cell bodies and cytoplasmic projections (Figure 4.3, columns I and IV). Colocalization patterns of Dicer were heterogeneous in that in some cases there was complete overlap, in some partial overlap, and in others the signal was adjacent to GWB. Colocalization of LSm4 and GWB was also observed in the cell bodies and cytoplasmic projections of primary mouse astrocytes (Figure 4.4A).

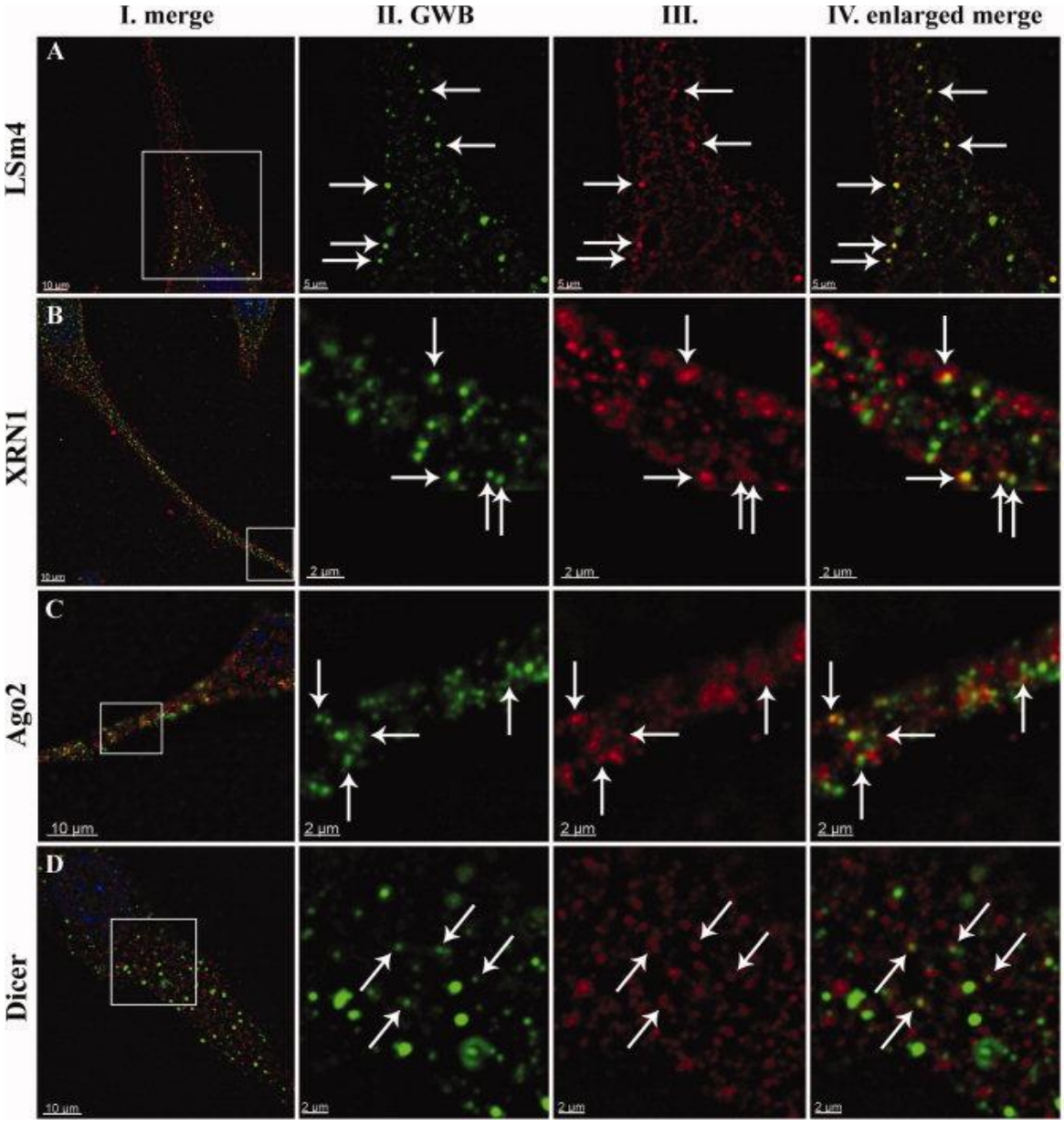

Figure 4.3: IIF analysis of U-87 glioblastoma/astrocytoma cell GWB shows that markers for 5'→3' mRNA degradation (LSm4 and XRN1) and RNA interference (Ago2 and Dicer) colocalize to GWB. Chicken anti-LSm4 antibody (1/200; A), rabbit anti-XRN1 antibody (1/500; B), mouse monoclonal to hAgo2 antibody (1/100; C), and mouse monoclonal to Dicer antibody (1/50; D) were stained with the secondary AF568 antibody (red; column III). GWB were marked with either mouse monoclonal antibodies to recombinant GW182 or human anti-GWB antibodies and were stained with the secondary AF488 antibody (green; column II). Images were merged and the nuclei stained with DAPI (column I). Merged images were enlarged in columns II-IV to focus on the GWB found in the astrocytoma cell body and processes. Arrows indicate cytoplasmic foci that colocalize.

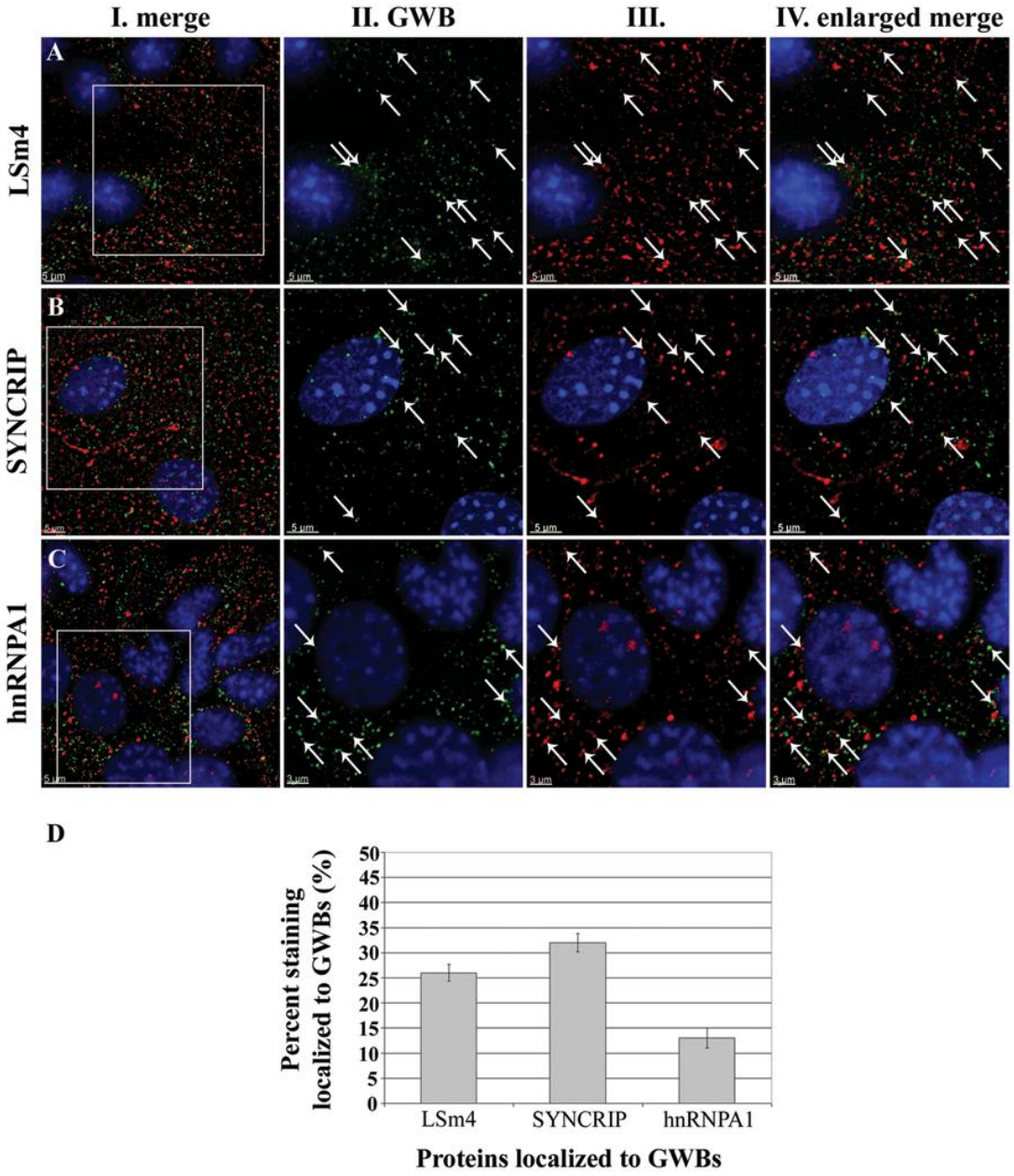

Figure 4.4: IIF analysis of GWB present in astrocytes from primary mouse hippocampal culture show that LSm4, SYNCRIP and hnRNPA1 localize to GWB. Chicken anti-LSm4 antibody (1/200, panel A), rabbit anti-SYNCRIP antibody (1/200, panel B) and human anti-hnRNPA1 antibody (1/200, panel C) were stained with the secondary AF568 antibody (red) (column I). GWB were marked with either mouse monoclonal antibodies to recombinant GW182 or human anti-GWB antibodies and were stained with the secondary AF488 antibody (green) (column II). The nuclei were stained with DAPI (columns I-III) and the images were merged (column III). Arrows indicate cytoplasmic foci that colocalized. Quantitative analysis of GWB in astrocytes shows

heterogeneity among GWB protein complexes as GWB contain varying percentages of proteins involved in mRNA degradation and mRNA transport/stabilization (panel D). Overlapping cytoplasmic foci with GWB were averaged from 3 to 10 cells observed over 3 independent experiments with each cell containing on average 100 foci. There was no statistical significant difference on percentages of overlap among the cells sampled for each respective marker: LSm4, $\chi 2$ (2)=1.869, p=0.392; SYNCRIP, $\chi 2$ (2)=1.496, p=0.475; and hnRNPA1, $\chi 2$ (2)=1.440, p=0.487. Error bars represent standard deviation from the mean percentages.

To determine the relative frequency of GWB that costained with the mRNA degradation and RNAi specific markers, we counted the GWB (>100 foci/cell) in nine to 12 astrocytoma cells observed from six independent experiments. With this approach, it was determined that approximately 22%, 25%, 27%, and 13% of GWB costained with antibodies to LSm4, XRN1, Ago2, and Dicer, respectively (Figures 4.3, 4.5). The value obtained for Dicer was derived only from those signals that demonstrated complete or partial overlap with GWB. Similar colocalization percentages were observed in counts of three to 10 primary astrocytes over three independent experiments, in which approximately 26% of GWB costained with the LSm4 antibody (Figure 4.4D). There was no statistical significant difference in the percentages of overlap among the cells sampled for each marker (see Figure 4.4 and Figure 4.5 legends for χ^2 values). The combined colocalization data indicated that there is microheterogeneity of GWB within astrocytes and astrocytoma cell bodies and cytoplasmic projections.

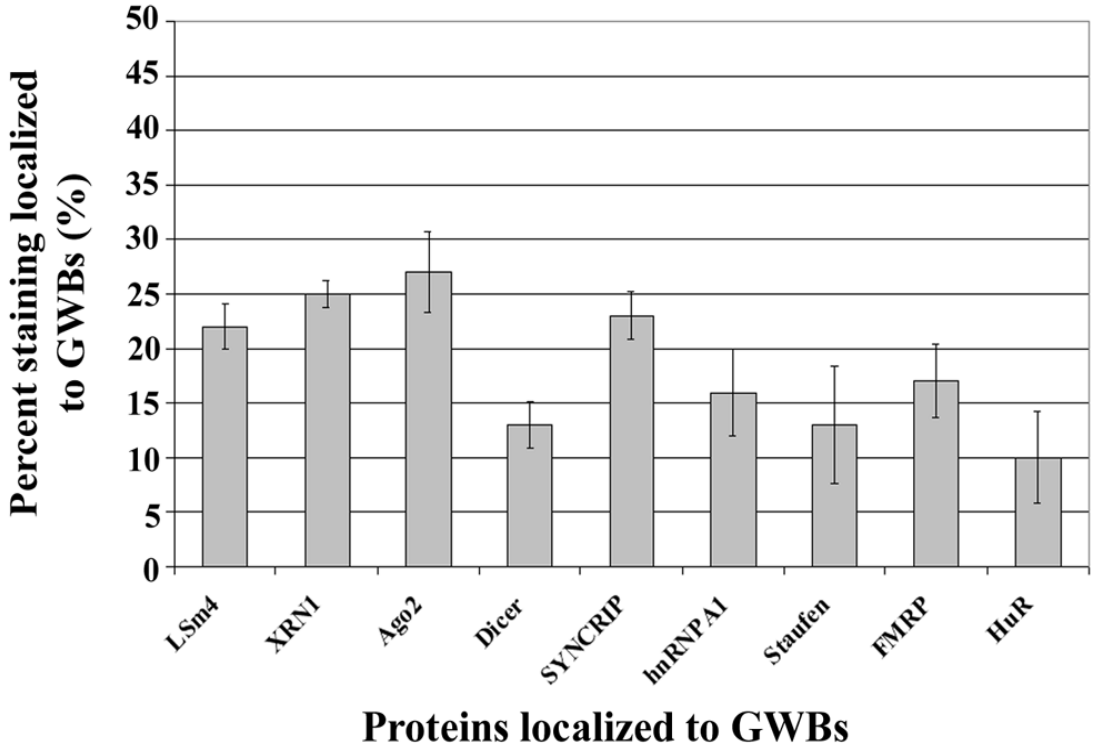

Figure 4.5: Quantitative analysis of U-87 glioblastoma/astrocytoma GWB shows heterogeneity among GWB protein complexes, in that GWB contain varying percentages of proteins involved in mRNA degradation and RNAi and mRNA transport and stabilization. Overlapping cytoplasmic foci with GWB were averaged over nine to twelve cells observed from six independent experiments with each cell containing on average 100 foci. There is no statistically significant difference in percentages of overlap for the following respective markers: LSm4, $\chi^2(5) = 1.061$, $P = 0.958$; XRN1, $\chi^2(5) = 0.388$, $P = 0.996$; Ago2, $\chi^2(5) = 3.542$, $P = 0.620$; Dicer, $\chi^2(5) = 2.269$, $P = 0.814$; SYNCRIP, $\chi^2(5) = 1.511$, $P = 0.913$; hnRNPA1, $\chi^2(5) = 6.696$, $P = 0.244$; FMRP, $\chi^2(5) = 4.071$, $P = 0.542$; and HuR $\chi^2(5) = 9.778$, $P = 0.082$. For Staufen, there is a statistical significant difference in percentage of overlap, with $\chi^2(5) = 12.957$, $P = 0.024$. Error bars represent standard deviation from the mean percentages.

4.2.3 Subset of astrocytoma GWB contain the proteins SYNCRIP, hnRNPA1, Staufen, FMRP and HuR

Several proteins that play a role in RNA stabilization, processing and transport have been identified in mRNA granules within soma and dendrites of neurons. These include SYNCRIP (synaptotagmin-binding, cytoplasmic RNA-interacting protein), hnRNPA1 (heterogeneous nuclear ribonucleoprotein A1), Staufen, FMRP (Fragile X mental retardation protein) and HuR (Hu antigen R) (Aschrafi et al., 2005;Atasoy et al., 1998;Bannai et al., 2004;Barbee et al., 2006;Belanger et al., 2003;Brennan and Steitz, 2001;Fan and Steitz, 1998;Jin et al., 2004;Keene, 1999;Kohrmann et al., 1999;Mazroui et al., 2002;Peng et al., 1998;Roegiers, 2003;Tang et al., 2001;Villacé et al., 2004). To determine whether neuronal mRNA granules have an analogous composition in astrocytoma cells, IIF colocalization studies were performed with antibodies to the aforementioned proteins and costained with the GWB antibodies. As shown in Figures 4.5 and 4.6, approximately 23% and 17% of GWB costained with antibodies to SYNCRIP and FMRP respectively. Approximately 16%, 13% and 10% of GWB costained with antibodies to hnRNPA1, Staufen and HuR respectively, however the standard deviations for these mean percentages ranged from 4% to over 5% (Figure 4.5 & Figure 4.6B, C, E). Similar colocalization percentages were observed in primary astrocytes where approximately 32% and 13% of GWB costained with antibodies to SYNCRIP and hnRNPA1 respectively (Figure 4.4, B, C and D). Staining with these markers was observed in both astrocyte and astrocytoma cell bodies and cytoplasmic projections. There was no statistical significant difference between the percentages of

overlap among the cells sampled for each marker, except for Staufen (see Figure 4.4 and 4.5 legends for respective χ^2 values).

We then set out to estimate the proportion of SYNCRIP and FMRP containing cytoplasmic granules that also contained markers of GWB components. Approximately <50% of the staining produced by SYNCRIP and FMRP, established markers of mRNA granules in neuronal cells, colocalized with markers for GWB (Figure 4.6, rows A and D). This suggested that there are different subsets of mRNA granules and that less than half of the cytoplasmic mRNA granules overlap with GWB. The presence of mRNA granule subsets was further supported by the observation that a smaller number of cytoplasmic granules marked by hnRNPA1, Staufen, and HuR also colocalized with GWB markers (Figure 4.6, rows B, C and E).

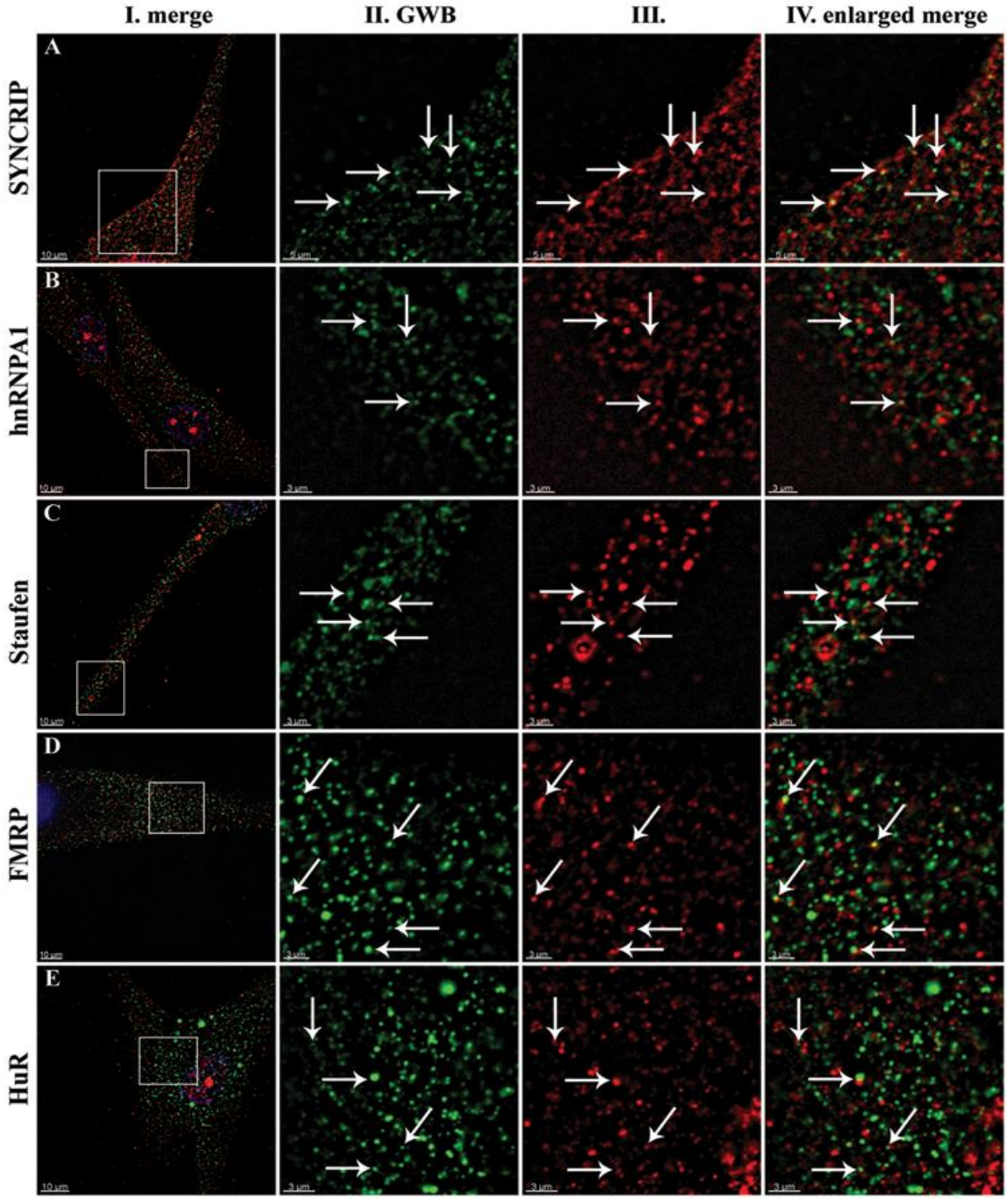

Figure 4.6: IIF analysis of U-87 glioblastoma/astrocytoma cell GWB shows that SYNCRIP and FMRP, mRNA/RNA binding proteins that are involved in mRNA transport and stabilization within neuronal mRNA granules, localize to GWB. Rabbit anti-SYNCRIP antibody (1/200, panel A), human anti-hnRNPA1 antibody (1/200, panel B), rabbit anti-Staufen antibody (1/100, panel C), mouse monoclonal to FMRP antibody (1/500, panel D) and rabbit anti-HuR antibody (1/100, panel E) were stained with the secondary AF568 antibody (red) (column III). GWB were marked with either

mouse monoclonal antibodies to recombinant GW182 or human anti-GWB antibodies, and were stained with the secondary AF488 antibody (green) (column II). Images were merged and the nuclei stained with DAPI (column I). Merged images were enlarged in columns II, III and IV to focus in on the colocalization between GWB and the mRNA granule proteins found in the astrocytoma cell body and cytoplasmic projections. Arrows indicate cytoplasmic foci that colocalize.

4.2.4 Biochemical Analysis of the GW182 protein complex

To determine whether any of the proteins that colocalized with GWB in U-87 glioblastoma/astrocytoma cells interacted with the GW182 protein, GWB protein complexes were immunoprecipitated and then probed with the appropriate antibodies for the presence of various components of mRNA degradation and RNAi pathways, and factors involved in mRNA processing/stabilization/transport. The Golgi complex protein golgin-97 was used as a control in immunoblot (IB) reactions to ensure that stringency was maintained as it is not expected to interact with GWB (Eystathioy et al., 2002a). The GW182 protein was immunoprecipitated using human anti-GWB antibodies and then probed with the mouse monoclonal 4B6 to GW182 by immunoblot to confirm the immunoprecipitation of the GW182 protein. As expected, the normal human serum did not IP the GW182 protein (Figure 4.7, 4B6 panel). As an assessment of the strength and stability of protein associations with GW182, IPs were carried out under physiological (150mM) and high (500mM) salt concentrations (Figure 4.7). Using this approach, it was noted that hDcp and Dicer were IP under both low and high salt stringency, whereas LSm4 was IP in lower amounts under high salt conditions (Figure 4.7). The molecular mass of LSm4 is ~15kDa as indicated in Figure 4.7; however, the antibody used to identify LSm was a polyclonal chicken serum that recognized multiple bands. The explanation of why polyclonal sera produce multiple bands is not completely known.

One explanation is that these additional bands represent intermolecular spreading from the LSm target antigen to other proteins of the decapping macromolecular complex. In addition, under high salt conditions there was a loss of the SYNCRIP, FMRP, and XRN1 proteins, all of which were found associated with the GW182 protein under low salt conditions. Staufen was not IP in these experimental conditions and thus does not seem to directly associate with GW182.

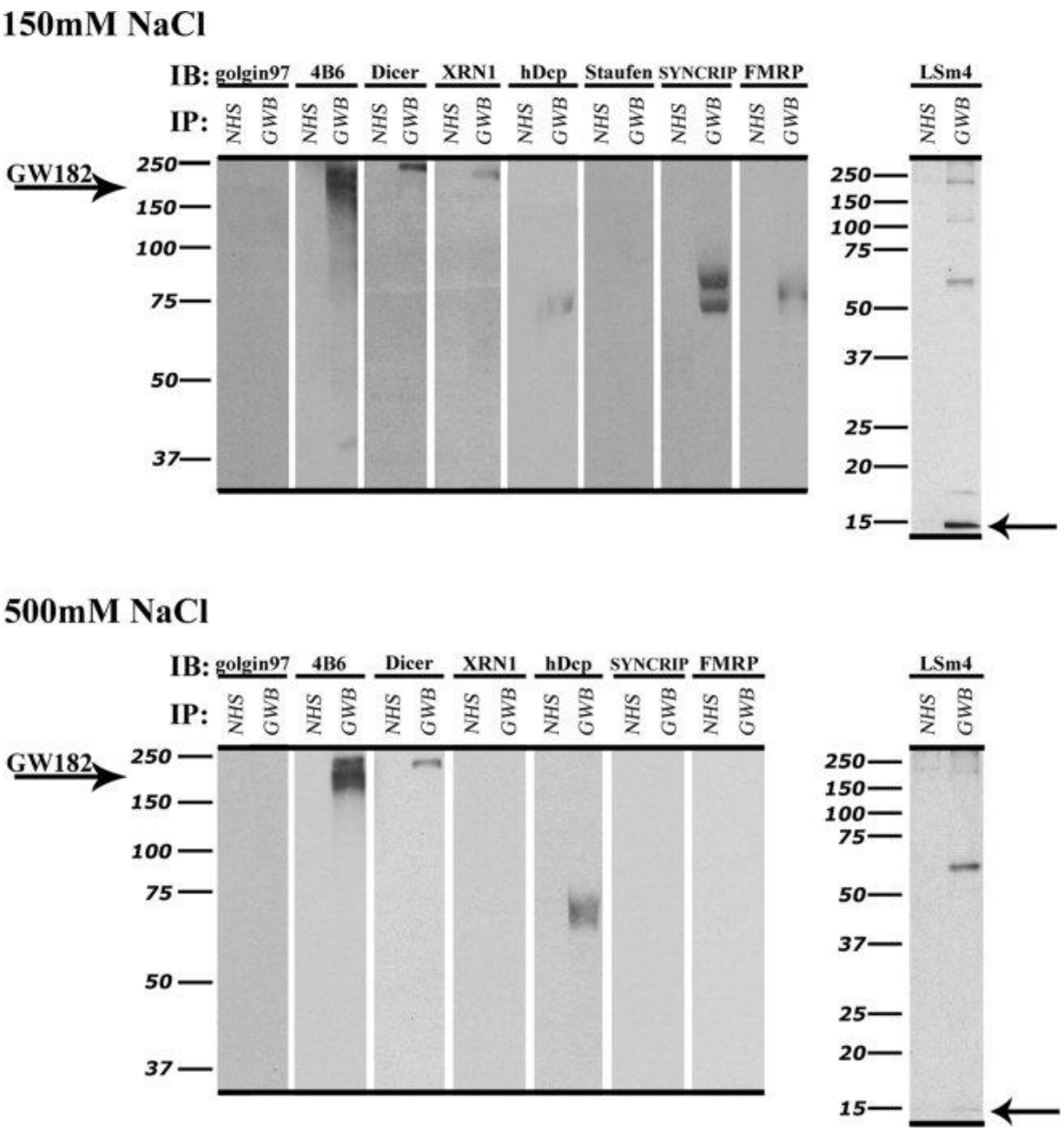

Figure 4.7: Dicer, hDcp, and LSm4 proteins remain associated with the GW182 protein in GWB, whereas XRN1 exonuclease, SYNCRIP and FMRP are released from GWB when the salt concentration of the IP buffer increases from physiological 150mM NaCl to 500mM NaCl. U-87 glioblastoma/astrocytoma lysate extracts were IP by 2 different human sera coupled to protein A-Sepharose beads: control NHS and human serum 18033 that recognizes GWB (i.e. GW182). The first IP set was analyzed by IB using a negative control mouse monoclonal to golgin 97 which produced no bands. The other IP sets were IB with mouse monoclonal 4B6 (1/50; 182 kDa), mouse monoclonal to Dicer (1/100; ~217 kDa), rabbit anti-XRN1 (1/1000; ~210 kDa), rabbit anti-hDcp (1/400; ~70 kDa), rabbit anti-SYNCRIP (1/500; ~65 & 85 kDa), mouse monoclonal FMRP (1/2000; ~80 kDa) and chicken anti-LSm4 (1/500; ~15 kDa band as

indicated by arrow). All antibodies (with the exception of Staufen) recognized their individual proteins that were IP using the GWB serum. None of the IB antibody probes recognized proteins IP by NHS. The rabbit anti-Staufen antibody (1/200) did not recognize any of the IP proteins.

4.3 Discussion

Studies to date have suggested that GWB have at least three overlapping functions (reviewed in (Eulalio et al., 2007) and (Jakymiw et al., 2007)): depots for specific subsets of mRNA (Brengues et al., 2005;Eystathioy et al., 2002a); sites for mRNA degradation (Cougot et al., 2004;Eystathioy et al., 2003c;Ingelfinger et al., 2002;Rehwinkel et al., 2005;Sheth and Parker, 2003;van Dijk et al., 2002); and sites for RNAi (Jakymiw et al., 2005;Liu et al., 2005a;Liu et al., 2005b;Pillai et al., 2005;Rehwinkel et al., 2005;Sen and Blau, 2005). This is the first report to describe GWB and the GW182 protein in association with markers of several pathways of mRNA processing in astrocytes and astrocytoma cells. Barbee *et al.* recently suggested neuronal mRNPs are functionally and structurally related to P bodies in *Drosophila* neurons (Barbee et al., 2006), but mammalian neural cells remain to be analyzed for GW proteins and their relationship to GW/P body structure and function. Casual observations indicate GWB are also present in mouse hippocampal neurons (unpublished data, see Chapter One). To date, oligodendrocyte cells have not been examined for GWB or mRNA granule localization. As discussed in Chapter One, mouse brain oligodendrocytes do not appear to contain GWB.

In astrocytes and astrocytoma cells, GWB contained some of the same proteins found previously in other mammalian cell lines. These include LSm1-7, hDcp (Andrei et al., 2005;Cougot et al., 2004;Eystathioy et al., 2003c;Fenger-Gron et al., 2005;Ingelfinger

et al., 2002;Rehwinkel et al., 2005;van Dijk et al., 2002), the XRN1 exonuclease (Bashkirov et al., 1997;Ingelfinger et al., 2002;Sheth and Parker, 2003), and the Ago2 endonuclease (Jakymiw et al., 2005;Liu et al., 2004;Pillai et al., 2005;Sen and Blau, 2005), which function in 5' $\rightarrow$ 3' mRNA degradation and RNAi respectively (summarized in Table 4.1). Although astrocytoma GWB contained these same proteins, astrocytoma GWB appeared to be more heterogeneous than GWB in other cells such as HeLa or HEp2 cells. This suggested that a subset of GWB function in mRNA degradation and RNAi within astrocytes.

The observation that Dicer was found in or adjacent to a proportion of GWB suggested that Dicer may interact with certain GWB in astrocytoma cells. In neuronal dendrites, Dicer has been reported to complex with FMRP and miRNAs which then act synergistically with Ago2 to regulate synaptogenesis (Tai and Schuman, 2006). We suggest that Dicer is found in close proximity to GWB to facilitate responses to various signals and perhaps are linked via a common "tethering/docking" protein such as Ago2, which is known to interact with GW182 (Ikeda et al., 2006;Jakymiw et al., 2005). Moreover, a study using AIN-1, a *C. elegans* protein that shares a partial sequence homology to GW182, showed that this protein interacted with protein complexes containing Dicer, Ago2 and miRNAs (Ding et al., 2005).

Table 4.1. Summary of the protein components of GWB in U-87 astrocytoma cells[*]

Protein class	Protein component	Protein function	Astrocytoma GWB		
				IP/IB	
			IIF	150	500
mRNA/RNA binding, stabilization and transport within mRNP complexes	hnRNPA1	Involved in the processing and transport of mRNA	+	ND	ND
	SYNCRIP[b]	Interacts with RNA to stabilize proteins localized to "mRNA granules" in neuronal cell bodies and dendrites	+	+	-
	Staufen[b]	Traffics mRNA to neuronal dendrites; Staufen-containing granules are essential in the localization and regulated translation of neuronal mRNAs	-	-	-
	FMRP[b]	An RNA-binding protein associated with fragile X mental retardation syndrome; involved in the transport and translational regulation of mRNAs in dendrites and localizes mRNA to "mRNA granules" or stress granules	+	+	-
	HuR[b]	A ubiquitously expressed, predominately nuclear protein involved in the shuttling and stabilization of mRNA from the nucleus to the cytoplasm, where the mRNAs are degraded, translated, or stabilized	-	ND	ND
Degradation	LSm4[a]	A component of the LSm 7-member complex that promotes 5'→3' mRNA decapping and degradation	+	+	+
	Dcp1/2[a]	Involved in mRNA decapping and other processes of 5'→3' mRNA degradation	ND	+	+
	XRN1[a]	Cytoplasmic 5'→3' exonuclease digests 5′ mRNA fragments generated from endonucleolytic cleavage by the RNA induced silencing complex (RISC)	+	+	-
RNAi	Dicer	An RNase III enzyme that cleaves long double-stranded RNA molecules into double-stranded small interfering RNA (siRNAs) duplexes of 19-21 base pairs; also cleaves premicroRNAs (premiRNAs) into microRNAs (miRNAs)	+	+	+
	Ago2[a]	Endonuclease protein is associated with RNAi function and is a key enzyme of the RISC	+	ND	ND
RNAi, mRNA binding	GW182[a]	The major autoantigen of GWB named for its apparent molecular mass of 182 kDa and the presence of multiple glycine-tryptophan repeats; the GW182 protein binds a subset of mRNAs, proteins involved in 5'→3' mRNA degradation pathways (LSm4 and Dcp), and proteins involved in RNAi (Ago2)	+	+	+

[*] Proteins marked with an

[a] have previously been published to localized to GWB in HeLa cells. Those proteins marked with a

[b] have previously been published to localize to neuronal "mRNA granules." IIF colocalization was represented as positive (+), whereas overlap with a large standard deviation equal to approximately one-half of the mean percentage was represented as negative (-). ND, no data.

Column 150 = NET2F IP buffer containing 150 mM NaCl; column 500 = NET2F IP buffer containing 500 mM NaCl. Bands present at their appropriate molecular mass were indicated as positive (+), whereas the absence of bands was indicated as negative (-).

This study is the first to report that markers of GWB colocalized with varying percentages of SYNCRIP, FMRP, hnRNPA1, Staufen and HuR in astrocytoma cells and, therefore, could potentially be similar to previously described neuronal "mRNA granules" (summarized in Table 4.1). A study using rat hippocampal neurons found that SYNCRIP, an RNA interacting and stabilizing protein, localized to mRNA granules within the cell body and the dendrites (Bannai et al., 2004). In our study, GWB were observed along the astrocyte/astrocytoma cell bodies and processes, similar to reports of the localization of SYNCRIP. FMRP is another RNA-binding protein that has been found to localize to "cytoplasmic granules" in neurons (Mazroui et al., 2002) and forms an mRNP complex that interacts with miRNA and components of the miRNA pathways including Dicer and Ago1 (Jin et al., 2004). Other studies showed that FMRP is present in polysomes as well as in neuronal "mRNA granules" and is thought to be involved in the transport and translational regulation of mRNAs within dendrites (Aschrafi et al., 2005). Large mRNA granules containing FMRP were also found to contain Staufen and other proteins involved in mRNA transport to dendrites (Kanai et al., 2004;Villacé et al., 2004). Of relevance to our study, a recent report showed that Staufen and FMRP containing neuronal RNPs are structurally and functionally related to *D. melanogaster* P bodies (Barbee et al., 2006). Our biochemical data suggested that FMRP is not associated with the GW182 protein *per se*, but the localization of FMRP to GWB may suggest multiple mRNA binding proteins complexed to their cognate mRNAs are

involved in mRNA regulation (perhaps via RNAi) within the GWB microenvironment. Another possibility stems from the results of a recent study showing that Ago2 and fragile X mental retardation-related protein (FXR1) interdependently function to upregulate the translational activation of AU-rich-elements (AREs) within the 3' UTR of mRNA, affecting mRNA stability and translation (Vasudevan and Steitz, 2007). The localization of miRNAs (Jakymiw et al., 2005; Liu et al., 2005b; Pillai et al., 2005) and ARE-binding proteins to GWB (Kedersha et al., 2005; Stoecklin et al., 2004) together with our data suggest that the observed heterogeneity of GWB within astrocyte/astrocytoma cells may be an effect of the various miRNA localized to specific GWB based on their intended target (see Chapter Five for related experiments).

The observation that SYNCRIP and FMRP localized in 17% up to 23% of astrocytoma GWB (and up to 32% in primary astrocyte GWB) suggests that a subset of GWB function in mRNA binding, transport and stabilization. A subset of GWB and the unique components of these structures (GW182 and GW2: TNRC6B/KIAA1093, (Meister et al., 2005)), may be essential in the transport, localization and regulated translation of mRNAs within astrocytes and possibly in other cells of the CNS such as neurons (for review see (Anderson and Kedersha, 2006)). An alternative interpretation is that these proteins are bound to mRNA exported from the nucleus and remain associated with mRNA that is targeted to GWB for RNAi and/or degradation.

GWB are clearly dynamic structures (Kedersha et al., 2005;Leung et al., 2006) and exist as different subsets containing various combinations of RNAi, mRNA degradation and RNA stabilization/processing/transport/storage proteins. As illustrated in Figures 4.3, 4.4, 4.5 and 4.6, a subset of GWB did not contain LSm4, XRN1, Ago2,

Dicer, SYNCRIP, hnRNPA1, Staufen, FMRP, or HuR, suggesting that more proteins associated with GWB have yet to be identified. Thus far, protein complexes containing the GW182 protein have been shown to include Ago2, Dicer, hDcp, and LSm4 but due to the dynamic nature of GWB, we hypothesize that GWB contain many more proteins that change in response to different stimuli such as stress responses (Kedersha et al., 2005;Leung et al., 2006) and cell division (Lian et al., 2006). One of these is Ge-1/Hedls (human enhancer of decapping large subunit), a 165 kDa protein that functions in mRNA decapping and was previously shown to be a component of GWB (Bloch et al., 2006;Fenger-Gron et al., 2005;Yu et al., 2005).

In summary, the data suggests that GWB function in 5' → 3' mRNA degradation, RNAi and mRNA processing/stabilization/transport. The inherent microheterogeneity of GWB within astrocytes and astrocytoma cells suggests a range of possible GWB functions depending on mRNA, protein or miRNA composition and their correlation to function. This is the first study to show that GWB are present in astrocytes and astrocytoma cells and colocalize to the mRNA granule proteins SYNCRIP and FMRP, and to a lesser extent with hnRNPA1, Staufen and HuR. The evidence for different subsets of GWB within astrocytes and astrocytoma cells reveals that GWB are not static in their protein composition or activity but could hypothetically be changing in response to signalling within these cells.

Chapter Five: **The MicroRNA and Messenger RNA Profile of the RNA-Induced Silencing Complex in Human Primary Astrocyte and Astrocytoma Cells***

* This work has been submitted for publication to PLoS ONE on May 04, 2010 (Moser JJ and Fritzler MJ. The MicroRNA and MessengerRNA Profile of the RNA-Induced Silencing Complex in Human Primary Astrocyte and Astrocytoma Cells).

5.1 Introduction

GW/P bodies are cytoplasmic ribonucleoprotein-rich foci that are involved in microRNA (miRNA)-mediated messenger RNA (mRNA) silencing and degradation. The mRNA regulatory functions within GW/P bodies are mediated by GW182 and its binding partner hAgo2 that bind miRNA within the RNA-induced silencing complex (RISC). To date there are no published reports of the profile of miRNA and mRNA targeted to the RISC or a comparison of the RISC-specific miRNA/mRNA profile differences in malignant and non-malignant cells.

Total cell RNA as well as RNA from immunoprecipitated RISC (as described in detail in Chapter Two) from malignant human U-87 astrocytoma cells and its non-malignant counterpart, primary human astrocytes were analyzed using miRNA and gene expression microarrays. The RISC mRNA and miRNA components were profiled by microarray analysis and the novel findings were fourfold: (1) miRNAs were highly enriched in astrocyte RISC compared to astrocytoma RISC, (2) astrocytoma and primary astrocyte cells each contained unique RISC miRNA profiles as compared to their respective cellular miRNA profiles, (3) miR-195, 10b, 29b, 19b, 34a and 455-3p levels were increased and the miR-181b level was decreased in U-87 astrocytoma RISC as compared to astrocyte RISC, and (4) the RISC contained decreased levels of mRNAs in primary astrocyte and U-87 astrocytoma cells. The observation that miR-34a and miR-195 levels were increased in the RISC of U-87 astrocytoma cells suggests an oncogenic role for these miRNAs. Differential regulation of mRNAs by specific miRNAs is evidenced by the observation that three miR34a-targeted mRNAs and two miR-195-targeted mRNAs appear to be downregulated while one miR-195-targeted mRNA was

upregulated. Biological pathway analysis of RISC mRNA components using Ingenuity Pathway Analysis software suggests that the RISC plays a pivotal role in malignancy and other conditions. This study points to the importance of the RISC and ultimately GW/P body composition and function in miRNA and mRNA deregulation in astrocytoma cells and possibly in other malignancies.

5.2 Results and Discussion

5.2.1 miRNAs are highly enriched in primary astrocyte RISC compared to U-87 astrocytoma RISC

MiRNA microarray analysis was undertaken to examine the spectrum of cellular miRNAs in primary human astrocytes and human U-87 astrocytoma cells and then compared them to those associated with the RISC of the respective cells. Several key observations were made from the examination of the four miRNA microarray data domains. First, comparison of U-87 astrocytoma cell and primary astrocyte global miRNA at equivalent RNA concentrations showed that the signal intensity of global miRNAs in the U-87 astrocytoma cells were generally increased compared to primary astrocytes (Figure 5.1, top and bottom left) suggesting that astrocytoma cells may have an increased number of individual miRNAs compared to the number in normal astrocytes. In addition, the global miRNA profile of astrocytoma cells was enriched in, and contained a greater variety of, miRNA than primary astrocytes. Second, comparison of global miRNA and RISC-immunoprecipitated (RISC-IP) miRNA in astrocytoma cells demonstrated that the signal intensity of the same miRNA species did not vary between

the RISC-enriched population and that of the global miRNA population (Figure 5.1, top left and right) suggesting that astrocytoma cell RISC are not as highly enriched in specific miRNAs and display the same relative signal intensity and contain many of the same miRNAs as astrocytoma cells. Third, comparison of global miRNA and RISC-IP miRNA revealed that the signal intensity and number of miRNAs of the RISC-IP miRNA was remarkably increased in primary astrocytes compared to that of the global astrocyte miRNAs (Figure 5.1, bottom left and right), suggesting that a greater number of miRNAs are enriched in primary astrocyte RISCs. Fourth, comparison of astrocytoma and astrocyte RISC-IP miRNA indicated that the number of miRNA species and the signal intensity of miRNAs present in the primary astrocyte RISC-IP were increased (Figure 5.1, right top and bottom) indicating that primary astrocyte RISC may be enriched in a relatively more diverse population of miRNAs and contain a greater number of individual miRNAs than U-87 astrocytoma RISC. These results suggest depletion or deregulation of the specific miRNA population in RISC could potentially have an important function in the malignant state.

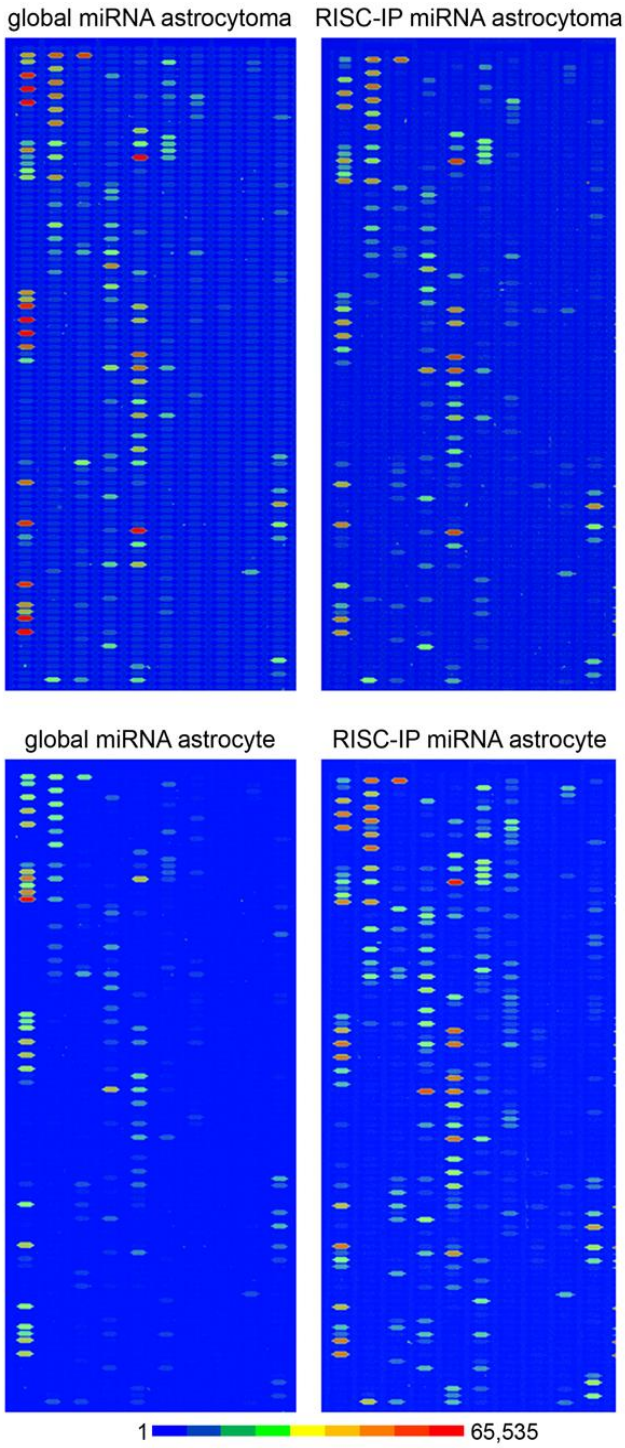

Figure 5.1: MiRNA microarray images of global and RISC-immunoprecipitated (RISC-IP) miRNA from human U-87 astrocytoma and primary human astrocyte cells. The representative chip images are displayed in pseudo colors to expand the visual dynamic range. As signal intensity increases from 1 to 65,535, the corresponding color changes from blue to green, to yellow and to red.

The signal probe intensity plot comparing the RISC-IP miRNAs to global miRNAs for U-87 astrocytoma cells and primary astrocytes showed many miRNAs that were equally expressed in cell fractions from both cell types (Figure 5.2). However, in both cell types, there was a subset of miRNAs that had higher signal intensity in RISC (Figure 5.2) and lower signal intensity in RISC (Figure 5.2). Furthermore, both cell types had their own unique miRNA signal distribution pattern indicating that each cell type had a unique RISC miRNA profile.

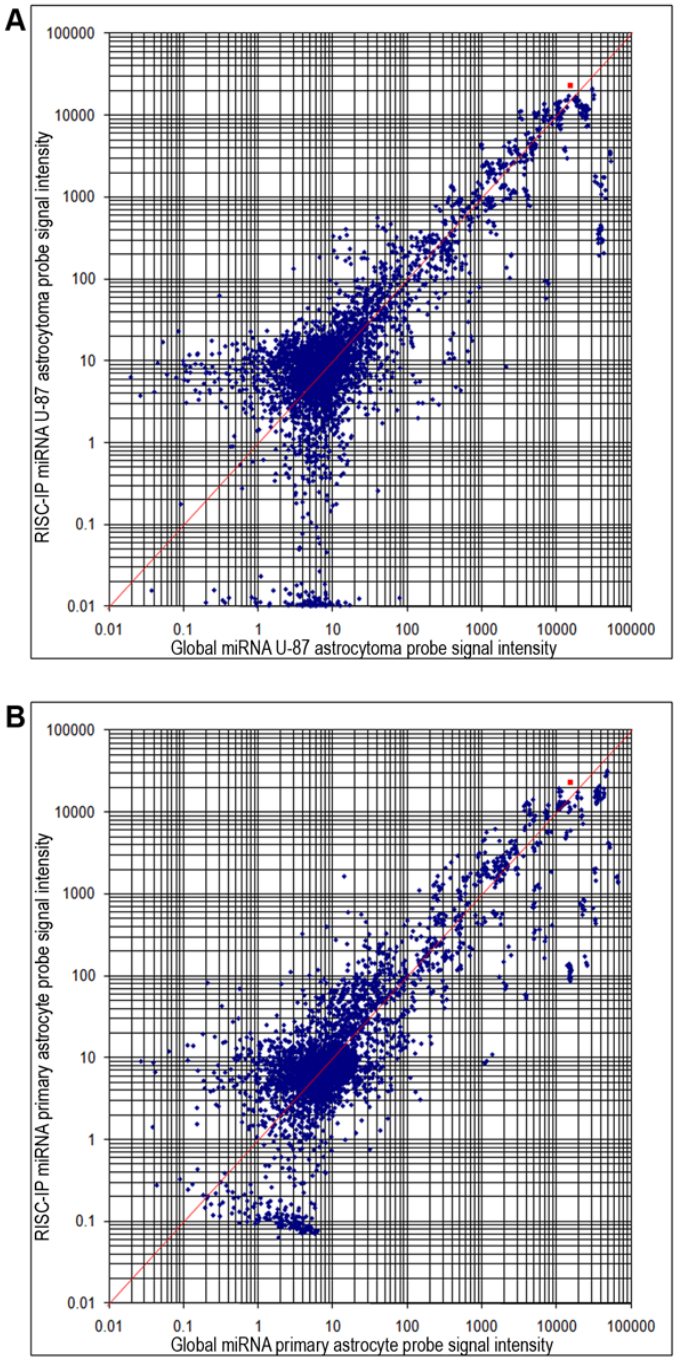

Figure 5.2: Global versus RISC-IP miRNA probe reporter signal intensity for (A) U-87 astrocytoma cells and (B) primary human astrocytes. The red line indicates a signal ratio of 1 between RISC-IP and global miRNA probe signal intensities. The miRNA probes that lie to the left of the red line indicate the miRNAs that are upregulated in the RISC-IP samples compared to the global samples. The miRNA probes that lie to the right of the red line indicate the miRNAs that are represented in the RISC-IP samples compared to the global samples.

5.2.2 RISC miRNA profile in primary human astrocytes

Primary astrocyte RISC contained a unique subset of significantly expressed ($p<0.01$) miRNAs when normalized to the expression levels of global astrocyte miRNAs (Figure 5.3). In this study, all significantly expressed miRNAs with a log2 fold change $>\pm2$ and a $p<0.01$ were regarded as miRNAs with significantly different expression. In astrocyte RISC, 13 miRNAs had a log2 fold change greater or equal to ±2 (Figure 5.3A) and of these, miR-424, miR-22, 125a-5p, 335 and 26b were increased by >2 fold change compared to global miRNA levels (Figure 5.3A). Notably, miR-424 was increased in RISC by ~5 fold. MiR-9*, 1280, 9, 720 and 1308 were all decreased in RISC with a log2 fold change below -3 and miR-455-3p, 155 and 923 were decreased between -2 and -3 fold (Figure 5.3A). Although only 13 miRNAs had a fold change $>\pm2$, many RISC-IP miRNA expression levels could still considered to be significantly different from global miRNA expression levels with $p<0.01$ (Figure 5.3B). Significant miRNA expression levels for 4 independent RISC-IP and global samples from primary astrocytes were plotted on a hierarchical clustered heatmap, illustrating that 60% of miRNAs (81 of 135) were increased while the remaining 40% (51/135) were decreased in RISC in primary astrocytes compared to the global cellular miRNA pool (Figure 5.3B).

Ingenuity Pathway Analysis (IPA) of the 13 key miRNAs with a log2 fold change $>\pm2$ in astrocyte RISC showed that these miRNAs were predominantly associated with genetic disorders and musculoskeletal disorders, however, these specific miRNAs have also been associated with inflammatory disease, cancer and reproductive system disease (Figure 5.3C, threshold set at $p<0.01$ using Fisher's exact test).

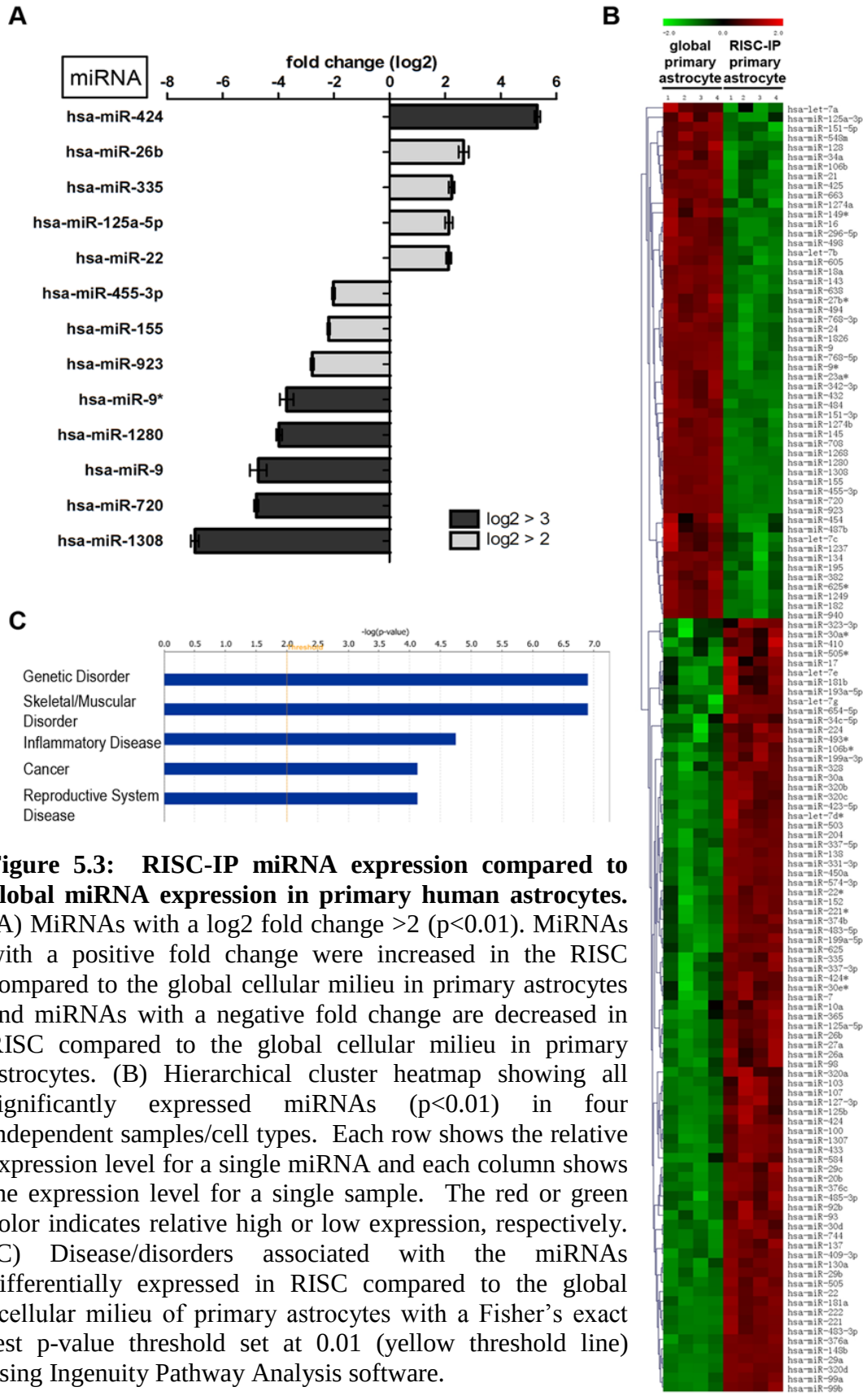

Figure 5.3: RISC-IP miRNA expression compared to global miRNA expression in primary human astrocytes. (A) MiRNAs with a log2 fold change >2 ($p<0.01$). MiRNAs with a positive fold change were increased in the RISC compared to the global cellular milieu in primary astrocytes and miRNAs with a negative fold change are decreased in RISC compared to the global cellular milieu in primary astrocytes. (B) Hierarchical cluster heatmap showing all significantly expressed miRNAs ($p<0.01$) in four independent samples/cell types. Each row shows the relative expression level for a single miRNA and each column shows the expression level for a single sample. The red or green color indicates relative high or low expression, respectively. (C) Disease/disorders associated with the miRNAs differentially expressed in RISC compared to the global ccellular milieu of primary astrocytes with a Fisher's exact test p-value threshold set at 0.01 (yellow threshold line) using Ingenuity Pathway Analysis software.

5.2.3 RISC miRNA profile in human U-87 astrocytoma cells

U-87 astrocytoma cell RISC also contained a unique subset of miRNAs when normalized to the global U-87 astrocytoma cell miRNA levels (Figure 5.4). As above, miRNAs having levels log2 fold >±2 and a $p<0.01$ were reported as miRNAs with key differences. In U-87 astrocytoma RISC, only 6 miRNAs had a log2 fold change >±2 (Figure 5.4A). Of these miRNAs, only miR-19b was increased by >±2 fold compared to global miRNA levels (Figure 5.4A). MiR-9, 29c, 768-5p and 1308 were all decreased in RISC with a log2 fold change below -3 and miR-1280 was decreased between -2 and -3 fold (Figure 5.4A). Of interest, in both U-87 astrocytoma and primary astrocyte RISC, miR-9 and miR-1308 were both decreased with the same relative log2 fold change value (Figure 5.3 and 5.4). Only 6 miRNAs had a fold change >±2, many U-87 astrocytoma RISC-IP miRNA levels were still considered to be significantly different from global miRNA levels with $p<0.01$ (Figure 5.4B). Significant miRNA levels for 4 independent RISC-IP and global samples from U-87 astrocytoma cells were plotted on a hierarchical clustered heat map and show that 52.8% of miRNAs (47 of 89) were increased in U-87 astrocytoma cells RISC as compared to the global cellular miRNA pool (Figure 5.4B). The remaining 47.2% of miRNAs (42 of 89) were decreased in U-87 astrocytoma RISC (Figure 5.4B). Of note, U-87 astrocytoma RISC contained 46 fewer miRNA species ($p<0.01$) than primary astrocyte RISC (Figure 5.3B compared to Figure 5.4B). In addition, comparison of the population of miRNAs that were increased, U-87 astrocytoma RISC contained 12.8% fewer miRNAs as compared to primary astrocyte RISC (compare Figure 5.3B and 5.4B).

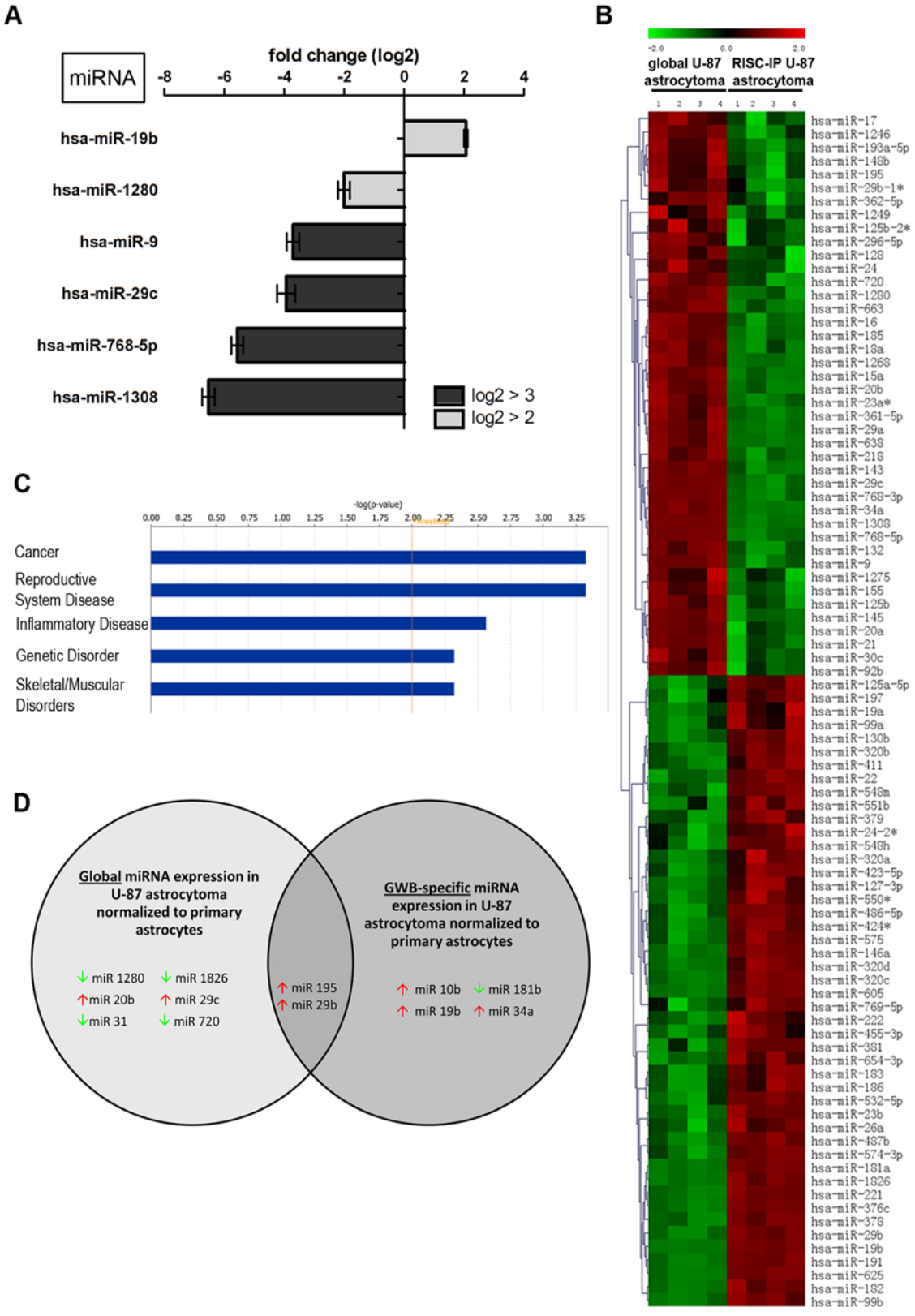
A
miRNA
fold change (log2)
-8
-6
-4
-2
0
2
4
hsa-miR-19b
hsa-miR-1280
hsa-miR-9
hsa-miR-29c
hsa-miR-768-5p
hsa-miR-1308
log2 > 3
log2 > 2
B
global U-87 astrocytoma
RISC-IP U-87 astrocytoma
hsa-miR-17
hsa-miR-1246
hsa-miR-193a-5p
hsa-miR-148b
hsa-miR-195
hsa-miR-29b-1*
hsa-miR-362-5p
hsa-miR-1249
hsa-miR-125b-2*
hsa-miR-296-5p
hsa-miR-128
hsa-miR-24
hsa-miR-720
hsa-miR-1280
hsa-miR-663
hsa-miR-16
hsa-miR-185
hsa-miR-18a
hsa-miR-1268
hsa-miR-15a
hsa-miR-20b
hsa-miR-23a*
hsa-miR-361-5p
hsa-miR-29a
hsa-miR-638
hsa-miR-218
hsa-miR-143
hsa-miR-29c
hsa-miR-768-3p
hsa-miR-34a
hsa-miR-1308
hsa-miR-768-5p
hsa-miR-132
hsa-miR-9
hsa-miR-1275
hsa-miR-155
hsa-miR-125b
hsa-miR-145
hsa-miR-20a
hsa-miR-21
hsa-miR-30c
hsa-miR-92b
hsa-miR-125a-5p
hsa-miR-197
hsa-miR-19a
hsa-miR-99a
hsa-miR-130b
hsa-miR-320b
hsa-miR-411
hsa-miR-22
hsa-miR-548m
hsa-miR-551b
hsa-miR-379
hsa-miR-24-2*
hsa-miR-548h
hsa-miR-320a
hsa-miR-423-5p
hsa-miR-127-3p
hsa-miR-550*
hsa-miR-486-5p
hsa-miR-424*
hsa-miR-575
hsa-miR-146a
hsa-miR-320d
hsa-miR-320c
hsa-miR-605
hsa-miR-769-5p
hsa-miR-222
hsa-miR-455-3p
hsa-miR-381
hsa-miR-654-3p
hsa-miR-183
hsa-miR-186
hsa-miR-532-5p
hsa-miR-23b
hsa-miR-26a
hsa-miR-487b
hsa-miR-574-3p
hsa-miR-181a
hsa-miR-1826
hsa-miR-221
hsa-miR-376c
hsa-miR-378
hsa-miR-29b
hsa-miR-19b
hsa-miR-191
hsa-miR-625
hsa-miR-182
hsa-miR-99b
C
-log(p-value)
Cancer
Reproductive System Disease
Inflammatory Disease
Genetic Disorder
Skeletal/Muscular Disorders
D
Global miRNA expression in U-87 astrocytoma normalized to primary astrocytes
miR 1280
miR 1826
miR 20b
miR 29c
miR 31
miR 720
miR 195
miR 29b
GWB-specific miRNA expression in U-87 astrocytoma normalized to primary astrocytes
miR 10b
miR 181b
miR 19b
miR 34a

Figure 5.4: RISC-IP miRNA expression compared to global miRNA expression in human U-87 astrocytoma cells. (A) MiRNAs with a log2 fold change >2 ($p<0.01$). MiRNAs with a positive fold change are increased in RISC compared to the global cellular milieu in astrocytoma cells and miRNAs with a negative fold change are decreased in RISC compared to the global cellular milieu in astrocytoma cells. (B) Hierarchical cluster heatmap showing all significantly expressed miRNAs ($p<0.01$) in four independent samples/cell type. Each row shows the relative expression level for a single miRNA and each column shows the expression level for a single sample. The red or green color indicates relative high or low expression, respectively. (C) Disease/disorders associated with the miRNAs differentially expressed in RISC compared to the global cellular milieu of U-87 astrocytoma cells with a Fisher's exact test p-value threshold set at 0.01 (yellow threshold line) using IPA software. (D) MiRNAs in RISC compared to the global cellular fraction in U-87 astrocytoma cells. U-87 astrocytoma cell miRNA expression was normalized to primary astrocytes miRNA expression. MiRNAs displayed have a log2 fold change >3. Green and red arrows indicate decreased and increased miRNA levels respectively.

IPA of the 6 key miRNAs with a log2 fold change >±2 in U-87 astrocytoma RISC showed that these miRNAs have been predominantly associated with cancer, however, these specific miRNAs have also been associated with inflammatory diseases and genetic disorders (Figure 5.4C, threshold set at $p<0.01$ using Fisher's exact test). Interestingly, U-87 astrocytoma RISC miRNAs were predominately associated with cancer (Figure 5.4C), whereas in primary astrocytes, RISC miRNAs are less associated with cancer and more with genetic disorders (Figure 5.3C). The –log (p-value) scale differs between Figures 5.3C and 5.4C due to the number of miRNAs used for IPA analysis (i.e. 13 vs 6), but functional trend analysis shows that miRNAs associated with inflammatory disease appear to be approximately the same for both U-87 astrocytoma cells and primary astrocytes (compare Figure 5.3C and 5.4C).

Upon normalization of significant ($p<0.01$) U-87 miRNA microarray values to primary astrocyte miRNA microarray values, RISC-specific miRNAs could be identified

and separated from miRNAs that were unique to the global cellular milieu (i.e. were not a part of RISC) in U-87 astrocytoma cells (Figure 5.4D). Unique to RISC in U-87 astrocytoma cells were miR10b, 19b, 34a and 181b. Of this U-87 astrocytoma RISC subset, all were increased with the exception of miR-181b which was decreased when compared to astrocytes (Figure 5.4D). MiRNAs not present in U-87 astrocytoma RISC included miR-1280, 1826, 31, 720, 20b and 29c all of which were decreased with the exception of miR-20b and 29c which were increased when compared to astrocytes (Figure 5.4D). MiR-195 and 29b were found in both U-87 astrocytoma RISC and in the cellular milieu and were both increased but with different levels (Figure 5.4D). Global miR-195 was increased with a log2 fold of 4.491, a difference of -0.977 from RISC expression. On the other hand, global miR-29b was increased by a log2 fold of 6.214 a difference of +1.580 from RISC expression, suggesting that miR-29b has a more significant regulatory role in the global cellular fraction than in the RISC.

The global and RISC-IP miRNA microarray results were subsequently validated by qkRT-PCR with miRNA normalized to the endogenous RNU6B control (Figure 5.5). A total of 18 miRNAs were examined by qkRT-PCR for global and RISC-IP miRNA in U-87 astrocytoma cells as normalized to primary astrocytes (Figure 5.5). The values of fold change cannot be directly compared between microarray and qkRT-PCR assays due to differences in calculation methods (log2 for microarray and $2^{-\Delta\Delta Ct}$ for qkRT-PCR), yet comparisons could be made based on the general trend of increased or decreased levels (Figure 5.5). For global miRNA, miR-29b, 29c, 195, 10b and 20b were increased in qkRT-PCR analyses and exhibited the same general trend as determined by microarray analysis (Figure 5.5A). The trend was not as evident for the decreased global miRNAs

where there was slightly greater variation in miR-181b, 1280 and 432 qkRT-PCR and microarray expression values; however miR-1826 levels coincided between assays (Figure 5.5A). For RISC-IP miRNA, the trend is similar for both microarray and qkRT-PCR assays (Figure 5.5B).

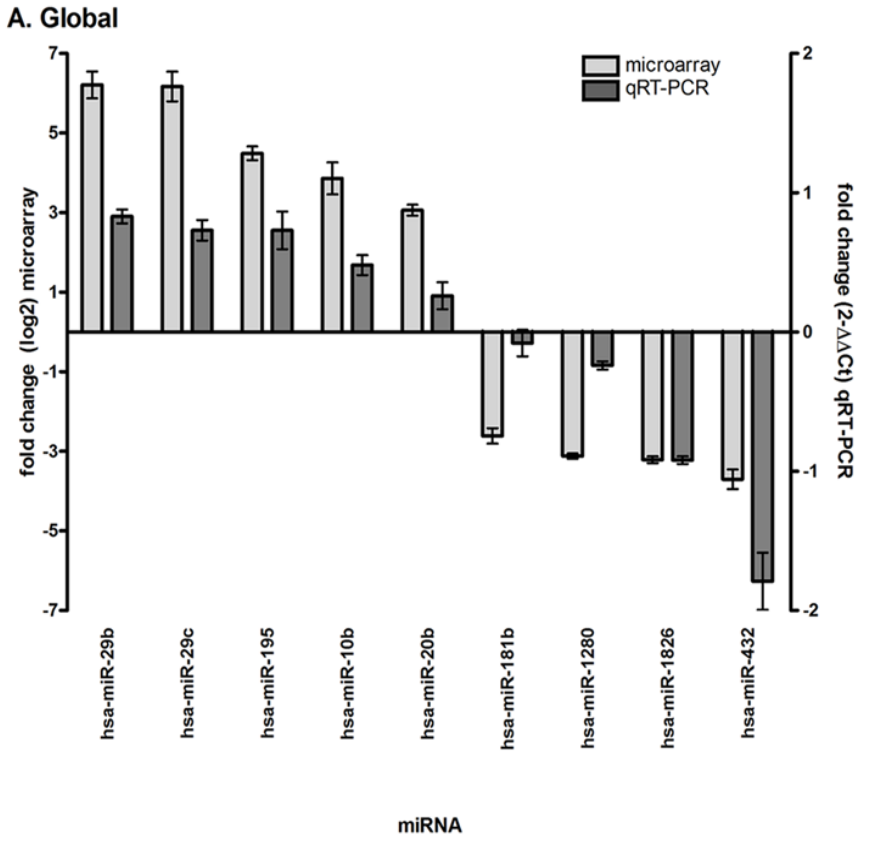
A. Global
microarray
qRT-PCR
fold change (log2) microarray
fold change (2-ΔΔCt) qRT-PCR
7
5
3
1
-1
-3
-5
-7
2
1
0
-1
-2
hsa-miR-29b
hsa-miR-29c
hsa-miR-195
hsa-miR-10b
hsa-miR-20b
hsa-miR-181b
hsa-miR-1280
hsa-miR-1826
hsa-miR-432
miRNA

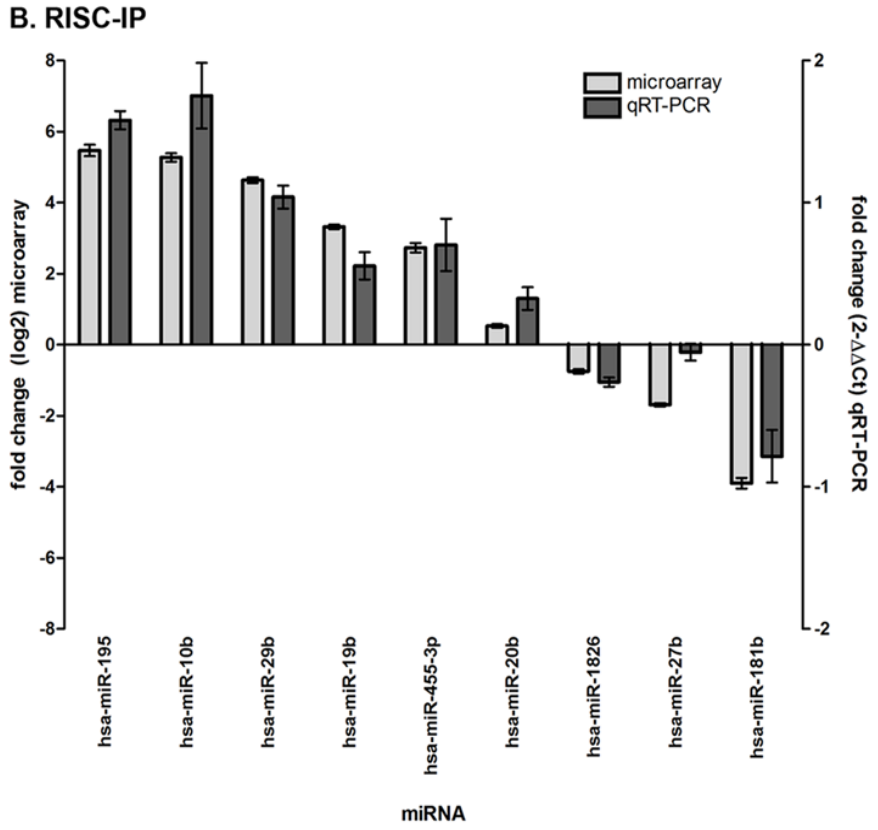
B. RISC-IP
microarray
qRT-PCR
fold change (log2) microarray
fold change (2-ΔΔCt) qRT-PCR
8
6
4
2
0
-2
-4
-6
-8
2
1
0
-1
-2
hsa-miR-195
hsa-miR-10b
hsa-miR-29b
hsa-miR-19b
hsa-miR-455-3p
hsa-miR-20b
hsa-miR-1826
hsa-miR-27b
hsa-miR-181b
miRNA

Figure 5.5: MiRNA microarray validation with qkRT-PCR analysis for (A) global miRNA and (B) RISC-specific miRNA. Nine random miRNAs were selected from the miRNA microarray datasets and examined by qkRT-PCR. Fold change from the miRNA microarray are given by log2 values (left y-axis, light grey bars). Fold change from the qkRT-PCR was determined using the $2^{-\Delta\Delta Ct}$ method and all miRNA expression values were normalized to the RNU6B endogenous control (right y-axis, dark grey bars). Error bars represent the standard deviation of the mean (SD). Note: only the general trend of up-regulation and down-regulation can be compared but the fold change (y-axis) cannot be directly compared between assays due to differences in calculation methods.

5.2.4 Specific miRNA levels are different in U-87 astrocytoma RISC compared to primary astrocyte RISC

Comparison of miRNA levels in RISC of U-87 astrocytoma and primary astrocytes by microarray also showed that RISC miRNA levels were cell type specific (Figure 5.6). As previously described, all significantly ($p<0.01$) expressed miRNAs with a log2 fold change > ±2 were denoted as miRNAs with key differences. Using cutoff, U-87 astrocytoma RISC contain a higher number of increased miRNA species compared to astrocyte RISC (Figure 5.6A). As such, miR-195, 10b, 29b, 19b, 34a and 455-3p were all increased in U-87 astrocytoma RISC as compared to primary astrocyte RISC (Figure 5.6A). MiR-181b was decreased with a log2 fold change > ±2 in U-87 astrocytoma RISC as compared to primary astrocyte RISC (Figure 5.6A). Notably, 6 RISC-IP miRNAs had a significant log2 fold change > ±3 (Figure 5.6A, Table 5.1).

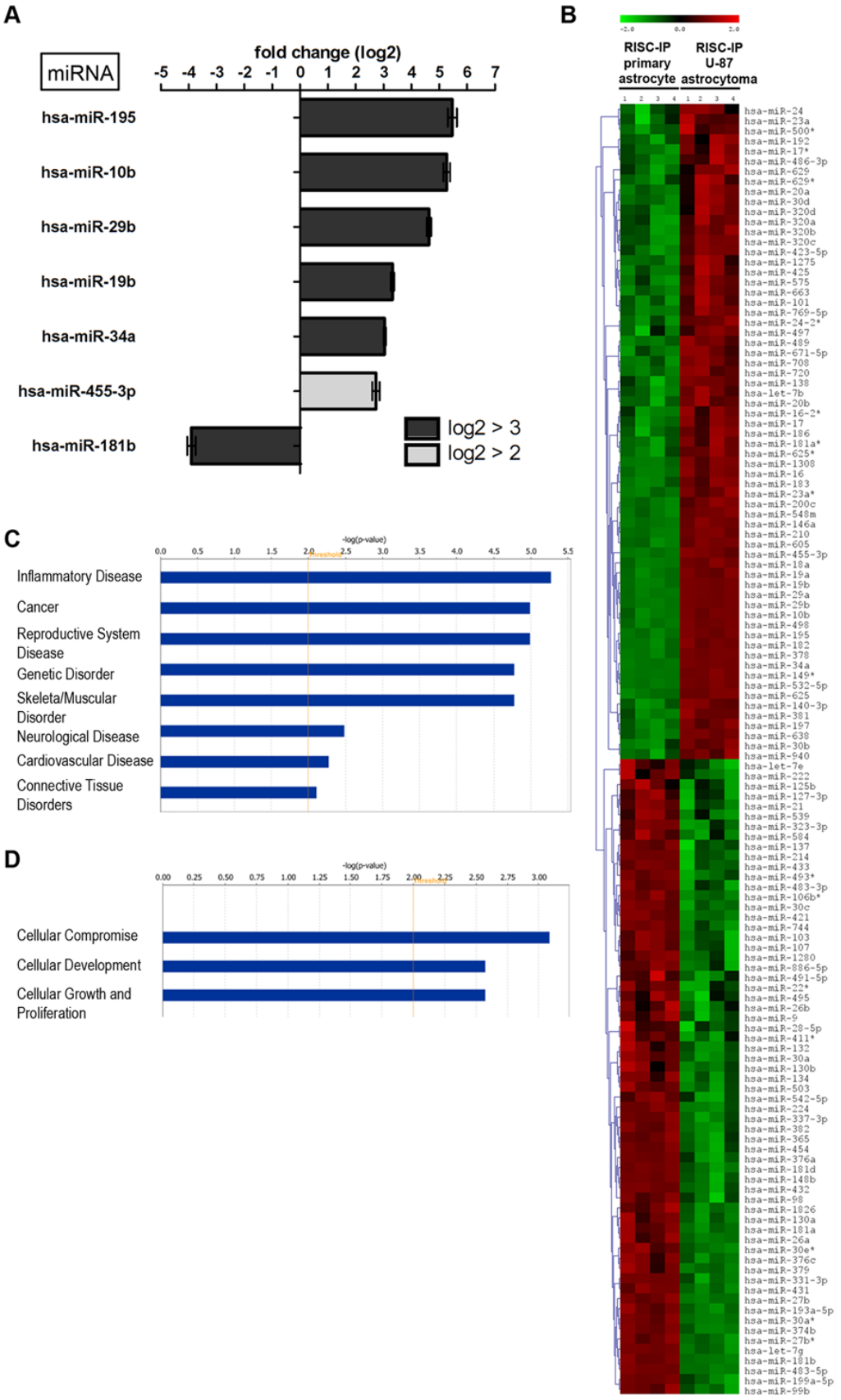
A
miRNA
fold change (log2)
-5 -4 -3 -2 -1 0 1 2 3 4 5 6 7
hsa-miR-195
hsa-miR-10b
hsa-miR-29b
hsa-miR-19b
hsa-miR-34a
hsa-miR-455-3p
hsa-miR-181b
log2 > 3
log2 > 2
B
RISC-IP primary astrocyte
RISC-IP U-87 astrocytoma
C
-log(p-value)
Inflammatory Disease
Cancer
Reproductive System Disease
Genetic Disorder
Skeleta/Muscular Disorder
Neurological Disease
Cardiovascular Disease
Connective Tissue Disorders
D
-log(p-value)
Cellular Compromise
Cellular Development
Cellular Growth and Proliferation

Figure 5.6: RISC-IP miRNA expression in human U-87 astrocytoma cells compared to primary human astrocytes. (A) MiRNAs with a log2 fold change >2 ($p<0.01$). MiRNAs with a positive fold change are increased in RISC-IP astrocytoma cells compared to RISC-IP astrocytes and miRNAs with a negative fold change are decreased in RISC-IP astrocytoma cells compared to RISC-IP astrocytes. (B) Hierarchical cluster heatmap showing all significantly expressed miRNAs ($p<0.01$) in four independent samples/cell type. Each row shows the relative expression level for a single miRNA and each column shows the expression level for a single sample. The red or green color indicates relative high or low expression, respectively. (C) Disease/disorders and (D) molecular and cellular functions associated with the miRNAs differentially expressed in RISC of U-87 astrocytoma cells compared to primary astrocytes with a Fisher's exact test p-value threshold set at 0.01 (yellow threshold line) using IPA software.

Table 5.1: Significantly expressed ($p<0.01$) RISC-immunoprecipitated miRNAs in human U-87 astrocytoma cells compared to primary human astrocytes with log2>3.

ID	Symbol	Fold Change	p-value
hsa-miR-195	MIR195	5.468	7.00E-07
hsa-miR-10b	MIR10B	5.273	2.91E-05
hsa-miR-29b	MIR29B	4.634	9.67E-07
hsa-miR-19b	MIR19B	3.320	6.17E-05
hsa-miR-34a	MIR34A	3.040	8.43E-09
hsa-miR-181b	MIR181B	-3.900	2.28E-06

Only 7 miRNAs had a fold change > ±2, yet many U-87 astrocytoma RISC-IP miRNA levels were still considered to be significantly different from levels in primary astrocyte RISC-IP miRNA (Figure 5.6B). When significant ($p<0.01$) miRNA levels for 4 independent U-87 astrocytoma and primary astrocyte RISC-IP samples were plotted on a hierarchical clustered heatmap, 50.8% of miRNAs (65 of 128) were increased in U-87 astrocytoma RISC compared to astrocyte RISC (Figure 5.6B). The remaining 49.2% of

miRNAs (63 of 128) were decreased in U-87 astrocytoma RISC in comparison to astrocyte RISC (Figure 5.6B).

These observations suggest U-87 astrocytoma cell RISC contain specific miRNAs that could potentially target tumor suppressor mRNA or act as oncogenes themselves resulting in increased proliferation, decreased cell death and tumor formation. Indeed, miR-19b located within the *mir-17–19b-1* cluster has been shown to function as an oncogene by targeting apoptotic factors that are activated in response to MYC overexpression, thereby allowing MYC to induce controlled cell proliferation (He et al., 2005). In human glioblastoma samples, miR-10b was increased whereas brain-enriched miR-181b was decreased in human glioblastoma samples and in 10 human glioblastoma cell lines one of which included U-87 astrocytoma cells (Ciafre et al., 2005). In support of increased miR-10b expression in gliomablastomas, another study showed that miR-10b was highly associated with higher grade gliomas suggesting that miR-10b may play a role in tumour invasiveness (Sasayama et al., 2009). Further, miR-10b was also highly expressed in metastatic breast cancer cells and was shown to be involved in cell migration, invasion and metastasis (Ma et al., 2007).

In contrast to our observation of miR-195 levels being increased in U-87 astrocytoma RISC, miR-195 has been shown to be downregulated in various cancer cells including hepatocellular carcinoma (Su et al., 2009;Iorio et al., 2007;Wang et al., 2008). MiR-195 was shown to play a fundamental role in cell cycle regulation and tumourigenesis where overexpression repressed phosphorylation of rentioblastoma (Rb)-E2F signalling downregulated mRNA targets such as cyclin D1, CDK6 and E2F3, thus suggesting miR-195 as a potential target for cancer therapy (Xu et al., 2009). MiR-195

expression has not been specifically reported in brain cancers to date Our results show miR-195 is in U-87 astrocytoma cell RISC as compared to primary astrocyte RISC, suggesting that U-87 astrocytoma RISC may be enriched in tumor suppressive miR-195 in an attempt to regulate the cell cycle and cell proliferation.

In this study, miR-34a was upregulated in U-87 astrocytoma RISC, however in other reports miR-34a was shown to be downregulated in cancer cells and tumors including colon cancer, leukemia, hepatocellular carcinoma and non-small cell lung cancer (Dijkstra et al., 2008;Li et al., 2009a;Gallardo et al., 2009). MiR-34a has been extensively studied in cancer and many studies point to miR-34a as a transcriptional target of p53 tumor suppressor whereby upregulation or activation of miR-34a contributes to p53-mediated apoptosis and G_1 cell cycle arrest (Chang et al., 2007;Raver-Shapira et al., 2007;Tarasov et al., 2007). Other studies have shown that miR-34 overexpression also takes place independent of p53 upregulation (Navarro et al., 2009;Christoffersen et al., 2009). In recent years, miR-34a has been found to affect tumor cell apoptosis, senescence, proliferation and invasion (Welch et al., 2007;Tarasov et al., 2007;Tazawa et al., 2007;Li et al., 2009a;Sun et al., 2008). In addition, a few mRNA targets of miR-34a are oncogenes such as MYC, CDK6, SIRT1 and c-Met (He et al., 2007a;Sun et al., 2008;Wei et al., 2008;Yamakuchi et al., 2008). In glioblastoma tumours, miR-34a was generally downregulated but when overexpressed, functioned to inhibit glioblastoma cell proliferation, survival, migration and invasion by targeting c-Met and Notch (Li et al., 2009b;Guessous et al., 2010). MiR-34a is generally thought to be a tumour suppressor, in our study and others it has been found to be upregulated in

several cancers including renal cell carcinoma (Dutta et al., 2007), colon cancer (Tazawa et al., 2007) and hepatocellular carcinoma (Meng et al., 2007).

The 7 key IPA miRNAs with a log2 fold change >±2 in U-87 astrocytoma RISC compared to primary astrocyte RISC showed that these miRNAs are associated with many diseases/disorders and have a role in specific molecular and cellular functions (Figure 5.6C, 5.6D). Specifically, U-87 astrocytoma RISC contain miRNAs that play a predominant role in inflammatory disease, cancer and genetic disorders and to a lesser extent in neurological disease and connective tissue disorders (Figure 5.6C, threshold set at $p<0.01$). In addition, U-87 astrocytoma RISC contain miRNAs that play a role in cellular compromise, development and growth and proliferation (Figure 5.6, threshold set at $p<0.01$ using Fisher's exact test). Not only are astrocytes important for neuronal survival and function, they contribute to the formation and preservation of a secure blood-brain barrier, control ionic and osmotic homeostasis (Amiry-Moghaddam and Ottersen, 2003), and play a role in the development and plasticity of the central nervous system by modifying the growth of axons and dendrites and regulating synapse formation (Helmuth, 2001). They also play a central role in the control of the immune response and surveillance in the central nervous system (Farina et al., 2007;Griffiths et al., 2009). Indeed, our finding that U-87 astrocytoma RISC-specific miRNAs function to regulate inflammatory and immune responses to a greater extent than neurological processes suggests astrocytoma cells are characterized by RISC-associated dysregulated immune surveillance and inflammatory responses.

A comparison of global miRNA expression between U-87 astrocytoma cells and primary astrocytes was not the primary focus of this study, yet this data has been included

for completeness (Figure 5.7). In brief, there were 40 global miRNAs that had a log2 fold change greater than or equal to 2 in U-87 astrocytoma cells when compared to primary astrocytes (Figure 5.7) with 8 of these global miRNAs having a significant log2 fold change >±3 (Figure 5.7A, Table 5.2).

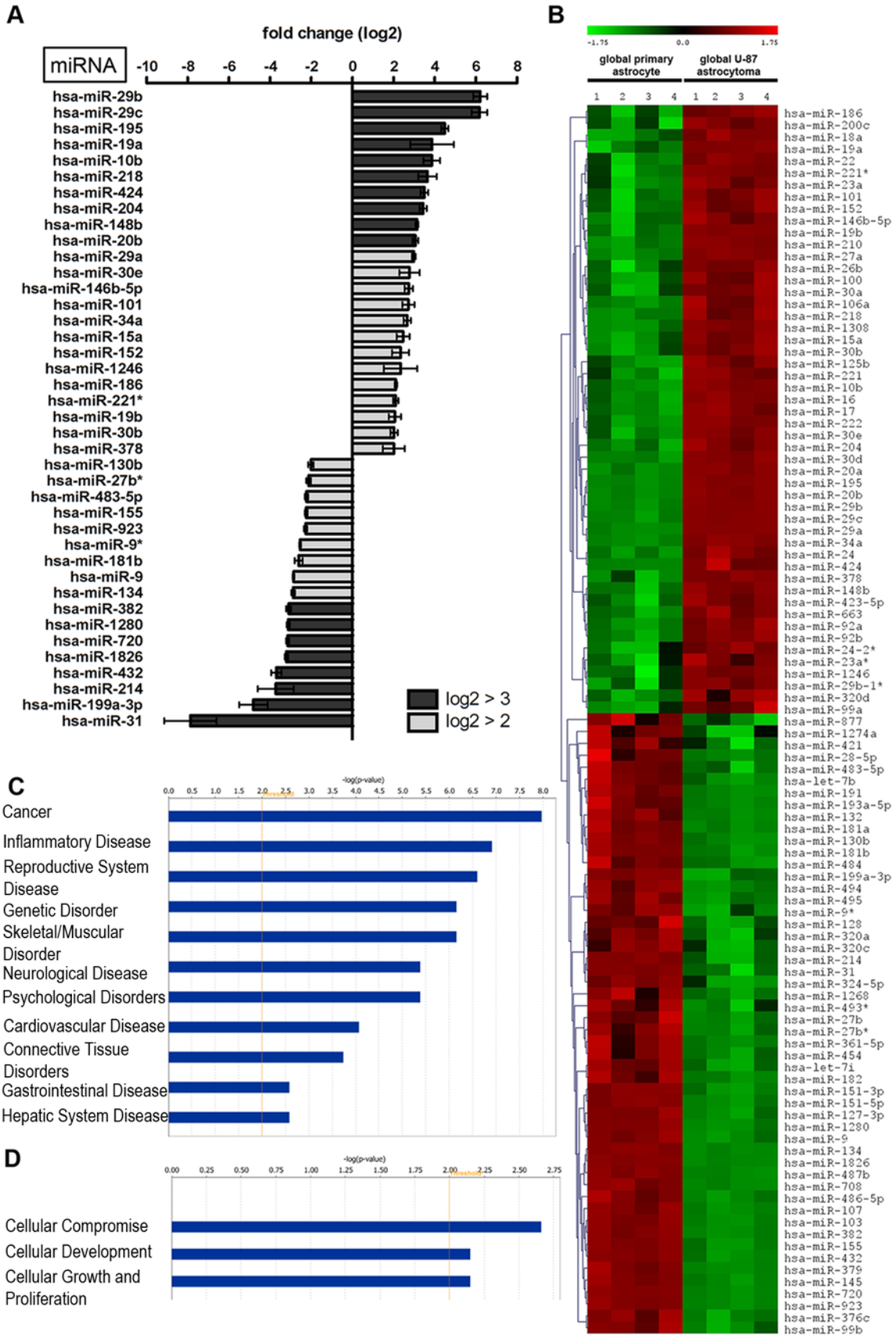
A
fold change (log2)
miRNA
-10 -8 -6 -4 -2 0 2 4 6 8
hsa-miR-29b
hsa-miR-29c
hsa-miR-195
hsa-miR-19a
hsa-miR-10b
hsa-miR-218
hsa-miR-424
hsa-miR-204
hsa-miR-148b
hsa-miR-20b
hsa-miR-29a
hsa-miR-30e
hsa-miR-146b-5p
hsa-miR-101
hsa-miR-34a
hsa-miR-15a
hsa-miR-152
hsa-miR-1246
hsa-miR-186
hsa-miR-221*
hsa-miR-19b
hsa-miR-30b
hsa-miR-378
hsa-miR-130b
hsa-miR-27b*
hsa-miR-483-5p
hsa-miR-155
hsa-miR-923
hsa-miR-9*
hsa-miR-181b
hsa-miR-9
hsa-miR-134
hsa-miR-382
hsa-miR-1280
hsa-miR-720
hsa-miR-1826
hsa-miR-432
hsa-miR-214
hsa-miR-199a-3p
hsa-miR-31
log2 > 3
log2 > 2
B
-1.75 0.0 1.75
global primary astrocyte
global U-87 astrocytoma
1 2 3 4 1 2 3 4
hsa-miR-186
hsa-miR-200c
hsa-miR-18a
hsa-miR-19a
hsa-miR-22
hsa-miR-221*
hsa-miR-23a
hsa-miR-101
hsa-miR-152
hsa-miR-146b-5p
hsa-miR-19b
hsa-miR-210
hsa-miR-27a
hsa-miR-26b
hsa-miR-100
hsa-miR-30a
hsa-miR-106a
hsa-miR-218
hsa-miR-1308
hsa-miR-15a
hsa-miR-30b
hsa-miR-125b
hsa-miR-221
hsa-miR-10b
hsa-miR-16
hsa-miR-17
hsa-miR-222
hsa-miR-30e
hsa-miR-204
hsa-miR-30d
hsa-miR-20a
hsa-miR-195
hsa-miR-20b
hsa-miR-29b
hsa-miR-29c
hsa-miR-29a
hsa-miR-34a
hsa-miR-24
hsa-miR-424
hsa-miR-378
hsa-miR-148b
hsa-miR-423-5p
hsa-miR-663
hsa-miR-92a
hsa-miR-92b
hsa-miR-24-2*
hsa-miR-23a*
hsa-miR-1246
hsa-miR-29b-1*
hsa-miR-320d
hsa-miR-99a
hsa-miR-877
hsa-miR-1274a
hsa-miR-421
hsa-miR-28-5p
hsa-miR-483-5p
hsa-let-7b
hsa-miR-191
hsa-miR-193a-5p
hsa-miR-132
hsa-miR-181a
hsa-miR-130b
hsa-miR-181b
hsa-miR-484
hsa-miR-199a-3p
hsa-miR-494
hsa-miR-495
hsa-miR-9*
hsa-miR-128
hsa-miR-320a
hsa-miR-320c
hsa-miR-214
hsa-miR-31
hsa-miR-324-5p
hsa-miR-1268
hsa-miR-493*
hsa-miR-27b
hsa-miR-27b*
hsa-miR-361-5p
hsa-miR-454
hsa-let-7i
hsa-miR-182
hsa-miR-151-3p
hsa-miR-151-5p
hsa-miR-127-3p
hsa-miR-1280
hsa-miR-9
hsa-miR-134
hsa-miR-1826
hsa-miR-487b
hsa-miR-708
hsa-miR-486-5p
hsa-miR-107
hsa-miR-103
hsa-miR-382
hsa-miR-155
hsa-miR-432
hsa-miR-379
hsa-miR-145
hsa-miR-720
hsa-miR-923
hsa-miR-376c
hsa-miR-99b
C
-log(p-value)
0.0 0.5 1.0 1.5 2.0 2.5 3.0 3.5 4.0 4.5 5.0 5.5 6.0 6.5 7.0 7.5 8.0
Cancer
Inflammatory Disease
Reproductive System Disease
Genetic Disorder
Skeletal/Muscular Disorder
Neurological Disease
Psychological Disorders
Cardiovascular Disease
Connective Tissue Disorders
Gastrointestinal Disease
Hepatic System Disease
D
-log(p-value)
0.00 0.25 0.50 0.75 1.00 1.25 1.50 1.75 2.00 2.25 2.50 2.75
Cellular Compromise
Cellular Development
Cellular Growth and Proliferation

Figure 5.7: Global miRNA expression in human U-87 astrocytoma cells compared to primary human astrocytes. (A) MiRNAs with a log2 fold change >2 ($p<0.01$). MiRNAs with a positive fold change are increased in astrocytoma cells compared to astrocytes and miRNAs with a negative fold change are decreased in astrocytoma cells compared to astrocytes. MiRNAs with a log2 fold change >3 (dark grey) represent the top 20% of miRNA that were significantly expressed ($p<0.01$). (B) Hierarchical cluster heatmap showing all significantly expressed miRNAs ($p<0.01$) in four independent samples/cell type. Each row shows the relative expression level for a single miRNA and each column shows the expression level for a single sample. The red or green color indicates relative high or low expression, respectively. (C) Disease/disorders and (D) molecular and cellular functions associated with the miRNAs differentially expressed in the global cellular milieu of U-87 astrocytoma cells compared to primary astrocytes with a Fisher's exact test p-value threshold set at 0.01 (yellow threshold line) using IPA software.

Table 5.2: Significantly expressed ($p<0.01$) global miRNAs in human U-87 astrocytoma cells compared to primary human astrocytes with log2>3.

ID	Symbol	Fold Change	p-value
hsa-miR-29b	MIR29B	6.214	3.52E-05
hsa-miR-29c	MIR29C	6.171	7.99E-05
hsa-miR-195	MIR195	4.491	5.75E-08
hsa-miR-20b	MIR20B	3.061	1.19E-07
hsa-miR-1280	MIR1280	-3.122	1.24E-06
hsa-miR-720	MIR720	-3.149	8.45E-08
hsa-miR-1826	MIR1826	-3.206	2.11E-09
hsa-miR-31	MIR31	-7.869	2.47E-03

As with the cell type specific RISC-IP miRNAs, there was a relatively equal representation of increased and decreased miRNAs in the global cellular milieu of both cell types (Figure 5.7B). IPA of the 40 key global miRNAs with a log2 fold change $\geq \pm 2$ in U-87 astrocytoma cells compared to primary astrocytes showed that these miRNAs

were associated with the same, albeit a higher number of diseases/disorders than those miRNAs that were specifically within RISC (Figure 5.7C). Global miRNAs play a role in cellular compromise, cellular development and cellular growth and proliferation as do RISC miRNAs, however to a lesser extent than RISC-specific miRNAs (Figure 5.7D).

5.2.5 RISC contain mostly decreased levels of mRNAs in primary astrocytes and U-87 astrocytoma cells

Global and RISC-IP gene expression in U-87 astrocytoma and primary astrocytes were analyzed on Affymetrix Human Genome U133A 2.0 Arrays as described in detail in the Methods section. There was slight variation in the specific global mRNA levels or RISC-IP mRNA levels between U-87 astrocytoma cells and primary astrocytes; however when significant ($p<0.01$) cell-specific expression values with a fold change $>\pm1.4$ (using the RMA algorithm) were grouped into a hierarchical clustered heat map of global versus RISC-IP sample sets, a unique profile of RISC-specific increased and decreased genes was observed (Figure 5.8A). Relative to global gene expression, U-87 astrocytoma and primary astrocyte RISC contained 93.9% of mRNA that were significantly ($p<0.01$) decreased (92 of 98 total) and 6.1% of mRNA that were significantly ($p<0.01$) increased (6 of 98 total) (Figure 5.8A), suggesting that the majority of mRNAs targeted to RISC are downregulated. Of the 98 genes expressed, 64 could be mapped to known genes in the Entrez gene database that encode enzymes, transcriptional regulators, transporters and other proteins (Table 5.3).

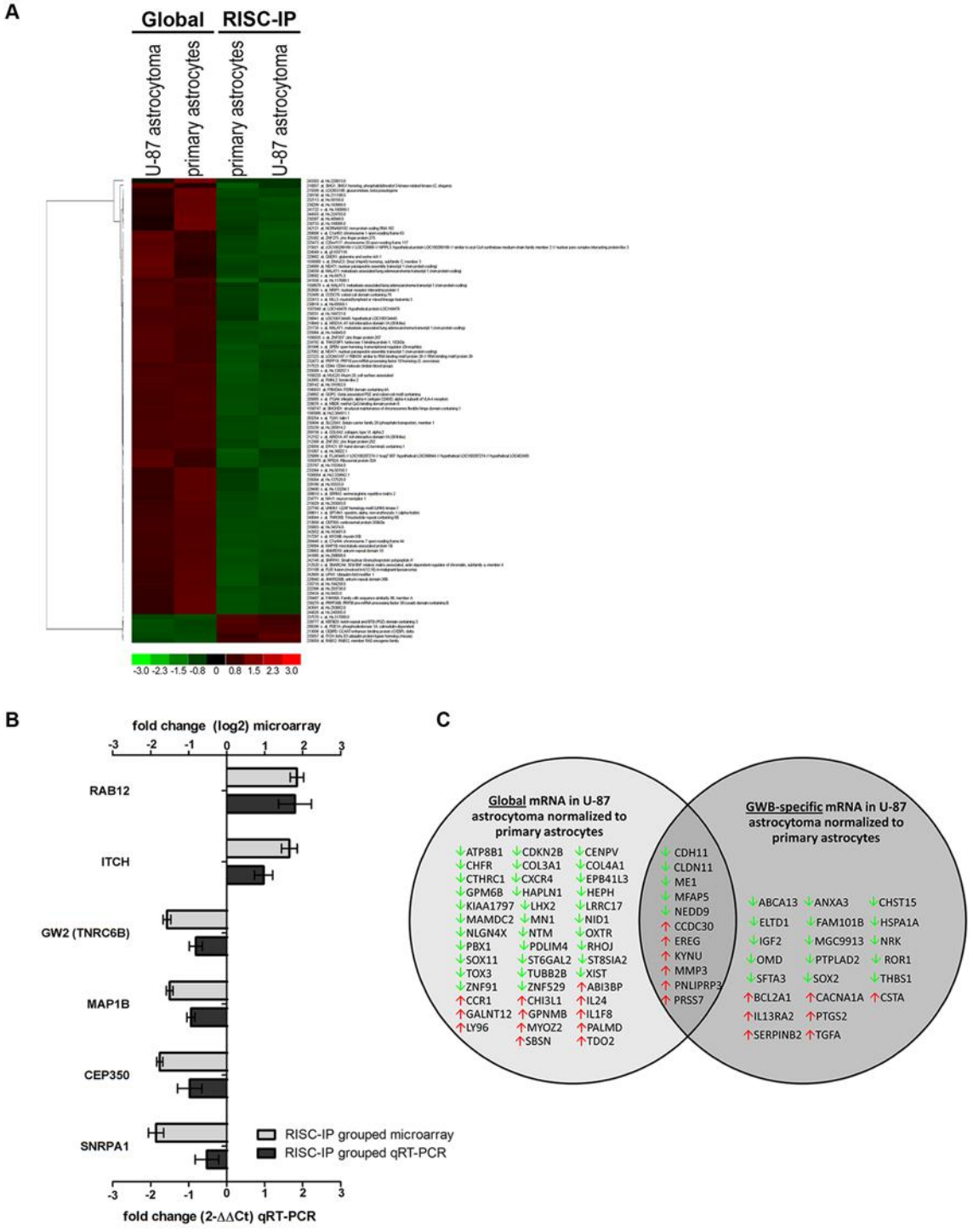

Figure 5.8: Global mRNA levels to RISC-IP mRNA levels in U-87 astrocytoma and primary astrocytes. (A) A hierarchical heatmap comparing global mRNA levels to RISC-IP mRNA levels in U-87 astrocytoma and primary astrocytes. MRNAs included in the heatmap had a fold change >1.4 and were significantly expressed ($p<0.01$). (B)

MRNA microarray validation with qkRT-PCR analysis in grouped RISC-IP U-87 astrocytoma and primary astrocytes samples. Grouped RISC-IP data were compared to the grouped global mRNA from U-87 astrocytoma and primary astrocytes samples. Eight mRNAs were selected from the grouped mRNA microarray dataset and examined by qkRT-PCR. Fold change from the mRNA microarray are given by log2 values (left y-axis, light grey bars). Fold change from the qkRT-PCR was determined using the $2^{-\Delta\Delta Ct}$ method and all mRNA expression values were normalized to the beta-actin endogenous control (right y-axis, dark grey bars). Error bars represent the standard deviation of the mean (SD). Importantly, the fold change (y-axis) cannot be directly compared between assays due to differences in calculation methods, but the general trend of up-regulation and down-regulation can be compared. (C) MRNAs in RISC compared to the global cellular milieu in U-87 astrocytoma cells. MRNA expression in U-87 astrocytoma cells were normalized to primary astrocytes mRNA expression. All mRNAs had a fold change >2.5 and were significantly expressed ($p<0.01$). Green and red arrows indicate decreased and increased levels respectively.

Table 5.3: RISC-immunoprecipitated mRNA levels compared to global cellular mRNA levels in U-87 astrocytoma cells and primary astrocytes with a fold change greater than ±1.4 with p<0.01.

Affymetrix ID	Symbol	Entrez Gene Name	Fold Change	Location	Type(s)
235059_at	RAB12	RAB12, member RAS oncogene family	1.850	Cytoplasm	enzyme
235057_at	ITCH	itchy E3 ubiquitin protein ligase homolog (mouse)	1.650	Nucleus	enzyme
208396_s_at	PDE1A	phosphodiesterase 1A, calmodulin-dependent	1.630	Cytoplasm	enzyme
213006_at	CEBPD	CCAAT/enhancer binding protein (C/EBP), delta	1.620	Nucleus	transcription regulator
228777_at	KBTBD3	kelch repeat and BTB (POZ) domain containing 3	1.540	unknown	other
209156_s_at	COL6A2	collagen, type VI, alpha 2	-1.430	Extracellular Space	other
203254_s_at	TLN1	talin 1	-1.450	Plasma Membrane	other
212152_x_at	ARID1A	AT rich interactive domain 1A (SWI-like)	-1.460	Nucleus	transcription regulator

208611_s_at	SPTAN1	spectrin, alpha, non-erythrocytic 1 (alpha-fodrin)	-1.460	Plasma Membrane	other
217297_s_at	MYO9B	myosin IXB	-1.470	Cytoplasm	enzyme
556035_s_at	ZNF207	zinc finger protein 207	-1.470	Nucleus	transcription regulator
212368_at	ZNF292	zinc finger protein 292	-1.470	Nucleus	transcription regulator
231108_at	FUS	fusion (involved in t(12;16) in malignant liposarcoma)	-1.490	Nucleus	transcription regulator
225473_at	C20ORF117	chromosome 20 open reading frame 117	-1.500	unknown	other
226084_at	MAP1B	microtubule-associated protein 1B	-1.500	Cytoplasm	other
226076_s_at	MBD6	methyl-CpG binding domain protein 6	-1.500	unknown	other
217523_at	CD44	CD44 molecule (Indian blood group)	-1.510	Plasma Membrane	other
205885_s_at	ITGA4	integrin, alpha 4 (antigen CD49D, alpha 4 subunit of VLA-4 receptor)	-1.510	Plasma Membrane	other
224792_at	TNKS1BP1	tankyrase 1 binding protein 1, 182kDa	-1.510	Nucleus	other
236862_at	GOPC	golgi associated PDZ and coiled-coil motif containing	-1.530	Cytoplasm	transporter
225656_at	EFHC1	EF-hand domain (C-terminal) containing 1	-1.540	Cytoplasm	other
225899_x_at	TCAG7.907	hypothetical LOC402483	-1.540	unknown	other
212520_s_at	SMARCA4	SWI/SNF related, matrix associated, actin dependent regulator of chromatin, subfamily a, member 4	-1.550	Nucleus	transcription regulator
1558747_at	SMCHD1	structural maintenance of chromosomes flexible hinge domain containing 1	-1.550	unknown	other
208610_s_at	SRRM2	serine/arginine repetitive matrix 2	-1.550	Nucleus	other

1557049_at	BTBD19	BTB (POZ) domain containing 19	-1.570	unknown	other
240044_x_at	TNRC6B	trinucleotide repeat containing 6B	-1.570	unknown	other
225382_at	ZNF275	zinc finger protein 275	-1.570	Nucleus	other
232473_at	PRPF18	PRP18 pre-mRNA processing factor 18 homolog (S. cerevisiae)	-1.590	Nucleus	transporter
224559_at	MALAT1	metastasis associated lung adenocarcinoma transcript 1 (non-protein coding)	-1.600	unknown	other
222413_s_at	MLL3	myeloid/lymphoid or mixed-lineage leukemia 3	-1.610	Nucleus	transcription regulator
201996_s_at	SPEN	spen homolog, transcriptional regulator (Drosophila)	-1.610	Nucleus	transcription regulator
242665_at	FMNL2 (includes EG:114793)	formin-like 2	-1.620	Cytoplasm	other
220940_at	ANKRD36B	ankyrin repeat domain 36B	-1.630	unknown	other
235589_s_at	MDM4	Mdm4 p53 binding protein homolog (mouse)	-1.630	Nucleus	other
227740_at	UHMK1	U2AF homology motif (UHM) kinase 1	-1.630	Nucleus	kinase
209006_s_at	C1ORF63	chromosome 1 open reading frame 63	-1.650	unknown	other
224771_at	NAV1	neuron navigator 1	-1.660	unknown	enzyme
215921_at	NPIPL3	nuclear pore complex interacting protein-like 3	-1.660	unknown	other
232489_at	CCDC76	coiled-coil domain containing 76	-1.670	unknown	other
215599_at	LOC653188	glucuronidase, beta pseudogene 3	-1.670	unknown	other
1558220_at	MUC20	mucin 20, cell surface associated	-1.670	Plasma Membrane	other
1555878_at	RPS24 (includes	ribosomal protein S24	-1.680	Cytoplasm	other

	EG:6229)				
202600_s_at	NRIP1	nuclear receptor interacting protein 1	-1.720	Nucleus	transcription regulator
1558678_s_at	MALAT1	metastasis associated lung adenocarcinoma transcript 1 (non-protein coding)	-1.740	unknown	other
229982_at	QSER1	glutamine and serine rich 1	-1.740	unknown	other
213956_at	CEP350	centrosomal protein 350kDa	-1.760	Cytoplasm	other
236841_at	LOC100134445	hypothetical LOC100134445	-1.770	unknown	other
209446_s_at	C7ORF44	chromosome 7 open reading frame 44	-1.790	unknown	other
226663_at	ANKRD10	ankyrin repeat domain 10	-1.820	Nucleus	transcription regulator
227223_at	RBM39	RNA binding motif protein 39	-1.820	Nucleus	transcription regulator
231735_s_at	MALAT1	metastasis associated lung adenocarcinoma transcript 1 (non-protein coding)	-1.830	unknown	other
210057_at	SMG1	SMG1 homolog, phosphatidylinositol 3-kinase-related kinase (C. elegans)	-1.830	Cytoplasm	kinase
239487_at	FAM98A	family with sequence similarity 98, member A	-1.840	unknown	other
242146_at	SNRPA1	small nuclear ribonucleoprotein polypeptide A'	-1.860	Nucleus	other
227062_at	NEAT1 (includes EG:283131)	nuclear paraspeckle assembly transcript 1 (non-protein coding)	-1.890	unknown	other
1560031_at	FRMD4A	FERM domain containing 4A	-1.900	unknown	other
242669_at	UFM1	ubiquitin-fold modifier 1	-1.900	Cytoplasm	other
558080_s_at	DNAJC3	DnaJ (Hsp40) homolog, subfamily C, member 3	-1.910	Cytoplasm	other
242121_at	NCRNA00	non-protein coding RNA 182	-1.930	unknown	other

	182				
210649_s_at	ARID1A	AT rich interactive domain 1A (SWI-like)	-1.980	Nucleus	transcription regulator
230270_at	PRPF38B	PRP38 pre-mRNA processing factor 38 (yeast) domain containing B	-2.050	unknown	other
234989_at	NEAT1 (includes EG:283131)	nuclear paraspeckle assembly transcript 1 (non-protein coding)	-2.100	unknown	other
230494_at	SLC20A1	solute carrier family 20 (phosphate transporter), member 1	-2.290	Plasma Membrane	transporter

The gene expression microarray results for RISC-IP (U-87 astrocytoma and primary astrocyte) were validated by qkRT-PCR with gene expression normalized to the beta-actin housekeeping gene (Figure 5.8B). As above, fold change values cannot be directly compared between microarray and qkRT-PCR assays due to differences in calculation methods (log2 for microarray and $2^{-\Delta\Delta Ct}$ for qkRT-PCR), however comparisons could be made based on the general trend (Figure 5.8B). The 6 mRNA cDNA examined by qkRT-PCR included RAB12, ITCH, GW2 (TNRC6B), MAP1B, CEP350 and SNRPA1 (Figure 5.8B). In general, the qkRT-PCR results for each of these mRNA cDNA were comparable with the microarray results, whereby RAB12 and ITCH expression were both increased in RISC and GW2, MAP1B, CEP350 and SNRPA1 expression were decreased when compared to the global cellular mRNA expression levels (Figure 5.8B).

There were many decreased mRNAs that were shared between U-87 astrocytoma cells and primary astrocytes in RISC, as well as differences in RISC-specific mRNA

levels (Figure 5.9A). Differences in significant ($p<0.01$) mRNA levels between U-87 astrocytoma and astrocytes were mapped onto a hierarchical clustered heatmap with mRNAs that exhibited a fold change $>\pm 2.3$ (Figure 5.9A, Table 5.4). U-87 astrocytoma cell RISC contained 41 decreased mRNAs and 30 increased mRNAs out of a total of 74 mRNAs as compared to primary astrocytes (Figure 5.9A) and include transmembrane receptors, growth factors, peptidases, transcription regulators, cytokines and other proteins as listed in Table 5.4. Globally, there were also specific mRNA level differences between U-87 astrocytoma cells and primary astrocytes (Figure 5.9B, Table 5.5). In brief, 71 mRNAs were decreased and 30 mRNAs were increased in the global cellular fraction of U-87 astrocytoma cells as compared to primary astrocytes (Figure 5.9B, $p<0.01$, log2 fold change $>\pm 2.3$) and include enzymes, peptidases, cytokines, growth factors, G-protein coupled receptors, transcription regulators and others (Table 5.5).

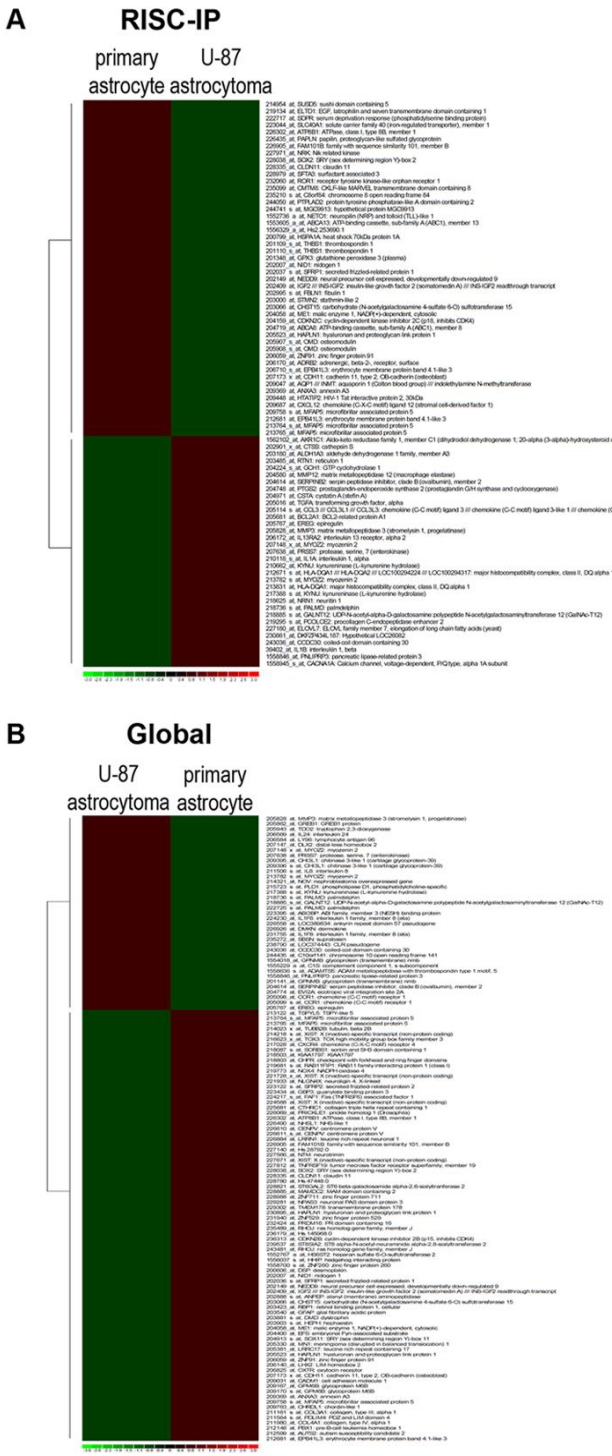

Figure 5.9: Hierarchical cluster heatmap of significant mRNA expression in primary astrocytes and U-87 astrocytoma cells isolated from (A) RISC-IP and (B) global total RNA samples. MRNAs included in the heatmap had a fold change > 2.3 and were significantly expressed ($p<0.01$).

Table 5.4: RISC-immunoprecipitated mRNA levels in human U-87 astrocytoma cells compared to RISC-immunoprecipitated mRNA levels in primary human astrocytes.

Affymetrix ID	Symbol	Entrez Gene Name	Fold Change	Location	Type(s)
243036_at	CCDC30	coiled-coil domain containing 30	3.320	unknown	other
206172_at	IL13RA2	interleukin 13 receptor, alpha 2	3.140	Plasma Membrane	transmembrane receptor
205767_at	EREG	epiregulin	3.100	Extracellular Space	growth factor
207638_at	PRSS7	protease, serine, 7 (enterokinase)	2.830	Extracellular Space	peptidase
205681_at	BCL2A1	BCL2-related protein A1	2.780	Cytoplasm	other
205828_at	MMP3	matrix metallopeptidase 3 (stromelysin 1, progelatinase)	2.770	Extracellular Space	peptidase
1558945_s_at	CACNA1A	calcium channel, voltage-dependent, P/Q type, alpha 1A subunit	2.660	Plasma Membrane	ion channel
204971_at	CSTA	cystatin A (stefin A)	2.660	Cytoplasm	other
205016_at	TGFA	transforming growth factor, alpha	2.660	Extracellular Space	growth factor
217388_s_at	KYNU	kynureninase (L-kynurenine hydrolase)	2.650	Cytoplasm	enzyme
1558846_at	PNLIPRP3	pancreatic lipase-related protein 3	2.600	unknown	other
204614_at	SERPINB2	serpin peptidase inhibitor, clade B (ovalbumin), member 2	2.570	Extracellular Space	other
204748_at	PTGS2	prostaglandin-endoperoxide synthase 2 (prostaglandin G/H synthase and cyclooxygenase)	2.530	Cytoplasm	enzyme
218625_at	NRN1	neuritin 1	2.480	Cytoplasm	other
213831_at	HLA-DQA1	major histocompatibility complex, class II, DQ alpha 1	2.470	Plasma Membrane	transmembrane receptor
203485_at	RTN1	reticulon 1	2.470	Cytoplasm	other
39402_at	IL1B	interleukin 1, beta	2.440	Extracellular Space	cytokine
202901_x_at	CTSS	cathepsin S	2.420	Cytoplasm	peptidase

1562102_at	AKR1C1	aldo-keto reductase family 1, member C1 (dihydrodiol dehydrogenase 1; 20-alpha (3-alpha)-hydroxysteroid dehydrogenase)	2.410	Cytoplasm	enzyme
203180_at	ALDH1A3	aldehyde dehydrogenase 1 family, member A3	2.410	Cytoplasm	enzyme
230861_at	DKFZP434L187	hypothetical LOC26082	2.410	unknown	other
18736_s_at	PALMD	palmdelphin	2.410	unknown	other
218885_s_at	GALNT12	UDP-N-acetyl-alpha-D-galactosamine:polypeptide N-acetylgalactosaminyltransferase 12 (GalNAc-T12)	2.380	Cytoplasm	enzyme
213782_s_at	MYOZ2	myozenin 2	2.360	Cytoplasm	other
210118_s_at	IL1A	interleukin 1, alpha	2.340	Extracellular Space	cytokine
204580_at	MMP12	matrix metallopeptidase 12 (macrophage elastase)	2.340	Extracellular Space	peptidase
205114_s_at	CCL3	chemokine (C-C motif) ligand 3	2.330	Extracellular Space	cytokine
204224_s_at	GCH1	GTP cyclohydrolase 1	2.330	Cytoplasm	enzyme
219295_s_at	PCOLCE2 (includes EG:26577)	procollagen C-endopeptidase enhancer 2	2.320	Extracellular Space	other
227180_at	ELOVL7	ELOVL family member 7, elongation of long chain fatty acids (yeast)	2.310	unknown	other
235099_at	CMTM8	CKLF-like MARVEL transmembrane domain containing 8	-2.300	Extracellular Space	cytokine
226435_at	PAPLN	papilin, proteoglycan-like sulfated glycoprotein	-2.310	unknown	other
206059_at	ZNF91	zinc finger protein 91	-2.310	Nucleus	transcription regulator
206170_at	ADRB2	adrenergic, beta-2-, receptor, surface	-2.330	Plasma Membrane	G-protein coupled receptor
204719_at	ABCA8	ATP-binding cassette, sub-family A (ABC1), member 8	-2.340	Plasma Membrane	transporter
203000_at	STMN2	stathmin-like 2	-2.340	Cytoplasm	other

02037_s_at	SFRP1	secreted frizzled-related protein 1	-2.350	Plasma Membrane	transmembrane receptor
209448_at	HTATIP2	HIV-1 Tat interactive protein 2, 30kDa	-2.360	Nucleus	transcription regulator
202995_s_at	FBLN1	fibulin 1	-2.370	Extracellular Space	other
1552736_a_at	NETO1	neuropilin (NRP) and tolloid (TLL)-like 1	-2.390	Extracellular Space	other
214954_at	SUSD5	sushi domain containing 5	-2.390	unknown	other
204159_at	CDKN2C	cyclin-dependent kinase inhibitor 2C (p18, inhibits CDK4)	-2.400	Nucleus	transcription regulator
205523_at	HAPLN1	hyaluronan and proteoglycan link protein 1	-2.400	Extracellular Space	other
235210_s_at	C8ORF84	chromosome 8 open reading frame 84	-2.410	unknown	other
223044_at	SLC40A1	solute carrier family 40 (iron-regulated transporter), member 1	-2.410	Plasma Membrane	transporter
201348_at	GPX3	glutathione peroxidase 3 (plasma)	-2.420	Extracellular Space	enzyme
222717_at	SDPR	serum deprivation response	-2.440	Plasma Membrane	other
226302_at	ATP8B1	ATPase, class I, type 8B, member 1	-2.470	Plasma Membrane	transporter
206710_s_at	EPB41L3	erythrocyte membrane protein band 4.1-like 3	-2.480	Plasma Membrane	other
209047_at	AQP1	aquaporin 1 (Colton blood group)	-2.490	Plasma Membrane	transporter
209687_at	CXCL12	chemokine (C-X-C motif) ligand 12 (stromal cell-derived factor 1)	-2.490	Extracellular Space	cytokine
202007_at	NID1	nidogen 1	-2.490	Extracellular Space	other
202149_at	NEDD9	neural precursor cell expressed, developmentally down-regulated 9	-2.500	Nucleus	other
209369_at	ANXA3	annexin A3	-2.520	Cytoplasm	enzyme
204058_at	ME1	malic enzyme 1, NADP(+)-dependent, cytosolic	-2.520	Cytoplasm	enzyme
203066_at	CHST15	carbohydrate (N-acetylgalactosamine 4-sulfate 6-O) sulfotransferase 15	-2.530	Plasma Membrane	enzyme

226905_at	FAM101B	family with sequence similarity 101, member B	-2.540	unknown	other
200799_at	HSPA1A	heat shock 70kDa protein 1A	-2.540	Cytoplasm	other
228038_at	SOX2	SRY (sex determining region Y)-box 2	-2.560	Nucleus	transcription regulator
219134_at	ELTD1	EGF, latrophilin and seven transmembrane domain containing 1	-2.620	Plasma Membrane	G-protein coupled receptor
1553605_a_at	ABCA13	ATP-binding cassette, sub-family A (ABC1), member 13	-2.630	unknown	transporter
244050_at	PTPLAD2	protein tyrosine phosphatase-like A domain containing 2	-2.650	unknown	other
244741_s_at	MGC9913	hypothetical protein MGC9913	-2.700	unknown	other
227971_at	NRK	Nik related kinase	-2.760	unknown	kinase
202409_at	IGF2	insulin-like growth factor 2 (somatomedin A)	-2.870	Extracellular Space	growth factor
207173_x_at	CDH11	cadherin 11, type 2, OB-cadherin (osteoblast)	-2.900	Plasma Membrane	other
232060_at	ROR1	receptor tyrosine kinase-like orphan receptor 1	-2.900	Plasma Membrane	kinase
228979_at	SFTA3	surfactant associated 3	-2.940	unknown	other
228335_at	CLDN11	claudin 11	-2.950	Plasma Membrane	other
205907_s_at	OMD	osteomodulin	-3.250	Extracellular Space	other
213764_s_at	MFAP5	microfibrillar associated protein 5	-3.330	Extracellular Space	other
201110_s_at	THBS1	thrombospondin 1	-3.710	Extracellular Space	other

Table 5.5: Global mRNA levels in human U-87 astrocytoma cells compared to primary human astrocytes with a fold change greater than 2.3 with p<0.01.

Affymetrix ID	Symbol	Entrez Gene Name	Fold Change	Location	Type(s)
217388_s_at	KYNU	kynureninase (L-kynurenine hydrolase)	3.340	Cytoplasm	enzyme
1554018_at	GPNMB	glycoprotein (transmembrane) nmb	3.220	Plasma Membrane	enzyme
213782_s_at	MYOZ2	myozenin 2	2.990	Cytoplasm	other
1558846_at	PNLIPRP3	pancreatic lipase-related protein 3	2.990	unknown	other
205828_at	MMP3	matrix metallopeptidase 3 (stromelysin 1, progelatinase)	2.940	Extracellular Space	peptidase
209395_at	CHI3L1	chitinase 3-like 1 (cartilage glycoprotein-39)	2.930	Extracellular Space	enzyme
223395_at	ABI3BP	ABI family, member 3 (NESH) binding protein	2.890	unknown	other
205098_at	CCR1	chemokine (C-C motif) receptor 1	2.890	Plasma Membrane	G-protein coupled receptor
205767_at	EREG	epiregulin	2.880	Extracellular Space	growth factor
243036_at	CCDC30	coiled-coil domain containing 30	2.810	unknown	other
231755_at	IL1F8	interleukin 1 family, member 8 (eta)	2.740	Extracellular Space	cytokine
206569_at	IL24	interleukin 24	2.700	Extracellular Space	cytokine
205943_at	TDO2	tryptophan 2,3-dioxygenase	2.700	Cytoplasm	enzyme
218736_s_at	PALMD	palmdelphin	2.680	unknown	other
207638_at	PRSS7	protease, serine, 7 (enterokinase)	2.680	Extracellular Space	peptidase
235272_at	SBSN	suprabasin	2.640	unknown	other
218885_s_at	GALNT12	UDP-N-acetyl-alpha-D-galactosamine:polypeptide N-acetylgalactosaminyltransferase 12 (GalNAc-T12)	2.510	Cytoplasm	enzyme
206584_at	LY96	lymphocyte antigen 96	2.500	Plasma Membrane	other
1555229_a_at	C1S	complement component 1, s subcomponent	2.490	Extracellular Space	peptidase
238790_at	LOC374443	CLR pseudogene	2.430	unknown	other
215723_s_at	PLD1	phospholipase D1, phosphatidylcholine-specific	2.410	Cytoplasm	enzyme

204614_at	SERPINB2	serpin peptidase inhibitor, clade B (ovalbumin), member 2	2.410	Extracellular Space	other
214321_at	NOV	nephroblastoma overexpressed gene	2.360	Extracellular Space	growth factor
1558636_s_at	ADAMTS5	ADAM metallopeptidase with thrombospondin type 1 motif, 5	2.350	Extracellular Space	peptidase
244435_at	FAM196A	family with sequence similarity 196, member A	2.350	unknown	other
204774_at	EVI2A	ecotropic viral integration site 2A	2.340	Plasma Membrane	transmembrane receptor
207147_at	DLX2	distal-less homeobox 2	2.330	Nucleus	transcription regulator
211506_s_at	IL8	interleukin 8	2.330	Extracellular Space	cytokine
226926_at	DMKN	dermokine	2.310	unknown	other
226558_at	LOC389834	ankyrin repeat domain 57 pseudogene	2.310	unknown	other
205862_at	GREB1	growth regulation by estrogen in breast cancer 1	2.300	Cytoplasm	other
219489_s_at	NXN	nucleoredoxin	-2.300	Nucleus	enzyme
232424_at	PRDM16	PR domain containing 16	-2.300	Nucleus	transcription regulator
235518_at	SLC8A1	solute carrier family 8 (sodium/calcium exchanger), member 1	-2.300	Plasma Membrane	transporter
229302_at	TMEM178	transmembrane protein 178	-2.300	unknown	other
226490_at	NHSL1	NHS-like 1	-2.310	unknown	other
202036_s_at	SFRP1	secreted frizzled-related protein 1	-2.310	Plasma Membrane	transmembrane receptor
218087_s_at	SORBS1	sorbin and SH3 domain containing 1	-2.310	Plasma Membrane	other
224217_s_at	FAF1	Fas (TNFRSF6) associated factor 1	-2.320	Nucleus	other
213122_at	TSPYL5	TSPY-like 5	-2.320	unknown	other
1558700_s_at	ZNF260	zinc finger protein 260	-2.320	Nucleus	other
203881_s_at	DMD	dystrophin	-2.330	Plasma Membrane	other
202409_at	IGF2	insulin-like growth factor 2 (somatomedin A)	-2.330	Extracellular Space	growth factor
209763_at	CHRDL1	chordin-like 1	-2.350	Extracellular Space	other
200606_at	DSP	desmoplakin	-2.350	Plasma	other

				Membrane	
229281_at	NPAS3	neuronal PAS domain protein 3	-2.350	Nucleus	other
202888_s_at	ANPEP	alanyl (membrane) aminopeptidase	-2.360	Plasma Membrane	peptidase
1556037_s_at	HHIP	hedgehog interacting protein	-2.360	Plasma Membrane	other
226884_at	LRRN1	leucine rich repeat neuronal 1	-2.360	unknown	other
209369_at	ANXA3	annexin A3	-2.370	Cytoplasm	enzyme
209031_at	CADM1	cell adhesion molecule 1	-2.370	Plasma Membrane	other
228988_at	ZNF711	zinc finger protein 711	-2.390	Nucleus	other
212599_at	AUTS2 (includes EG:26053)	autism susceptibility candidate 2	-2.400	unknown	other
204400_at	EFS	embryonal Fyn-associated substrate	-2.400	Cytoplasm	other
219773_at	NOX4	NADPH oxidase 4	-2.400	Cytoplasm	enzyme
226069_at	PRICKLE1	prickle homolog 1 (Drosophila)	-2.410	Nucleus	other
219681_s_at	RAB11FIP1	RAB11 family interacting protein 1 (class I)	-2.410	Cytoplasm	other
228038_at	SOX2	SRY (sex determining region Y)-box 2	-2.420	Nucleus	transcription regulator
227812_at	TNFRSF19	tumor necrosis factor receptor superfamily, member 19	-2.430	Plasma Membrane	transmembrane receptor
552767_a_at	HS6ST2	heparan sulfate 6-O-sulfotransferase 2	-2.440	Extracellular Space	enzyme
226905_at	FAM101B	family with sequence similarity 101, member B	-2.450	unknown	other
223122_s_at	SFRP2	secreted frizzled-related protein 2	-2.450	Plasma Membrane	transmembrane receptor
203540_at	GFAP	glial fibrillary acidic protein	-2.460	Cytoplasm	other
223434_at	GBP3	guanylate binding protein 3	-2.470	Cytoplasm	enzyme
203066_at	CHST15	carbohydrate (N-acetylgalactosamine 4-sulfate 6-O) sulfotransferase 15	-2.480	Plasma Membrane	enzyme
203423_at	RBP1	retinol binding protein 1, cellular	-2.480	Extracellular Space	transporter
217028_at	CXCR4	chemokine (C-X-C motif) receptor 4	-2.500	Plasma Membrane	G-protein coupled receptor
218503_at	KIAA1797	KIAA1797	-2.500	unknown	other

231940_at	ZNF529	zinc finger protein 529	-2.510	unknown	other
204058_at	ME1	malic enzyme 1, NADP(+)-dependent, cytosolic	-2.520	Cytoplasm	enzyme
216623_x_at	TOX3	TOX high mobility group box family member 3	-2.520	unknown	other
203903_s_at	HEPH	hephaestin	-2.540	Plasma Membrane	transporter
239537_at	ST8SIA2	ST8 alpha-N-acetyl-neuraminide alpha-2,8-sialyltransferase 2	-2.540	Cytoplasm	enzyme
206059_at	ZNF91	zinc finger protein 91	-2.540	Nucleus	transcription regulator
211564_s_at	PDLIM4	PDZ and LIM domain 4	-2.550	Cytoplasm	other
218803_at	CHFR	checkpoint with forkhead and ring finger domains	-2.590	Nucleus	enzyme
226302_at	ATP8B1	ATPase, class I, type 8B, member 1	-2.600	Plasma Membrane	transporter
206140_at	LHX2	LIM homeobox 2	-2.600	Nucleus	transcription regulator
228885_at	MAMDC2	MAM domain containing 2	-2.600	Extracellular Space	other
228821_at	ST6GAL2	ST6 beta-galactosamide alpha-2,6-sialyltranferase 2	-2.600	Cytoplasm	enzyme
202007_at	NID1	nidogen 1	-2.610	Extracellular Space	other
206825_at	OXTR	oxytocin receptor	-2.610	Plasma Membrane	G-protein coupled receptor
226611_s_at	CENPV	centromere protein V	-2.630	Nucleus	other
212681_at	EPB41L3	erythrocyte membrane protein band 4.1-like 3	-2.640	Plasma Membrane	other
205381_at	LRRC17	leucine rich repeat containing 17	-2.660	unknown	other
209170_s_at	GPM6B	glycoprotein M6B	-2.730	Plasma Membrane	other
205330_at	MN1	meningioma (disrupted in balanced translocation) 1	-2.750	Nucleus	other
235489_at	RHOJ	ras homolog gene family, member J	-2.750	Cytoplasm	enzyme
224588_at	XIST	X (inactive)-specific transcript (non-protein coding)	-2.760	Nucleus	other
228335_at	CLDN11	claudin 11	-2.770	Plasma Membrane	other
11161_s_at	COL3A1	collagen, type III, alpha 1	-2.780	Extracellular Space	other

202149_at	NEDD9	neural precursor cell expressed, developmentally down-regulated 9	-2.780	Nucleus	other
212148_at	PBX1	pre-B-cell leukemia homeobox 1	-2.780	Nucleus	transcription regulator
225681_at	CTHRC1	collagen triple helix repeat containing 1	-2.820	Extracellular Space	other
214023_x_at	TUBB2B	tubulin, beta 2B	-2.860	Cytoplasm	other
221933_at	NLGN4X	neuroligin 4, X-linked	-2.880	Plasma Membrane	enzyme
236313_at	CDKN2B	cyclin-dependent kinase inhibitor 2B (p15, inhibits CDK4)	-2.890	Nucleus	transcription regulator
227566_at	NTM	neurotrimin	-2.890	Plasma Membrane	other
213764_s_at	MFAP5	microfibrillar associated protein 5	-2.900	Extracellular Space	other
207173_x_at	CDH11	cadherin 11, type 2, OB-cadherin (osteoblast)	-3.000	Plasma Membrane	other
204913_s_at	SOX11	SRY (sex determining region Y)-box 11	-3.060	Nucleus	transcription regulator
205523_at	HAPLN1	hyaluronan and proteoglycan link protein 1	-3.070	Extracellular Space	other
211980_at	COL4A1	collagen, type IV, alpha 1	-3.380	Extracellular Space	other

Comparison of mRNA levels in U-87 astrocytoma cell RISC and the global cellular fraction as compared to primary astrocytes provided a unique RISC mRNA profile, a unique global mRNA profile and a list of mRNAs that are shared between RISC and the global cellular milieu (Figure 5.8C). Overall, a greater number of mRNA species were unique to the global cellular fraction and were not found within the RISC in U-87 astrocytoma ($p<0.01$, log2 fold change $>\pm 2.5$). Of these global-specific, 32 mRNA were decreased compared to 12 mRNAs that were increased (Figure 5.8C). RISC contained less mRNAs than the global cellular fraction and specifically contained 15

decreased mRNAs and 7 increased mRNAs (Figure 5.8C). Common to both fractions were 5 decreased mRNAs and 6 increased mRNAs (Figure 5.8C).

Significant ($p<0.01$) mRNA levels with a log2 fold change $>\pm2.5$ in RISC and in the global cellular milieu of U-87 astrocytoma cells as compared to primary astrocytes were assessed using IPA for their association with various diseases or disorders (Figure 5.10) and their role in molecular and cellular functions (Figure 5.11). RISC were more highly enriched in mRNA that are involved in cancer, inflammatory, immunological and neurological disorders, among others (Figure 5.10). In comparison, the global cellular fraction was more highly enriched with mRNA that are involved in infectious diseases as well as hematological and dermatological disorders (Figure 5.10). U-87 astrocytoma RISC were more highly enriched in mRNA components that are involved in multiple cell functions and processes including the cell cycle, cellular growth and proliferation, DNA replication, DNA recombination and repair, and cellular assembly and organization, among others (Figure 5.11). In comparison, the global cellular fraction was more highly enriched with mRNA that are involved in antigen presentation and amino acid metabolism (Figure 5.11). Given that mRNAs important in cell cycle control and cancer are specifically enriched in the RISC within astrocytoma cells suggests the possibility that the RISC may be a future target for brain cancer therapies.

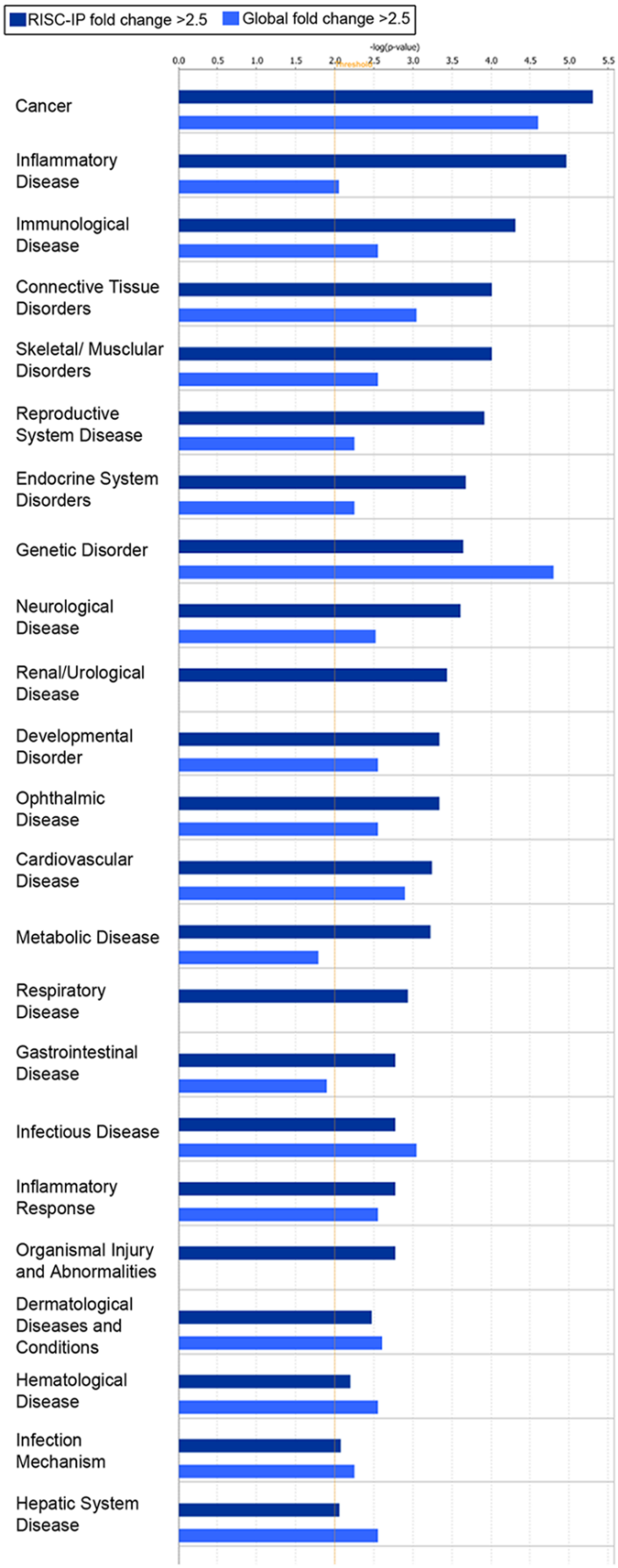

Figure 5.10: Disease and disorder representation of the mRNA in the RISC of U-87 astrocytoma cells compared to primary astrocytes and the mRNA in the global cellular milieu of U-87 astrocytoma cells compared to primary astrocytes. Bar charts display the relative number (-log(p-value)) of mRNAs with a fold change >2.5 and were considered significant ($p<0.01$). RISC-IP mRNA were indicated with dark blue bars and the global mRNA were indicated with light blue bars. The threshold (yellow lines) were set at $p<0.01$ and were calculated using Fischer's exact p-value test using IPA software.

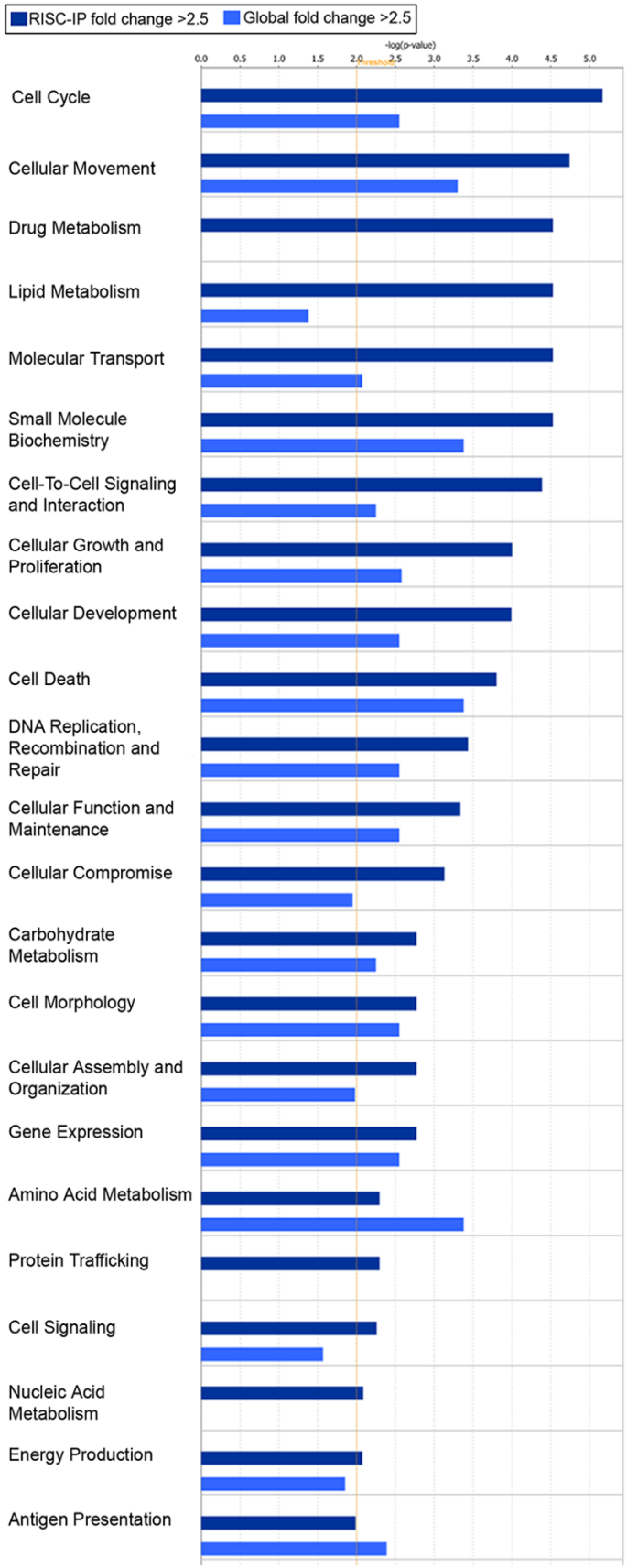

Figure 5.11: Molecular and cellular functional assessment of the mRNA in the RISC of U-87 astrocytoma cells compared to primary astrocytes and the mRNA in the global cellular milieu of U-87 astrocytoma cells compared to primary astrocytes. Bar charts display the relative number (-log(p-value)) of mRNAs with a fold change >2.5 and were considered significant ($p<0.01$). RISC-IP mRNA were indicated with dark blue bars and the global mRNA were indicated with light blue bars. The threshold (yellow lines) were set at $p<0.01$ and were calculated using Fischer's exact p-value test using IPA software.

5.2.6 Biological pathway analysis of miRNA and mRNA profile in U-87 astrocytoma RISC

RISC miRNA and mRNA microarray data was examined using IPA software to help appreciate the key mRNA-miRNA connections and biological pathways that were associated directly with the RISC and GW/P bodies (Figure 5.12). In this analysis, all selected miRNA had a fold change >±3 and all mRNA had a fold change >±2 (Figure 5.12). Each mRNA or miRNA was colored based upon the experimental expression level (i.e. green signified decreased expression and red specified increased expression) and the exact log2 fold change values were indicated below the molecule (Figure 5.12).

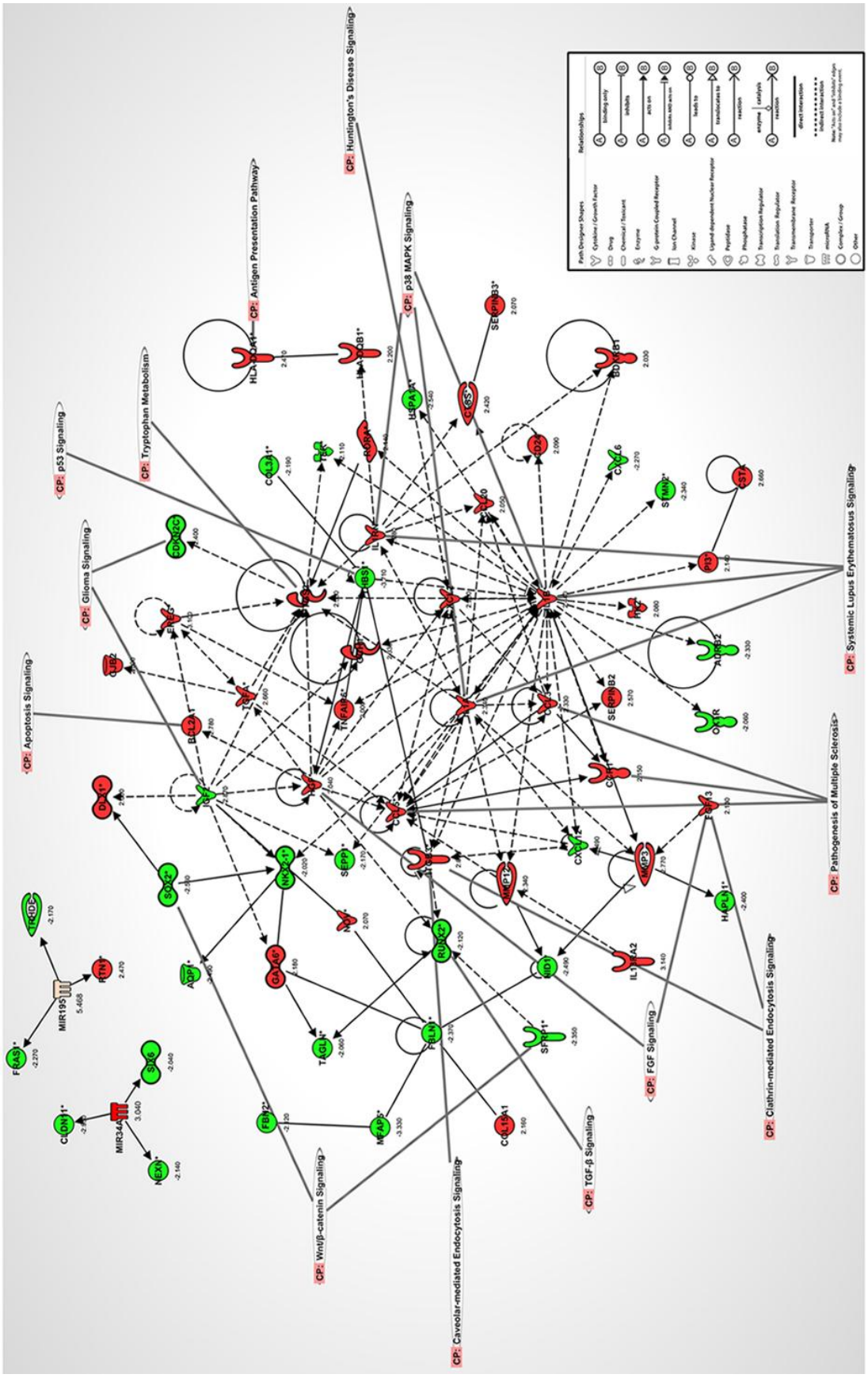
CP: Huntington's Disease Signaling
CP: Antigen Presentation Pathway
CP: p38 MAPK Signaling
CP: p53 Signaling
CP: Tryptophan Metabolism
CP: Glioma Signaling
CP: Apoptosis Signaling
CP: Systemic Lupus Erythematosus Signaling
CP: Pathogenesis of Multiple Sclerosis
CP: Clathrin-mediated Endocytosis Signaling
CP: Caveolar-mediated Endocytosis Signaling
CP: Wnt/β-catenin Signaling
CP: TGF-β Signaling
CP: FGF Signaling
Path Designer Shapes
Relationships

Figure 5.12: Biological pathway analysis showing the links between miRNA and mRNAs within RISC in U-87 astrocytoma cells compared to primary astrocytes using IPA software. All miRNA and mRNA were significantly expressed ($p<0.01$). MiRNA had a log2 fold change >3 and mRNA had a log2 fold change >2. Some key canonical pathways are indicated by labels.

As noted above, miR-34a levels were increased in U-87 astrocytoma RISC compared to primary astrocyte RISC with a log2 fold change of 3.040 (Figure 5.4D, Table 5.1, p-value $8.43x10^{-9}$). In U-87 astrocytoma RISC, increased miR-34a levels corresponded specifically with the significantly ($p<0.01$) decreased levels of miR-34a predicted targets: claudin 11 (CLDN11*, -2.950), nexilin F actin binding protein (NEXN*, -2.140) and six homeobox 6 (SIX6, -2.040) which have roles in cell adhesion, permeability, migration and proliferation (Figure 5.12, Table 5.6).

Table 5.6: Specific messenger RNA fold change linked to the increased levels of miR-34a in U-87 astrocytoma RISC.

Name	Entrez gene name	Fold Change	Role in cell	Canonical pathway/ Biological process	Entrez gene summary
CLDN11	claudin 11	-2.950	adhesion, permeability, sealing in, formation, migration, proliferation, sealing	leukocyte extravasation signaling, tight junction signaling, cell adhesion, spermatogenesis, axon ensheathment, calcium-independent cell-cell adhesion	The protein encoded by this gene belongs to the claudin family of tight junction associated proteins and is a major component of central nervous system myelin that is necessary for normal CNS function. There is growing evidence that the protein determines the permeability between layers of myelin sheaths via focal adhesion and, with its expression highly regulated during development, may play an important role in cellular proliferation and migration. In addition, the protein is a candidate autoantigen in the development of autoimmune demyelinating disease.
NEXN	nexilin (F actin binding protein)	-2.140	migration	regulation of cell migration, regulation of cytoskeleton organization	NEXN is a filamentous actin (F-actin)-binding protein that localizes to focal contacts and may be involved in cell adhesion and migration (Ohtsuka et al., 1998 [PubMed 9832551]; Wang et al., 2005 [PubMed 15823560]).
SIX6	SIX homeobox 6	-2.040	proliferation	regulation of transcription, DNA-dependent, multicellular organism development, visual perception, organ morphogenesis	The protein encoded by this gene is a homeobox protein that is similar to the Drosophila 'sine oculis' gene product. This gene is found in a cluster of related genes on chromosome 14 and is thought to be involved in eye development. Defects in this gene are a cause of isolated microphthalmia with cataract type 2 (MCOPCT2).

MiR-195 expression was also increased in U-87 astrocytoma GW/P bodies compared to primary astrocyte GW/P bodies with a log2 fold change of 5.468 (Figure 5.4D, Table 5.1, p-value $7.00x10^{-7}$). Increased miR-195 expression in U-87 astrocytoma RISC correlated with the significantly ($p<0.01$) decreased levels of miR-195 predicted targets: Fraser syndrome 1 (FRAS1*, -2.270) and thyrotropin-releasing hormone degrading enzyme (TRHDE, -2.170), which are involved in in cell communication and signalling (Figure 5.12, Table 5.7). MiR-195 is also predicted to silence reticulon 1 (RTN1*) which has a role in apoptosis, however the mRNA microarray results of our study show that RTN1* levels were increased by a log2 fold change of 2.470 in U-87 astrocytoma RISC, suggesting that miR-195 upregulation may have activated RTN1* (Figure 5.12, Table 5.7). Perhaps as in other cells, miR-195 function may have switched from repression to activation of target translation depending on the cell cycle status of astrocytoma cells (Vasudevan et al., 2008;Vasudevan et al., 2007;Vasudevan and Steitz, 2007). Since U-87 astrocytoma cells actively and rapidly proliferate in culture, it is unlikely that these cells had arrested and moved into quiescence (G_o) thereby questioning the potential activation role of miR-195. Indeed, rather than being activated, RTN1* was possibly stabilized by another binding protein that would prevent miR-195 from its repressive activity. Recent studies have suggested there are two populations of miRNA, one that positively correlates with its target mRNAs and others that negatively correlate with cognate targets (Nunez-Iglesias et al., 2010;Wang et al., 2009;Wang and Li, 2009). Thus, it is possible that miR-195 may have a dual function depending on the status of the mRNA target or where the mRNA is localized within the cell. This 'ying-yang' area of miRNA biology remains to be fully elucidated.

Table 5.7: Specific messenger RNA fold change linked to increased levels of miR-195 in U-87 astrocytoma RISC.

Name	Entrez gene name	Fold Change	Role in cell	Canonical pathway/ Biological process	Entrez gene summary
FRAS1	Fraser syndrome 1	-2.270	unknown	cell communication	This gene encodes an extracellular matrix protein that appears to function in the regulation of epidermal-basement membrane adhesion and organogenesis during development. Mutations in this gene cause Fraser syndrome, a multisystem malformation that can include craniofacial, urogenital and respiratory system abnormalities. Alternative splicing results in multiple transcript variants.
TRHDE	thyrotropin-releasing hormone degrading enzyme	-2.170	signaling	glutathione metabolism, proteolysis, signal transduction, cell-cell signaling	This gene encodes a member of the peptidase M1 family. The encoded protein is an extracellular peptidase that specifically cleaves and inactivates the neuropeptide thyrotropin-releasing hormone.
RTN1	reticulon 1	2.470	apoptosis	signal transduction, neuron differentiation	This gene belongs to the family of reticulon encoding genes. Reticulons are associated with the endoplasmic reticulum, and are involved in neuroendocrine secretion or in membrane trafficking in neuroendocrine cells. Alternatively spliced transcript variants encoding different isoforms have been identified. Multiple promoters rather than alternative splicing of internal exons seem to be involved in this diversity.

Beyond the 6 mRNAs targeted by miR-34a and miR-195, there were many mRNAs that were increased and decreased in U-87 astrocytoma RISC that were directly (solid black arrows) or indirectly (dashed black arrows) connected through another molecule within the same pathway (Figure 5.12). Central mRNAs with decreased expression in which 4 or more other mRNAs converged included insulin-like growth factor 2 (IGF2, -2.870), fibulin 1 (FBLN1*, -2.370), thrombospondin 1 (THBS1*, -3.710) and chemokine C-X-C motif ligand 12 (CXCL12*, -2.490) all of which have functions in apoptosis, proliferation and migration (Figure 5.12). Central mRNAs with increased expression in which 4 or more other mRNAs converged included epiregulin (EREG, 3.100), chemokine C-C motif ligand 3 (CCL3, 2.330), chemokine C-X-C motif ligand 2 (CXCL2, 2.250), interleukin 1 alpha (IL1A*, 2.340), interleukin 1 beta (IL1B*, 2.440), interleukin 1 receptor antagonist (IL1RN*, 2.280), tumor necrosis factor alpha induced protein factor 6 (TNFAIP6, 2.000), transforming growth factor alpha (TGFA*, 2.660), prostaglandin-endoperoxide synthase 2 (PTGS2*, 2.530), matrix metallopeptidase 3 (MMP3, 2.770) and matrix metallopeptidase 12 (MMP12, 2.340) which have functions in apoptosis, migration, proliferation and invasion (Figure 5.12). The mRNAs that are involved in key canonical pathways are indicated by labels and include Systemic Lupus Erythematosus signalling, p38 MAPK signalling, clathrin-mediated endocytosis signalling, pathogenesis of multiple sclerosis and others (Figure 5.12). The majority (>90%) of these mRNAs localized to U-87 astrocytoma RISC are associated with tumorigenesis and cancer (label not shown on biological pathway to avoid figure crowding), which suggests the miRNA-loaded RISC is a key regulator of mRNAs involved in cancer and cell cycle regulation in U-87 astrocytoma cells.

5.3 Summary and Conclusions

The hypothesis was the RISC-specific miRNA and mRNA components will not only differ between malignant and non-malignant cells of the same cell lineage, but will also differ between cells originating from different organs. In this study, evidence is provided that RISC contain miRNAs and mRNAs whose levels are increased or decreased compared to the global cellular miRNA and mRNA levels and differ in miRNA and mRNA composition between malignant and non-malignant cell types, although the overall functional impact of these differences remains to be elucidated. We suspect that the RISC-rich GW/P body microenvironment may serve to physically focus and more efficiently increase the expression of tumour suppressor miRNAs that may otherwise be too dispersed within the global cellular milieu of cancer cells to have a suppressive effect. In this way, miRNA could effectively repress target mRNA that are shuttled specifically to GW/P bodies. Shuttling downregulated miRNAs to the RISC within the microenvironment of GW/P bodies may prevent degradation of target mRNA while they are stored in structural GW/P bodies, however this hypotheses remain to be tested. Further RISC and GW/P body RNA component profiling is required. The current study provides a methodological framework that produced a set of unique profiles from human primary astrocytes and U-87 astrocytoma cells in which to start building the RISC-miRNA and RISC-mRNA component repository.

Chapter Six: **Conclusions, Limitations of Research Approach and Future Studies**

6.1 Conclusions

The studies undertaken to complete the objectives and test the initial hypotheses proposed for this thesis work have lead to the following conclusions:

Hypothesis #1: GW/P bodies are more highly expressed in astrocytoma cells than in primary astrocytes.

- GW/P bodies were found in the cell bodies and cytoplasmic projections of mouse brain astrocytes, cultured astrocytes isolated from the mouse hippocampus and human U-87 astrocytoma cells.
- GW/P bodies were more numerous in U-87 astrocytoma cells as compared to mouse brain astrocytes and cultured astrocytes. The exact reason for this increased GWP body expression in malignant cells has not been a goal of this thesis. It may be partly due to the rapidly proliferating characteristics of malignant cells in general. Lian *et al.* (2006) showed GW/P bodies are highly expressed in proliferating HeLa cells, disassemble prior to mitosis, start to reassemble in early G_1 phase and then increase in size and number in late S and G_2 phase (Lian et al., 2006). Recently, an immunohistochemical study by Yoo *et al.* (2010) showed that GW182 (and Ago2) proteins are more highly expressed in prostate and esophageal cancers compared to normal prostate and esophageal cells (Yoo et al., 2010). In normal human astrocyte culture 87.77% of cells are in G_1, 5.09% are in G_2 and 7.14% are in S phase (Figure 6.1A). However in malignant U-87 astrocytoma cell culture there are less cells in G_1 (62.70%) and more in G_2 (15.57%) and S (21.73%) phase compared to normal astrocytes (Figure 6.1B).

These cell cycle observations may account for the increased number of GW/P bodies observed in malignant U-87 astrocytoma cells compared to normal astrocytes because ~37% of astrocytoma cells are in S/G_2 phase where GW/P bodies are more numerous (compared to ~12% S/G_2 for astrocytes).

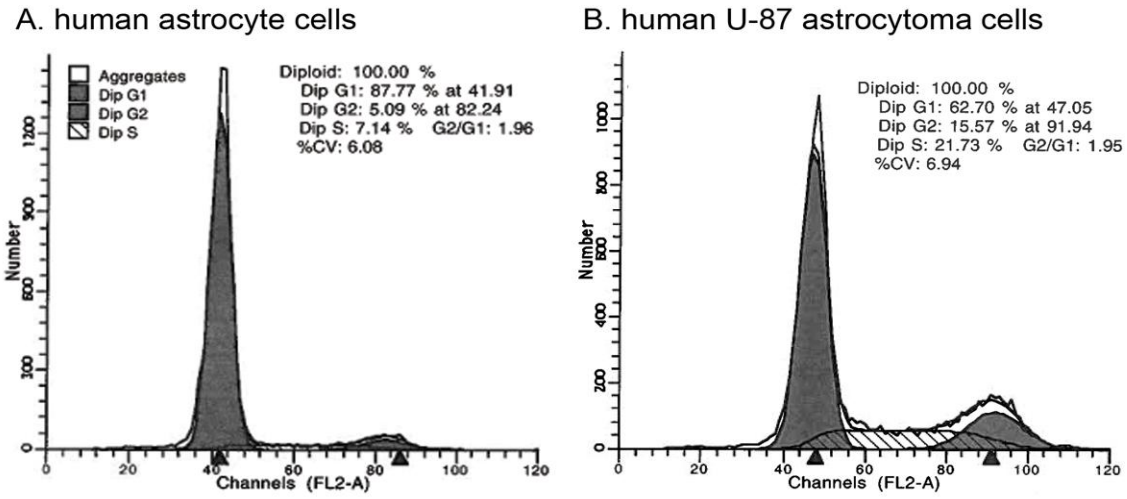

Figure 6.1: Cell cycle analysis showing the percentage of human (A) U-87 astrocytoma and (B) astrocyte cells in G_1, G_2 and S phase during normal growth conditions. Cells ($1x10^6$) were washed in PBS, resuspended in 500 µl PBS, fixed in 500 µl of 100% ethanol for 24 hours at 4°C, centrifuged, washed in PBS and resuspended in 500 µl propidium iodide staining buffer (50µg/ml propidium iodide, 0.1% Triton X-100, 0.2mg Dnase free Rnase A in PBS) for 45 min at RT prior to flow cytometry analysis.

<u>Hypothesis #2</u>: GW/P bodies will have significant heterogeneity in astrocytes and astrocytoma cells as evidenced by variable content of proteins involved in mRNA degradation, RNAi and mRNA transport and stabilization that colocalize to apparently different but overlapping subsets of GW/P bodies. The proteins involved in the various mRNA functions are expected to be co-immunoprecipiated by antibodies to GW/P body components in astrocytoma cells.

- Human astrocytoma GW/P bodies exhibited remarkable compositional heterogeneity as evidenced by varying percentages of these structures that colocalized with LSm4 (22%) and XRN1 (25%) as well as hAgo2 (27%) and Dicer (13%), key proteins involved in mRNA degradation and RNAi respectively. Similar percentages of GW/P colocalization were observed in mouse astrocytes with approximately 26% of GW/P bodies colocalized to LSm4.
- Human astrocytoma GW/P bodies also exhibited complex heterogeneity with varying percentages of colocalization with SYNCRIP (23%), FMRP (17%), hnRNPA1 (16%), Staufen (13%) and HuR (10%), key proteins involved in mRNA transport and stabilization. Similar percentages of GW/P colocalization were observed in mouse astrocytes with approximately 32% and 13% of GW/P bodies colocalized to SYNCRIP and hnRNPA1 respectively.
- A key to examining this hypothesis was the optimization of an IP-WB protocol for the immunoprecipitation of the GW182 protein and the RISC complex in order to determine the natural ligands of GW/P bodies/RISC complex. Employing the optimized IP-WB protocol in astrocytes and astrocytoma cells lead to the novel discovery that certain proteins are part of at least subsets of the GW/P

body/RISC complex. For example, subsets of GW/P bodies containing the GW182 and hAgo2 proteins immunoprecipitated the mRNA transport and stabilization proteins SYNCRIP, hnRNPA1 and FMRP. RISC (GW182/hAgo2) subsets of GW/P bodies also immunoprecipitated Dicer, hDcp, LSm4, XRN1, SYNCRIP and FMRP. Staufen colocalized with GW/P body foci, yet it was not immunoprecipitated along with GW182 and hAgo2 suggesting it is not a natural ligand of either GW182 or hAgo2.

Hypothesis #3: The GW/P body/RISC-specific miRNA profile will differ between human astrocytes and astrocytoma cells. MiRNAs involved in the repression of mRNAs involved in cancer progression pathways will have an increased expression level in astrocytoma cells compared to astrocytes.

- Unexpectedly, miRNAs were more highly enriched in astrocyte RISC compared to U-87 astrocytoma RISC indicating that primary astrocyte RISC may contain a relatively more diverse population of miRNAs and contain a greater number of individual miRNAs than U-87 astrocytoma RISC. These results suggest depletion or deregulation of the specific miRNA population in RISC could potentially have an important function in the malignant state.
- Astrocytoma and primary astrocyte cells each contained unique RISC miRNA profiles as compared to their respective cellular miRNA profiles.
- MiR-195, 10b, 29b, 19b, 34a and 455-3p levels were increased and the miR-181b level was decreased in U-87 astrocytoma RISC as compared to astrocyte RISC. Of these miRNAs, differential expression of miR-195, 10b, 19b, 34a and 181b

have been implicated in targeting mRNAs involved in cancer progression. These astrocytoma RISC miRNAs also play a predominant role in inflammatory disease, cancer and genetic disorders and to a lesser extent in neurological disease and connective tissue disorders. Astrocytoma RISC miRNAs also are predicted to play a role in various cellular processes including cellular compromise, development and growth and proliferation.

Hypothesis #4: The GW/P body/RISC-specific mRNA profile will be similar in human astrocytes and astrocytoma cells; however the mRNAs involved in cancer progression pathways will have an increased expression in astrocytoma GW/P bodies/RISC compared to astrocyte GW/P bodies/RISC.

- As expected, the RISC contained decreased levels of mRNAs in astrocyte and astrocytoma cells compared to global mRNA levels in these cells. Relative to global gene expression, U-87 astrocytoma and primary astrocyte RISC contained 93.9% of mRNA that were significantly ($p<0.01$) decreased and 6.1% of mRNA that were significantly ($p<0.01$) increased, suggesting that the majority of mRNAs targeted to RISC were downregulated. The small percentage (6.1%) of mRNAs that were upregulated in RISC may contain AREs that could potentially be activated by RISC-specific miRNA.
- A greater number of mRNAs were unique to the global cellular fraction and were not found within the RISC in U-87 astrocytoma as normalized and compared to primary astrocytes.

- The astrocytoma RISC contained less mRNAs than the global cellular fraction but specifically contained 15 decreased mRNAs and 7 increased mRNAs relative to the astrocyte RISC. Astrocytoma RISC were more highly enriched in mRNA that are involved in cancer, inflammatory, immunological and neurological disorders, among other diseases. Astrocytoma RISC were more highly enriched in mRNA components involved in multiple cell functions and processes including the cell cycle, cellular growth and proliferation, DNA replication, DNA recombination and repair, and cellular assembly and organization, among others.
- Biological pathway analysis showed that the majority (>90%) of mRNAs localized to astrocytoma RISC were associated with cancer.

6.2 Limitations of Research Approach

At the start of this thesis project, purified human primary astrocytes cells were not commercially available, so the study in Chapter Four relied on normal astrocytes cultured from mouse brain. Optimally, all the studies should have been performed using human astrocytes and compared them to the chosen human U87 astrocytoma cell line. However, no significant difference was noted between the GW/P body expression in mouse brain astrocytes, cultured mouse astrocytes and cultured human astrocytes. In addition, tissue culture cell lines are commonly used in research studies but have been reported to change and incorporate epigenetic mutations while in culture. During the course of experimentation, every attempt was made to ensure similar cell passage numbers were used for each experiment and no remarkable changes in GW/P body expression were noted; however future studies of GW/P body component expression would benefit from using tissue extracted from human brain tumours of varying pathological grade (i.e. World Health Organization (WHO) well-circumscribed grade 1 pilocytic astrocytomas, diffusely infiltrating grade 2 astrocytomas, grade 3 anaplastic astrocytomas and grade 4 glioblastoma multiforme tumours (Buckner et al., 2007)) and normal brain. Obtaining human brain tumour tissue would require obtaining ethics consent and, in our experience, has been complicated by limited availability at the University of Calgary. Even then, human brain tumour samples generally have a mixture of cell types (blood cells, fibroblasts, necrotic and apoptotic cells, etc.) so a homogeneous sample of astrocytoma cells would likely be difficult to obtain. In addition, obtaining a tumour with the grade of choice (i.e. grade IV) may be difficult since pathological diagnosis sometimes differs after a pathological review is conducted by an experienced neuropathologist (Buckner et

al., 2007). Obtaining normal astrocytes from human brain tissue would be even more difficult because cadaver tissues are typically not processed sooner than 4-5 hours post-mortem making observations on viable cells problematic.

Another limitation to the research approach was the use of static fixed and permeabilized cells to examine GW/P bodies which, as was demonstrated early in my research studies, move dynamically throughout the cell. In these studies, GW182 coupled to green fluorescent protein (GFP) was examined in transfected human astrocytes and U-87 astrocytoma cells; however these experiments showed an over-expression of GW/P bodies in transfected cells when compared to cells that were not transfected (Figure 6.2). This would likely have opened the question of the reliability and validity of real time imaging studies.

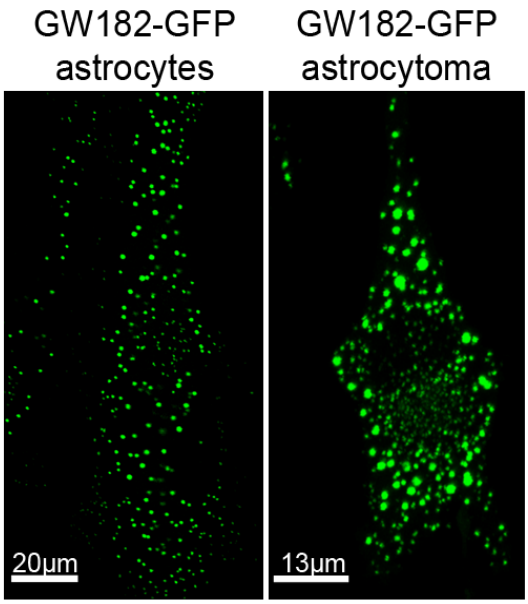

Figure 6.2: Transfected GW182-GFP expression in live human astrocytes and astrocytoma cells after 30 hours using Lipofectamine LTX with Plus reagent (Invitrogen). The GW182-GFP construct was a kind gift from Dr. Edward K.L. Chan (University of Florida, Gainesville, FL).

Nevertheless, when examining the real time dynamics of GW/P bodies in transfected GW182-GFP astrocytes and astrocytoma cells, their movement was relatively random but some foci moved distances of 2 – 3 µm over a 45 min period (Figure 6.3) and their average velocity was between 5.7 nm/sec - 5.9 nm/sec and ranged from 3 nm/sec to 12 nm/sec.

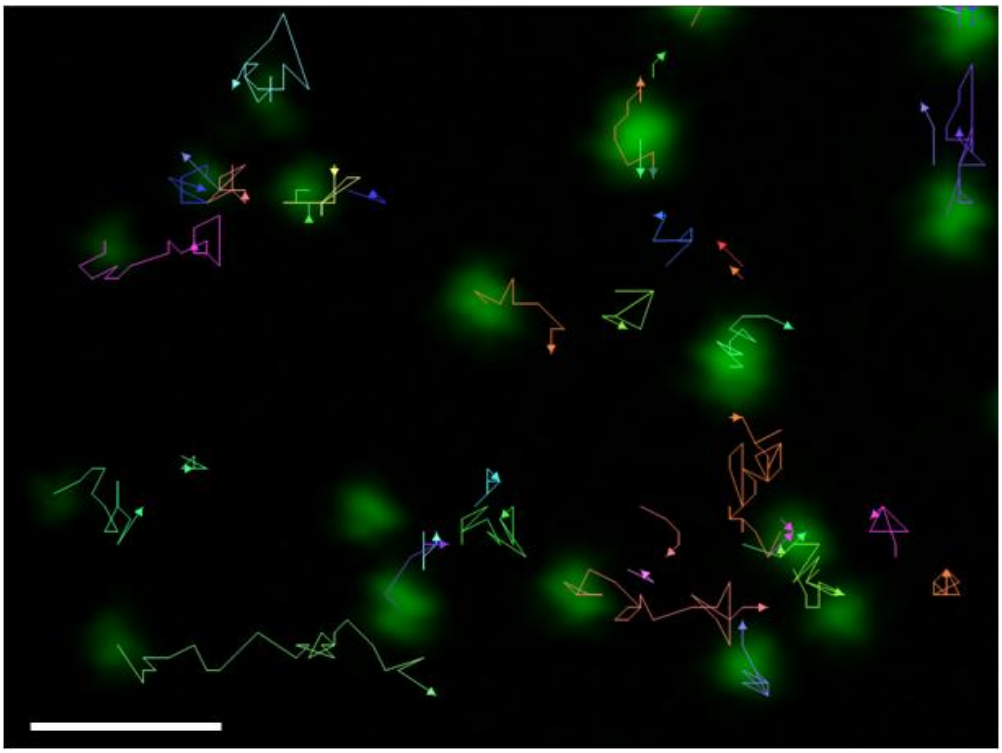

Figure 6.3: Directional tracking of GW182-GFP foci in live human astrocytes and astrocytoma using Volocity software (PerkinElmer, Woodbridge, ON). Astrocytes and astrocytoma cells were transfected with the GW182-GFP construct using Lipofectamine LTX with Plus reagent (Invitrogen) and imaged after 30 hours. Scale bar = 1.2µm.

Live cell imaging of dynamic GW/P bodies may be preferable to using fixed cell methods when examining movement. The basal/normal expression of GW/P bodies was

determined in each cell type and was preferable to the over-expressed GW/P bodies in the GW182-GFP transfected cells to examine the experimental objectives of this thesis.

6.3 Future Studies

Throughout the course of the experiments, it has become apparent that in attempting to answer any single question, many more have been generated that could easily form core studies of a productive post-doctoral fellowship, or another PhD thesis. Consequently, the field of GW/P body research would significantly benefit from 1) **basic research studies** focused on the components of GW/P bodies in neurons from the central and peripheral nervous systems at basal levels of function and physiologically relevant stimulatory excitation and 2) **clinical research studies** that examine other autoimmune diseases associated with GW/P bodies and the relevance of circulating antibodies to GW/P body protein components in disease initiation pathogenesis, and/or the immune mechanisms that lead to loss of tolerance to GW/P body autoantigens.

6.3.1 Basic Research Studies

Some new GW/P body associated proteins, mRNAs and miRNAs have been identified in astrocyte and astrocytoma cells in this thesis work. Future studies would benefit from a parallel analysis in CNS neurons and cells of the peripheral nervous system to examine if these GW/P body components are unique to astrocytes and astrocytoma cells or if they are common among all neural cells. GW/P body expression in peripheral nervous system dorsal root ganglion is currently being investigated in

collaboration with Dr. Doug Zochodne's lab in a murine diabetic neuropathy disease model.

Once the protein, mRNA and miRNA components of GW/P bodies had been investigated in cultured CNS neurons and compared to astrocyte GW/P body components, it would be interesting to investigate the change that occurs in GW/P bodies when physiologically relevant signals such as calcium (Ca^{2+}) influx occur in neurons and astrocytes. As discussed in Chapter One (section 1.4.1), synaptic stimulation of post-synaptic densities mediated by Ca^{2+} induced calpain activation released pre-miRNA, Dicer, FMRP and Ago2 from PSDs into the cytosol where activated Dicer cleaved pre-miRNA into mature miRNA (Lugli et al., 2005;Lugli et al., 2008). Lugli *et al.* (2005, 2008) did not examine the response of GW182 to Ca^{2+} induced calpain activation specifically, yet the data suggest mature miRNA in association with hAgo2 and GW182 are capable of regulating target mRNA perhaps within GW/P body components that may be present in the soluble components of synaptic fractions. It would be interesting to examine the effects of Ca^{2+} influx on GW182 and its interaction with Ago2 and FMRP within GW/P bodies. The hypothesis would be that excitatory stimulation would cause an increased number of GW/P bodies present in the postsynaptic neural cytosol and in astrocyte processes.

The hypothesis that Ca^{2+} influx can lead directly to an increase in miRNA-mediated translational repression may be complicated by two factors: (1) miRNAs have significant diversity within the nervous system and target a wide range of mRNAs and (2) synapses are not simply on-off switches that are involved in transmitting action potentials at a single moment in time. For example, neurons are often continually activated in a process

known as long term potentiation (LTP) which is thought to be important for certain aspects of physiology such as learning and memory. LTP is the long-lasting enhancement in communication between two neurons that results from stimulating them simultaneously. Regular activation of a synapse may activate certain miRNAs to translationally repress a subset of mRNAs while upregulating another subset of mRNAs. In any event, miRNAs would undoubtedly implement complex changes in the translational profile of dendritic mRNAs. For example, miRNAs in the postsynaptic cell may upregulate the translation of voltage-gated Ca^{2+} channels, metabotropic Ca^{2+} channels or signaling proteins such as calcium/calmodulin–dependent protein kinase that would ultimately enhance sensitivity to signals received from the presynaptic cell. Consequently, miRNAs may fine tune the translational response to synaptic activation by repressing the translation of some mRNA but not affecting other mRNA.

Another area of GW/P body biology that has yet to be elucidated is the functional role of phosphorylation of the GW182/TNRC6A, GW2/TNRC6B and GW3/TNRC6C paralogs. GW182 was shown to be a phosphoprotein when immunoprecipitated from HeLa cells labelled with [32P]orthophosphate using the index 18033 serum (Eystathioy et al., 2002a). However, to date, no studies have been published on the physiological role of phosphorylated versus unphosphorylated GW182, GW2 or GW3 proteins. A considered hypothesis is that phosphorylated GW182 protein may be the active hAgo2-binding form whereas unphosphorylated GW182 may be inactive and unable to bind to hAgo2. Interestingly, hAgo2 has been shown to be post-translationally modified by phosphorylation of serine-387 by the p38 MAPK (mitogen-activated protein kinase) signalling pathway, which when mutated to alanine, led to a reduction in localization of

hAgo2 to GW/P bodies (Zeng et al., 2008). This study by Zeng *et al.* (2008) suggested that phosphorylation of hAgo2 is essential for localization to GW/P bodies, but they did not specifically investigate if the phosphorylation state of hAgo2 influenced binding to GW182. In addition, this study suggested that hAgo2-mediated gene silencing may be linked to distinct signalling pathways and prompts the question of what signalling pathway phosphorylates GW182.

From protein colocalization studies, GW/P bodies are heterogeneous in protein composition and at any given time a subset of GW/P bodies may contain protein cargo that is different from another subset of GW/P bodies. The complete proteome of GW/P bodies as analyzed by mass spectrometry analysis has not yet been elucidated and, therefore, other functions of these important bodies remains to be discovered.

6.3.2 Clinical Research Studies

As the list of GW/P body-protein components expands, there is a continued effort to identify the autoimmune diseases associated with GW/P bodies which may provide clues to the etiology of these GW/P body-associated diseases. To date, numerous autoantigens within GW/P bodies include GW182/TNRC6A, GW2/TNRC6B, GW3/TNRC6C, Ge-1/Hedls/RCD8, hLSm1-7, Ago2/EIF2C2, Ro52/TRIM21, RAP55/LSm14A, Su and diacyl-phosphatidylethanolamine which have been correlated with clinical autoimmune disease (Table 6.1).

Table 6.1: Summary of GW/P body autoantigens as recognized by human sera with autoimmune diseases.

GW/P body Autoantigens	Autoimmune Disease	Reference
Ge-1/Hedls/RCD8	primary biliary cirrhosis (PBC)	(Bloch et al., 2005;Yu et al., 2005)
hLSm1-7 complex	SLE	(Eystathioy et al., 2002b)
GW182/TNRC6A	SLE/SjS/neurological symptoms[I]	(Eystathioy et al., 2002b;Eystathioy et al., 2003b;Bhanji et al., 2007)
Ago2/ EIF2C2	SLE/SjS/neurological symptoms[I]	(Bhanji et al., 2007)
GW2/TNRC6B	SjS, ataxia, SLE, sensory neuropathy, limited cutaneous systemic sclerosis (SSc), PBC, hypothyroidism	(Bhanji et al., 2007)
GW3/TNRC6C	SjS, arthritis, celiac disease, PBC, limited cutaneous SSc, hypothyroidism, neuropathy	(Bhanji et al., 2007)
Ro52/TRIM21	SjS	(Bhanji et al., 2007)
RAP55/LSm14A	PBC	(Marnef et al., 2009;Yang et al., 2006)
Su	SLE	(Jakymiw et al., 2006)
diacyl-phosphatidylethanolamine[II]	SLE, other autoimmune disease (no clinical anti-phospholipid syndrome	(Laurino et al., 2006)

[I]Neurological symptoms include ataxia, motor and sensory neuropathy.
[II]only partial colocalization with GW/P bodies.

The most common autoantigens targeted by patients containing autoantibodies to GW/P bodies were previously identified as Ge-1/Hedls (58%), GW182 (40%), and Ago2 (16%) (n=55) (Bhanji et al., 2007). Noteworthy is that 18% of GW/P body reactive sera did not react to any of the antigens analyzed suggesting that there are other target autoantigens yet to be discovered (Bhanji et al., 2007). Currently, studies are being initiated to examine if some of the other autoantigens recognized by anti-GW/P body positive humans sera may be directed against SYNCRIP, FMRP, LSm4, XRN1, TNGW1 (Li et al., 2008) and others.

The relevance of circulating antibodies to GW/P body protein components in disease onset, loss of tolerance to autoantigens and/or prognosis is currently unknown, however recent miRNA expression studies in RA (Nakasa et al., 2008;Pauley et al., 2008;Stanczyk et al., 2008) and SLE (Dai et al., 2007;Dai et al., 2009) patients suggests that there is an autoimmune response to key components of the RNAi/miRNA pathway (reviewed in (Pauley et al., 2009)). In future, it would be interesting to investigate the possibility that RNAi protein components of GW/P bodies may be involved in the pathogenesis of circulating antibodies. To answer this question, a study analyzing the genetic sequences of TNGW1, GW182 or hAgo2 in patients with autoantibodies to GW/P bodies to determine if genetic mutations exist that may alter post-transcriptional regulation of their respective proteins and perturb the integrity or miRNA regulatory function of GW/P bodies potentially leading to a loss of tolerance to these GW/P body autoantigens. Alternatively, gene alterations in the TNR (trinucleotide repeat) region of *TNRC6A*, for example, may simply alter the TNGW1 or GW182 protein enough to break B cell tolerance leading to autoantibodies and then intra- and inter-molecular epitope

spreading which would lead to the spectrum of GW/P body autoantibodies that have been described to date.

6.4 Concluding Comments

PhD thesis work in Dr. Fritzler's laboratory has been an immensely rewarding experience. Looking back, I have learned the skills and acquired knowledge essential for making what I believe is a significant contribution to the literature on GW/P bodies and the cell and molecular biology of astrocytes and astrocytomas. In addition to 'enjoyment of all things GWB', other investigations with Dr. JB Rattner into primary cilia expression in astrocytes and astrocytoma cells of varying malignancy grades has blossomed into two further first-authored publications (see Appendix 2 for a complete list of publications during thesis work). I look forward to continuing my academic research career and incorporating my love of science with my love of medicine as I enter Medical School at the University of Calgary in July 2010.

References

Aizer A, Brody Y, Ler LW, Sonenberg N, Singer RH, Shav-Tal Y (2008) The dynamics of mammalian P Body transport, assembly and disassembly *in vivo*. Mol Biol Cell 19:4154-4166.

Amiry-Moghaddam M, Ottersen OP (2003) The molecular basis of water transport in the brain. Nat Rev Neurosci 4:991-1001.

Anderson P, Kedersha N (2006) RNA granules. J Cell Biol 172:803-808.

Anderson P, Kedersha N (2009) RNA granules: post-transcriptional and epigenetic modulators of gene expression. Nat Rev Mol Cell Biol 10:430-436.

Andrei MA, Ingelfinger D, Heintzmann R, Achsel T, Rivera-Pomar R, Luhrmann R (2005) A role for eIF4E and eIF4E-transporter in targeting mRNPs to mammalian processing bodies. RNA 11:717-727.

Ares M, Jr., Proudfoot NJ (2005) The Spanish connection: Transcription and mRNA processing get even closer. Cell 120:163-166.

Aschrafi A, Cunningham BA, Edelman GM, Vanderklish PW (2005) The fragile X mental retardation protein and group I metabotropic glutamate receptors regulate levels of mRNA granules in brain. Proc Natl Acad Sci USA 102:2180-2185.

Ashraf SI, Kunes S (2006) A trace of silence: memory and microRNA at the synapse. Curr Opin Neurobiol 16:535-539.

Atasoy U, Watson J, Patel D, Keene JD (1998) ELAV protein HuA (HuR) can redistribute between nucleus and cytoplasm and is upregulated during serum stimulation and T cell activation. J Cell Sci 111:3145-3156.

Baillat D, Shiekhattar R (2009) Functional dissection of the human TNRC6 (GW182-related) family of proteins. Mol Cell Biol 29:4144-4155.

Bannai H, Fukatsu K, Mizutani A, Natsume T, Iemura S, Ikegami T, Inouie T, Mikoshiba K (2004) An RNA-interacting protein, SYNCRIP (heterogeneous nuclear ribonuclear protein Q1/NSAP1) is a component of mRNA granule transported with inositol 1,4,5-trisphosphate receptor type 1 mRNA in neuronal dendrites. J Biol Chem 279:53427-53434.

Barbee SA, Estes PS, Cziko AM, Hillebrand J, Luedeman RA, Coller JM, Johnson N, Howlett IC, Geng C, Ueda R, Brand AH, Newbury SF, Wilhelm JE, Levine RB,

Nakamura A, Parker R, Ramaswami M (2006) Staufen- and FMRP-containing neuronal RNPs are structurally and functionally related to somatic P Bodies. Neuron 52:997-1009.

Baroni TE, Chittur SV, George AD, Tenenbaum SA (2008) Advances in RIP-chip analysis : RNA-binding protein immunoprecipitation-microarray profiling. Methods Mol Biol 419:93-108.

Bashkirov VI, Scherthan H, Solinger JA, Buerstedde JM, Heyer WD (1997) A mouse cytoplasmic exoribonuclease (mXRN1p) with preference for G4 tetraplex substrates. J Cell Biol 136:761-773.

Behm-Ansmant I, Rehwinkel J, Doerks T, Stark A, Bork P, Izaurralde E (2006) mRNA degradation by miRNAs and GW182 requires both CCR4:NOT deadenylase and DCP1:DCP2 decapping complexes. Genes Dev 20:1885-1898.

Belanger G, Stocksley MA, Vandromme M, Schaeffer L, Furic L, DesGroseillers L, Jasmin BJ (2003) Localization of the RNA-binding proteins Staufen1 and Staufen2 at the mammalian neuromuscular junction. J Neurochem 86:669-677.

Bhanji R, Eystathioy T, Chan EKL, Bloch DB, Fritzler MJ (2007) Clinical and serological features of patients with autoantibodies to GW/P Bodies. Clin Immunol 123:247-256.

Bloch DB, Gulick T, Bloch KD, Yang WH (2006) Processing body autoantibodies reconsidered. RNA 12:707-709.

Bloch DB, Yu JH, Yang WH, Graeme-Cook F, Lindor KD, Viswanathan A, Bloch KD, Nakajima A (2005) The cytoplasmic dot staining pattern is detected in a subgroup of patients with primary biliary cirrhosis. J Rheumatol 32:477-483.

Bolstad BM, Irizarry RA, Astrand M, Speed TP (2003) A comparison of normalization methods for high density oligonucleotide array data based on variance and bias. Bioinformatics 19:185-193.

Brengues M, Teixeira D, Parker R (2005) Movement of eukaryotic mRNAs between polysomes and cytoplasmic processing bodies. Science 310:486-489.

Brennan CM, Steitz JA (2001) HuR and mRNA stability. Cell Mol Life Sci 58:266-277.

Buckner JC, Brown PD, O'Neill BP, Meyer FB, Wetmore CJ, Uhm JH (2007) Central nervous system tumors. Mayo Clin Proc 82:1271-1286.

Calin GA, Croce CM (2006) MicroRNA signatures in human cancers. Nat Rev Cancer 6:857-866.

Calin GA, Sevignani C, Dumitru CD, Hyslop T, Noch E, Yendamuri S, Shimizu M, Rattan S, Bullrich F, Negrini M, Croce CM (2004) Human microRNA genes are

frequently located at fragile sites and genomic regions involved in cancers. Proc Natl Acad Sci USA 101:2999-3004.

Chan JA, Krichevsky AM, Kosik KS (2005) MicroRNA-21 is an antiapoptotic factor in human glioblastoma cells. Cancer Res 65:6029-6033.

Chang TC, Wentzel EA, Kent OA, Ramachandran K, Mullendore M, Lee KH, Feldmann G, Yamakuchi M, Ferlito M, Lowenstein CJ, Arking DE, Beer MA, Maitra A, Mendell JT (2007) Transactivation of miR-34a by p53 broadly influences gene expression and promotes apoptosis. Mol Cell 26:745-752.

Christoffersen NR, Shalgi R, Frankel LB, Leucci E, Lees M, Klausen M, Pilpel Y, Nielsen FC, Oren M, Lund AH (2009) p53-independent upregulation of miR-34a during oncogene-induced senescence represses MYC. Cell Death Differ 17:236-245.

Chu CY, Rana TM (2006) Translation repression in human cells by microRNA-induced gene silencing requires RCK/p54. PLoS Biol 4:e210.

Ciafre SA, Galardi S, Mangiola A, Ferracin M, Liu CG, Sabatino G, Negrini M, Maira G, Croce CM, Farace MG (2005) Extensive modulation of a set of microRNAs in primary glioblastoma. Biochem Biophys Res Commun 334:1351-1358.

Cougot N, Babajko S, Seraphin B (2004) Cytoplasmic foci are sites of mRNA decay in human cells. J Cell Biol 165:31-40.

Cougot N, Bhattacharyya SN, Tapia-Arancibia L, Bordonne R, Filipowicz W, Bertrand E, Rage F (2008) Dendrites of mammalian neurons contain specialized P-Body-like structures that respond to neuronal activation. J Neurosci 28:13793-13804.

Dai Y, Huang YS, Tang M, Lv TY, Hu CX, Tan YH, Xu ZM, Yin YB (2007) Microarray analysis of microRNA expression in peripheral blood cells of systemic lupus erythematosus patients. Lupus 16:939-946.

Dai Y, Sui W, Lan H, Yan Q, Huang H, Huang Y (2009) Comprehensive analysis of microRNA expression patterns in renal biopsies of lupus nephritis patients. Rheumatol Int 29:749-754.

Dijkstra MK, van Lom K, Tielemans D, Elstrodt F, Langerak AW, Veer MB, Jongen-Lavrencic M (2008) 17p13//TP53 deletion in B-CLL patients is associated with microRNA-34a downregulation. Leukemia 23:625-627.

Ding L, Spencer A, Morita K, Han M (2005) The developmental timing regulator AIN-1 interacts with miRISCs and may target the Argonaute protein ALG-1 to cytoplasmic P Bodies in *C. elegans*. Mol Cell 19:437-447.

Dutta KK, Zhong Y, Liu YT, Yamada T, Akatsuka S, Hu Q, Yoshihara M, Ohara H, Takehashi M, Shinohara T, Masutani H, Onuki J, Toyokuni S (2007) Association of

microRNA-34a overexpression with proliferation is cell type-dependent. Cancer Science 98:1845-1852.

Eddy EM (1975) Germ plasm and the differentiation of the germ cell line. Int Rev Cytol 43:229-80.:229-280.

Eulalio A, Behm-Ansmant I, Izaurralde E (2007) P bodies: at the crossroads of post-transcriptional pathways. Nat Rev Mol Cell Biol 8:9-22.

Eulalio A, Helms S, Fritzsch C, Fauser M, Izaurralde E (2009a) A C-terminal silencing domain in GW182 is essential for miRNA function. RNA 15:1067-1077.

Eulalio A, Huntzinger E, Izaurralde E (2008) GW182 interaction with Argonaute is essential for miRNA-mediated translational repression and mRNA decay. Nat Struct Mol Biol 15:346-353.

Eulalio A, Huntzinger E, Nishihara T, Rehwinkel J, Fauser M, Izaurralde E (2009b) Deadenylation is a widespread effect of miRNA regulation. RNA 15:21-32.

Eulalio A, Tritschler F, Buttner R, Weichenrieder O, Izaurralde E, Truffault V (2009c) The RRM domain in GW182 proteins contributes to miRNA-mediated gene silencing. Nucleic Acids Res 37:2974-2983.

Eulalio A, Tritschler F, Izaurralde E (2009d) The GW182 protein family in animal cells: New insights into domains required for miRNA-mediated gene silencing. RNA 15:1433-1442.

Eystathioy T, Chan EKL, Mahler M, Luft LM, Fritzler ML, Fritzler MJ (2003a) A panel of monoclonal antibodies to cytoplasmic GW bodies and the mRNA binding protein GW182. Hybridoma & Hybridomics 22:79-86.

Eystathioy T, Chan EKL, Tenenbaum SA, Keene JD, Griffith KJ, Fritzler MJ (2002a) A phosphorylated cytoplasmic autoantigen, GW182, associates with a unique population of human mRNAs within novel cytoplasmic speckles. Mol Biol Cell 13:1338-1351.

Eystathioy T, Chan EKL, Yang Z, Takeuchi K, Mahler M, Luft LM, Zochodne DW, Fritzler MJ (2003b) Clinical and serological associations of autoantibodies to a novel cytoplasmic autoantigen, GW182 and GW bodies. J Mol Med 81:811-818.

Eystathioy T, Jakymiw A, Chan EKL, Séraphin B, Cougot N, Fritzler MJ (2003c) The GW182 protein co-localizes with mRNA degradation associated proteins hDcp1 and hLSm4 in cytoplasmic GW bodies. RNA 9:1171-1173.

Eystathioy T, Peebles C, Hamel JC, Vaughan JH, Chan EKL (2002b) Autoantibody to hLSm4 and the hepatameric LSm complex in anti-Sm sera. Arthritis Rheum 46:726-734.

Fan XC, Steitz JA (1998) Overexpression of HuR, a nuclear-cytoplasmic shuttling protein, increases the in vivo stability of ARE-containing mRNAs. EMBO J 17:3448-3460.

Farina C, Aloisi F, Meinl E (2007) Astrocytes are active players in cerebral innate immunity. Trends Immunol 28:138-145.

Fenger-Gron M, Fillman C, Norrild B, Lykke-Andersen J (2005) Multiple processing body factors and the ARE binding protein TTP activate mRNA decapping. Mol Cell 20:905-915.

Fierro-Monti I, Mohammed S, Matthiesen R, Santoro R, Burns JS, Williams DJ, Proud CG, Kassem M, Jensen ON, Roepstorff P (2006) Quantitative proteomics identifies Gemin5, a scaffolding protein involved in ribonucleoprotein assembly, as a novel partner for eukaryotic initiation factor 4E. J Proteome Res 5:1367-1378.

Friedman RC, Farh KK, Burge CB, Bartel DP (2009) Most mammalian mRNAs are conserved targets of microRNAs. Genome Res 19:92-105.

Fritzler MJ (1996) Clinical relevance of autoantibodies in systemic rheumatic diseases. Mol Biol Rep 23:133-145.

Gallardo E, Navarro A, Vinolas N, Marrades RM, Diaz T, Gel B, Quera A, Bandres E, Garcia-Foncillas J, Ramirez J, Monzo M (2009) miR-34a as a prognostic marker of relapse in surgically resected non-small-cell lung cancer. Carcinogenesis 30:1903-1909.

Gao X, Gulari E, Zhou X (2004) In situ synthesis of oligonucleotide microarrays. Biopolymers 73:579-596.

Gibbings DJ, Ciaudo C, Erhardt M, Voinnet O (2009) Multivesicular bodies associate with components of miRNA effector complexes and modulate miRNA activity. Nat Cell Biol 11:1143-1149.

Gregory RI, Chendrimada TP, Cooch N, Shiekhattar R (2005) Human RISC couples microRNA biogenesis and posttranscriptional gene silencing. Cell 123:631-640.

Griffis ER, Stuurman N, Vale RD (2007) Spindly, a novel protein essential for silencing the spindle assembly checkpoint, recruits dynein to the kinetochore. J Cell Biol 177:1005-1015.

Griffiths MR, Gasque P, Neal JW (2009) The multiple roles of the innate immune system in the regulation of apoptosis and inflammation in the brain. J Neuropathol Exp Neurol 68:217-226.

Guessous F, Zhang Y, Kofman A, Catania A, Li Y, Schiff D, Purow B, Abounader R (2010) microRNA-34a is tumor suppressive in brain tumors and glioma stem cells. Cell Cycle 9:[Epub ahead of print].

He L, He X, Lim LP, de Stanchina E, Xuan Z, Liang Y, Xue W, Zender L, Magnus J, Ridzon D, Jackson AL, Linsley PS, Chen C, Lowe SW, Cleary MA, Hannon GJ (2007a) A microRNA component of the p53 tumour suppressor network. Nature 447:1130-1134.

He L, He X, Lowe SW, Hannon GJ (2007b) microRNAs join the p53 network - another piece in the tumour-suppression puzzle. Nat Rev Cancer 7:819-822.

He L, Thomson JM, Hemann MT, Hernando-Monge E, Mu D, Goodson S, Powers S, Cordon-Cardo C, Lowe SW, Hannon GJ, Hammond SM (2005) A microRNA polycistron as a potential human oncogene. Nature 435:828-833.

Helmuth L (2001) Neuroscience. Glia tell neurons to build synapses. Science 291:569-570.

Hillebrand J, Barbee SA, Ramaswami M (2007) P-body components, microRNA regulation, and synaptic plasticity. ScientificWorldJournal 7:178-190.

Hirokawa N (2006) mRNA transport in dendrites: RNA granules, motors, and tracks. J Neurosci 26:7139-7142.

Ikeda K, Satoh M, Pauley KM, Fritzler MJ, Reeves WH, Chan EK (2006) Detection of the argonaute protein Ago2 and microRNAs in the RNA induced silencing complex (RISC) using a monoclonal antibody. J Immunol Methods 317:38-44.

Ingelfinger D, Arndt-Jovin DJ, Luhrmann R, Achsel T (2002) The human LSm1-7 proteins colocalize with the mRNA-degrading enzymes Dcp1/2 and Xrnl in distinct cytoplasmic foci. RNA 8:1489-1501.

Iorio MV, Ferracin M, Liu CG, Veronese A, Spizzo R, Sabbioni S, Magri E, Pedriali M, Fabbri M, Campiglio M, Ménard S, Palazzo JP, Rosenberg A, Musiani P, Volinia S, Nenci I, Calin GA, Querzoli P, Negrini M, Croce CM (2005) MicroRNA gene expression deregulation in human breast cancer. Cancer Res 65:7065-7070.

Iorio MV, Visone R, Di Leva G, Donati V, Petrocca F, Casalini P, Taccioli C, Volinia S, Liu CG, Alder H, Calin GA, Menard S, Croce CM (2007) MicroRNA signatures in human ovarian cancer. Cancer Res 67:8699-8707.

Irizarry RA, Hobbs B, Collin F, Beazer-Barclay YD, Antonellis KJ, Scherf U, Speed TP (2003) Exploration, normalization, and summaries of high density oligonucleotide array probe level data. Biostatistics 4:249-264.

Jakymiw A, Eystathioy T, Satoh M, Hamel JC, Fritzler MJ, Chan EKL (2005) Disruption of GW bodies impairs mammalian mRNA interference. Nat Cell Biol 7:1167-1174.

Jakymiw A, Ikeda K, Fritzler MJ, Reeves WH, Satoh M, Chan EK (2006) Autoimmune targeting of key components of RNA interference. Arthritis Res Ther 8:R87.

Jakymiw A, Pauley KM, Li S, Ikeda K, Lian S, Eystathioy T, Satoh M, Fritzler MJ, Chan EKL (2007) The role of GW/P bodies in RNA processing and silencing. J Cell Sci 120:1317-1323.

Jin P, Zarnescu DC, Ceman S, Nakamoto M, Mowrey J, Jongens TA, Nelson DL, Moses K, Warren ST (2004) Biochemical and genetic interaction between the fragile X mental retardation protein and the microRNA pathway. Nat Neurosci 7:113-117.

Kanai Y, Dohmae N, Hirokawa N (2004) Kinesin transports RNA: isolation and characterization of an RNA-transporting granule. Neuron 19:513-525.

Kedersha N, Stoecklin G, Ayodele M, Yacono P, Lykke-Andersen J, Fritzler MJ, Scheuner D, Kaufman RJ, Golan DE, Anderson P (2005) Stress granules and processing bodies are dynamically linked sites of mRNP remodeling. J Cell Biol 169:871-884.

Keene JD (1999) Why is Hu where? Shuttling of early-response-gene messenger RNA subsets. Proc Natl Acad Sci USA 96:14085-14090.

Kiebler MA, Bassell GJ (2006) Neuronal RNA granules: movers and makers. Neuron 51:685-690.

Kohrmann M, Luo M, Kaether C, DesGroseillers L, Dotti CG, Kiebler MA (1999) Microtubule-dependent recruitment of Staufen-green fluorescent protein into large RNA-containing granules and subsequent dendritic transport in living hippocampal neurons. Mol Biol Cell 10:2945-2953.

Korzhevskii DE, Otellin VA, Grigor'ev IP (2005) Glial fibrillary acidic protein in astrocytes in the human neocortex. Neurosci Behav Physiol 35:789-792.

Krichevsky AM, Kosik KS (2001) Neuronal RNA granules: a link between RNA localization and stimulation-dependent translation. Neuron 32:683-696.

Laurino CFC, Fritzler MJ, Mortara RA, Silva NP, Almeida IC, Andrade LEC (2006) Human autoantibodies to diacyl-phosphatidylethanolamine recognize a specific set of discrete cytoplasmic domains. Clin Exp Immunol 143:572-584.

Lazzaretti D, Tournier I, Izaurralde E (2009) The C-terminal domains of human TNRC6A, TNRC6B, and TNRC6C silence bound transcripts independently of Argonaute proteins. RNA 15:1059-1066.

Lee YS, Dutta A (2009) MicroRNAs in cancer. Annu Rev Pathol 4:199-227.

Lee YS, Pressman S, Andress AP, Kim K, White JL, Cassidy JJ, Li X, Lubell K, Lim DH, Cho IS, Nakahara K, Preall JB, Bellare P, Sontheimer EJ, Carthew RW (2009) Silencing by small RNAs is linked to endosomal trafficking. Nat Cell Biol 11:1150-1156.

Leung AK, Calabrese JM, Sharp PA (2006) Quantitative analysis of Argonaute protein reveals microRNA-dependent localization to stress granules. Proc Natl Acad Sci U S A 103:18125-18130.

Li N, Fu H, Tie Y, Hu Z, Kong W, Wu Y, Zheng X (2009a) miR-34a inhibits migration and invasion by down-regulation of c-Met expression in human hepatocellular carcinoma cells. Cancer Let 275:44-53.

Li S, Lian SL, Moser JJ, Fritzler ML, Fritzler MJ, Satoh M, Chan EKL (2008) Identification of GW182 and its novel isoform TNGW1 as translational repressors in Ago-2-mediated silencing. J Cell Sci 121:4134-4144.

Li Y, Guessous F, Zhang Y, DiPierro C, Kefas B, Johnson E, Marcinkiewicz L, Jiang J, Yang Y, Schmittgen TD, Lopes B, Schiff D, Purow B, Abounader R (2009b) MicroRNA-34a inhibits glioblastoma growth by targeting multiple oncogenes. Cancer Res 69:7569-7576.

Lian S, Jakymiw A, Eystathioy T, Hamel JC, Fritzler MJ, Chan EK (2006) GW Bodies, microRNAs and the cell cycle. Cell Cycle 5:242-245.

Lian SL, Li S, Abadal GX, Pauley BA, Fritzler MJ, Chan EK (2009) The C-terminal half of human Ago2 binds to multiple GW-rich regions of GW182 and requires GW182 to mediate silencing. RNA 15:804-813.

Liu J, Carmell MA, Rivas FV, Marsden CG, Thomson JM, Song JJ, Hammond SM, Joshua-Tor L, Hannon GJ (2004) Argonaute2 is the catalytic engine of mammalian RNAi. Science 305:1437-1441.

Liu J, Rivas FV, Wohlschlegel J, Yates JR, III, Parker R, Hannon GJ (2005a) A role for the P-body component GW182 in microRNA function. Nat Cell Biol 7:1161-1166.

Liu J, Valencia-Sanchez MA, Hannon GJ, Parker R (2005b) MicroRNA-dependent localization of targeted mRNAs to mammalian P-bodies. Nat Cell Biol 7:719-723.

Lu J, Getz G, Miska EA, varez-Saavedra E, Lamb J, Peck D, Sweet-Cordero A, Ebert BL, Mak RH, Ferrando AA, Downing JR, Jacks T, Horvitz HR, Golub TR (2005) MicroRNA expression profiles classify human cancers. Nature 435:834-838.

Luft LM (2005) Thesis Dissertation: Characterization of GWBs in Breast Cancer. University of Calgary.

Lugli G, Larson J, Martone ME, Jones Y, Smalheiser NR (2005) Dicer and eIF2c are enriched at postsynaptic densities in adult mouse brain and are modified by neuronal activity in a calpain-dependent manner. J Neurochem 94:896-905.

Lugli G, Torvik VI, Larson J, Smalheiser NR (2008) Expression of microRNAs and their precursors in synaptic fractions of adult mouse forebrain. J Neurochem 106:650-661.

Ma L, Teruya-Feldstein J, Weinberg RA (2007) Tumour invasion and metastasis initiated by microRNA-10b in breast cancer. Nature 449:682-688.

Mansfield KD, Keene JD (2009) The ribonome: a dominant force in co-ordinating gene expression. Biol Cell 101:169-181.

Marnef A, Sommerville J, Ladomery MR (2009) RAP55: Insights into an evolutionarily conserved protein family. Int J Biochem Cell Biol 41:977-981.

Matranga C, Tomari Y, Shin C, Bartel DP, Zamore PD (2005) Passenger-strand cleavage facilitates assembly of siRNA into Ago2-containing RNAi enzyme complexes. Cell 123:607-620.

Mazroui R, Huot ME, Tremblay S, Filion C, Labelle Y, Khandjian EW (2002) Trapping of messenger RNA by Fragile X Mental Retardation protein into cytoplasmic granules induces translation repression. Human Molecular Genetics 11:3007-3017.

McLellan A (2009) Exosome release by primary B cells. Crit Rev Immunol 29:203-217.

Meister G, Landthaler M, Peters L, Chen PY, Urlaub H, Luhrmann R, Tuschl T (2005) Identification of novel Argonaute-associated proteins. Curr Biol 15:2149-2155.

Meister G, Tuschl T (2004) Mechanisms of gene silencing by double-stranded RNA. Nature 431:343-349.

Meng F, Henson R, Wehbe-Janek H, Ghoshal K, Jacob ST, Patel T (2007) MicroRNA-21 regulates expression of the PTEN tumor suppressor gene in human hepatocellular cancer. Gastroenterol 133:647-658.

Moser JJ, Chan EK, Fritzler MJ (2009) Optimization of immunoprecipitation-western blot analysis in detecting GW182-associated components of GW/P bodies. Nat Protoc 4:674-685.

Moser JJ, Eystathioy T, Chan EKL, Fritzler MJ (2007) Markers of mRNA stabilization and degradation, and RNAi within astrocytoma GW bodies. J Neurosci Res 85:3619-3631.

Moser JJ, Fritzler MJ (2010) Cytoplasmic ribonucleoprotein (RNP) bodies and their relationship to GW/P bodies. Int J Biochem Cell Biol 42:828-843.

Musunuru K, Darnell RB (2001) Paraneoplastic neurologic disease antigens: RNA-binding proteins and signaling proteins in neuronal degeneration. Ann Rev Neurosci 24:239-262.

Nakasa T, Miyaki S, Okubo A, Hashimoto M, Nishida K, Ochi M, Asahara H (2008) Expression of microRNA-146 in rheumatoid arthritis synovial tissue. Arthritis Rheum 58:1284-1292.

Navarro F, Gutman D, Meire E, Caceres M, Rigoutsos I, Bentwich Z, Lieberman J (2009) miR-34a contributes to megakaryocytic differentiation of K562 cells independently of p53. Blood 114:2181-2192.

Nedergaard M, Ransom B, Goldman SA (2003) New roles for astrocytes: redefining the functional architecture of the brain. Trends Neurosci 26:523-530.

Newman EA (2003) New roles for astrocytes: regulation of synaptic transmission. Trends Neurosci 26:536-542.

Nunez-Iglesias J, Liu CC, Morgan TE, Finch CE, Zhou XJ (2010) Joint genome-wide profiling of miRNA and mRNA expression in Alzheimer's disease cortex reveals altered miRNA regulation. PLoS ONE 5:e8898.

O'Donnell KA, Wentzel EA, Zeller KI, Dang CV, Mendell JT (2005) c-Myc-regulated microRNAs modulate E2F1 expression. Nature 435:839-843.

Pare JM, Tahbaz N, Lopez-Orozco J, Lapointe P, Lasko P, Hobman TC (2009) Hsp90 regulates the function of Argonaute 2 and its recruitment to stress granules and P-bodies. Mol Biol Cell 20:3273-3284.

Parker R, Sheth U (2007) P bodies and the control of mRNA translation and degradation. Mol Cell 25:635-646.

Pauley KM, Cha S, Chan EK (2009) MicroRNA in autoimmunity and autoimmune diseases. J Autoimmun 32:189-194.

Pauley KM, Eystathioy T, Jakymiw A, Hamel JC, Fritzler MJ, Chan EK (2006) Formation of GW bodies is a consequence of microRNA genesis. EMBO Rep 7:904-910.

Pauley KM, Satoh M, Chan AL, Bubb MR, Reeves WH, Chan EK (2008) Upregulated miR-146a expression in peripheral blood mononuclear cells from rheumatoid arthritis patients. Arthritis Res Ther 10:R101.

Peng SS, Chen CY, Xu N, Shyu AB (1998) RNA stabilization by the AU-rich element binding protein, HuR, an ELAV protein. EMBO J 17:3461-3470.

Perl A (2009) Emerging new pathways of pathogenesis and targets for treatment in systemic lupus erythematosus and Sjogren's syndrome. Curr Opin Rheumatol 21:443-447.

Pillai RS, Bhattacharyya SN, Artus CG, Zoller T, Cougot N, Basyuk E, Bertrand E, Filipowicz W (2005) Inhibition of translational initiation by Let-7 microRNA in human cells. Science 309:1573-1576.

Rabinowits G, Gercel-Taylor C, Day JM, Taylor DD, Kloecker GH (2009) Exosomal microRNA: a diagnostic marker for lung cancer. Clin Lung Cancer 10:42-46.

Rana TM (2007) Illuminating the silence: understanding the structure and function of small RNAs. Nat Rev Mol Cell Biol 8:23-36.

Raver-Shapira N, Marciano E, Meiri E, Spector Y, Rosenfeld N, Moskovits N, Bentwich Z, Oren M (2007) Transcriptional activation of miR-34a contributes to p53-mediated apoptosis. Mol Cell 26:731-743.

Rehwinkel J, Behm-Ansmant I, Gatfield D, Izaurralde E (2005) A crucial role for GW182 and the DCP1:DCP2 decapping complex in miRNA-mediated gene silencing. RNA 11:1640-1647.

Roegiers F (2003) Insights into mRNA transport in neurons. Proc Natl Acad Sci USA 100:1465-1466.

Rosen A, Casciola-Rosen L (2009) Autoantigens in systemic autoimmunity: critical partner in pathogenesis. J Intern Med 265:625-631.

Sasayama T, Nishihara M, Kondoh T, Hosoda K, Kohmura E (2009) MicroRNA-10b is overexpressed in malignant glioma and associated with tumor invasive factors, uPAR and RhoC. Int J Cancer 125:1407-1413.

Scheller N, Resa-Infante P, de la Luna S, Galao RP, Albrecht M, Kaestner L, Lipp P, Lengauer T, Meyerhans A, Diez J (2007) Identification of PatL1, a human homolog to yeast P body component Pat1. Biochim Biophys Acta 1773:1786-1792.

Schipke CG, Kettenmann H (2004) Astrocyte responses to neuronal activity. Glia 47:226-232.

Schratt GM, Tuebing F, Nigh EA, Kane CG, Sabatini ME, Kiebler M, Greenberg ME (2006) A brain-specific microRNA regulates dendritic spine development. Nature 439:283-289.

Sen GL, Blau HM (2005) Argonaute 2/RISC resides in sites of mammalian mRNA decay known as cytoplasmic bodies. Nat Cell Biol 7:633-636.

Serman A, LeRoy F., Aigueperse C, Kress M, Dautry F, Weil D (2007) GW body disassembly triggered by siRNAs independently of their silencing activity. Nucleic Acids Res 35:4715-4727.

Sheth U, Parker R (2003) Decapping and decay of messenger RNA occur in cytoplasmic processing bodies. Science 300:805-808.

Simpson RJ, Lim JW, Moritz RL, Mathivanan S (2009) Exosomes: proteomic insights and diagnostic potential. Expert Rev Proteomics 6:267-283.

Sossin WS, DesGroseillers L (2006) Intracellular trafficking of RNA in neurons. Traffic 7:1581-1589.

Souquere S, Mollet S, Kress M, Dautry F, Pierron G, Weil D (2009) Unravelling the ultrastructure of stress granules and associated P-bodies in human cells. J Cell Sci 122:3619-3626.

St Johnston D (2005) Moving messages: The intracellular localization of mRNAs. Nat Rev Mol Cell Biol 6:363-375.

Stanczyk J, Pedrioli DM, Brentano F, Sanchez-Pernaute O, Kolling C, Gay RE, Detmar M, Gay S, Kyburz D (2008) Altered expression of MicroRNA in synovial fibroblasts and synovial tissue in rheumatoid arthritis. Arthritis Rheum 58:1001-1009.

Stinton LM, Eystathioy T, Selak S, Chan EKL, Fritzler MJ (2004) Autoantibodies to protein transport and messenger RNA processing pathways: Endosomes, lysosomes, Golgi complex, proteasomes, assemblyosomes, exosomes and GW Bodies. Clin Immunol 110:30-44.

Su H, Yang JR, Xu T, Huang J, Xu L, Yuan Y, Zhuang SM (2009) MicroRNA-101, down-regulated in hepatocellular carcinoma, promotes apoptosis and suppresses tumorigenicity. Cancer Res 69:1135-1142.

Sun F, Fu H, Liu Q, Tie Y, Zhu J, Xing R, Sun Z, Zheng X (2008) Downregulation of CCND1 and CDK6 by miR-34a induces cell cycle arrest. FEBS Lett 582:1564-1568.

Sutton MA, Schuman EM (2006) Dendritic protein synthesis, synaptic plasticity, and memory. Cell 127:49-58.

Tai HC, Schuman EM (2006) MicroRNA: MicroRNAs reach out into dendrites. Current Biology 16:R121-R123.

Tan EM (1991) Autoantibodies in pathology and cell biology. Cell 67:841-842.

Tang SJ, Meulemans D, Vazquez L, Colaco N, Schuman E (2001) A role for a rat homolog of staufen in the transport of RNA to neuronal dendrites. Neuron 32:463-475.

Tarasov V, Jung P, Verdoot B, Lodygin D, Epanchintsev A, Menssen A, Meister G, Hermeking H (2007) Differential regulation of microRNAs by p53 revealed by massively parallel sequencing: miR-34a is a p53 target that induces apoptosis and G1-arrest. Cell Cycle 6:1586-1593.

Tazawa H, Tsuchiya N, Izumiya M, Nakagama H (2007) Tumor-suppressive miR-34a induces senescence-like growth arrest through modulation of the E2F pathway in human colon cancer cells. Proc Natl Acad Sci USA 104:15472-15477.

Teixeira D, Sheth U, Valencia-Sanchez MA, Brengues M, Parker R (2005) Processing bodies require RNA for assembly and contain nontranslating mRNAs. RNA 11:371-382.

Tenenbaum SA, Carson CC, Lager PJ, Keene JD (2000) Identifying mRNA subsets in messenger ribonucleoprotein complexes by using cDNA arrays. Proc Natl Acad Sci USA 97:14085-14090.

Thomas MG, Tosar LJM, Loschi M, Pasquini JM, Correale J, Kindler S, Boccaccio GL (2005) Staufen recruitment into stress granules does not affect early mRNA transport in oligodendrocytes. Mol Biol Cell 16:405-420.

van Dijk E, Cougot N, Meyer S, Babajko S, Wahle E, Séraphin B (2002) Human Dcp2: a catalytically active mRNA decapping enzyme located in specific cytoplasmic structures. EMBO J 21:6915-6924.

Vasudevan S, Steitz JA (2007) AU-rich-element-mediated upregulation of translation by FXR1 and Argonaute 2. Cell 128:1105-1118.

Vasudevan S, Tong Y, Steitz JA (2007) Switching from repression to activation: microRNAs can up-regulate translation. Science 318:1931-1934.

Vasudevan S, Tong Y, Steitz JA (2008) Cell-cycle control of microRNA-mediated translation regulation. Cell Cycle 7:1545-1549.

Villacé P, Marión RM, Ortín J (2004) The composition of Staufen-containing RNA granules from human cells indicates their role in the regulated transport and translation of messenger RNAs. Nucleic Acids Res 32:2411-2420.

Volinia S, Calin GA, Liu CG, Ambs S, Cimmino A, Petrocca F, Visone R, Iorio M, Roldo C, Ferracin M, Prueitt RL, Yanaihara N, Lanza G, Scarpa A, Vecchione A, Negrini M, Harris CC, Croce CM (2006) A microRNA expression signature of human solid tumors defines cancer gene targets. Proc Natl Acad Sci USA 103:2257-2261.

Volterra A, Meldolesi J (2005) Astrocytes, from brain glue to communication elements: the revolution continues. Nat Rev Neurosci 6:626-640.

Wang L, Oberg AL, Asmann YW, Sicotte H, McDonnell SK, Riska SM, Liu W, Steer CJ, Subramanian S, Cunningham JM, Cerhan JR, Thibodeau SN (2009) Genome-wide transcriptional profiling reveals microRNA-correlated genes and biological processes in human lymphoblastoid cell lines. PLoS ONE 4:e5878.

Wang X, Tang S, Le SY, Lu R, Rader JS, Meyers C, Zheng ZM (2008) Aberrant expression of oncogenic and tumor-suppressive microRNAs in cervical cancer is required for cancer cell growth. PLoS ONE 3:e2557.

Wang YP, Li KB (2009) Correlation of expression profiles between microRNAs and mRNA targets using NCI-60 data. BMC Genomics 10:218.

Wei JS, Song YK, Durinck S, Chen QR, Cheuk ATC, Tsang P, Zhang Q, Thiele CJ, Slack A, Shohet J, Khan J (2008) The MYCN oncogene is a direct target of miR-34a. Oncogene 27:5204-5213.

Welch C, Chen Y, Stallings RL (2007) MicroRNA-34a functions as a potential tumor suppressor by inducing apoptosis in neuroblastoma cells. Oncogene 26:5017-5022.

Xu T, Zhu Y, Xiong Y, Ge YY, Yun JP, Zhuang SM (2009) MicroRNA-195 suppresses tumorigenicity and regulates G1/S transition of human hepatocellular carcinoma cells. Hepatology 50:113-121.

Yamakuchi M, Ferlito M, Lowenstein CJ (2008) miR-34a repression of SIRT1 regulates apoptosis. Proc Natl Acad Sci USA 105:13421-13426.

Yanaihara N, Caplen N, Bowman E, Seike M, Kumamoto K, Yi M, Stephens RM, Okamoto A, Yokota J, Tanaka T, Calin GA, Liu CG, Croce CM, Harris CC (2006) Unique microRNA molecular profiles in lung cancer diagnosis and prognosis. Cancer Cell 9:189-198.

Yang WH, Yu JH, Gulick T, Bloch KD, Bloch DB (2006) RNA-associated protein 55 (RAP55) localizes to mRNA processing bodies and stress granules. RNA 12:547-554.

Yang Z, Jakymiw A, Wood MR, Eystathioy T, Rubin RL, Fritzler MJ, Chan EK (2004) GW182 is critical for the stability of GW bodies expressed during the cell cycle and cell proliferation. J Cell Sci 117:5567-5578.

Yoo NJ, Hur SY, Kim MS, Lee JY, Lee SH (2010) Immunohistochemical analysis of RNA-induced silencing complex-related proteins AGO2 and TNRC6A in prostate and esophageal cancers. APMIS 118:271-276.

Yu JH, Yang WH, Gulick T, Bloch KD, Bloch DB (2005) Ge-1 is a central component of the mammalian cytoplasmic mRNA processing body. RNA 11:1795-1802.

Zee JM, Shideler KK, Eystathioy T, Bruecks AK, Fritzler MJ, Mydlarski PR (2008) GW bodies: cytoplasmic compartments in normal human skin. J Invest Dermatol 128:2902-2912.

Zeitelhofer M, Karra D, Macchi P, Tolino M, Thomas S, Schwarz M, Kiebler M, Dahm R (2008) Dynamic interaction between P-bodies and transport ribonucleoprotein particles in dendrites of mature hippocampal neurons. J Neurosci 28:7555-7562.

Zeng F, Peritz T, Kannanayakal TJ, Kilk K, Eiriksdottir E, Langel U, Eberwine J (2006) A protocol for PAIR: PNA-assisted identification of RNA binding proteins in living cells. Nat Protoc 1:920-927.

Zeng Y, Sankala H, Zhang X, Graves PR (2008) Phosphorylation of Argonaute 2 at serine-387 facilitates its localization to processing bodies. Biochem J 413:429-436.

Zhu Q, Hong A, Sheng N, Zhang X, Matejko A, Jun KY, Srivannavit O, Gulari E, Gao X, Zhou X (2007) microParaflo biochip for nucleic acid and protein analysis. Methods Mol Biol 382:287-312.

Zipprich JT, Bhattacharyya S, Mathys H, Filipowicz W (2009) Importance of the C-terminal domain of the human GW182 protein TNRC6C for translational repression. RNA 20:781-793.

APPENDIX B: COMPLETE LIST OF PUBLICATIONS DURING THESIS

Moser JJ and Fritzler MJ. The MicroRNA and MessengerRNA Profile of the RNA-Induced Silencing Complex in Human Primary Astrocyte and Astrocytoma Cells. *Submitted to PLoS ONE May 04, 2010.*

Moser JJ and Fritzler MJ. Cytoplasmic ribonucleoprotein (RNP) bodies and their relationship to GW/P bodies. International Journal of Biochemistry and Cell Biology, 2010 Jun;42(6):828-43.

Moser JJ, Fritzler MJ, Ou Y, Rattner JB. The PCM-Basal Body/Primary Cilium Coalition. Seminars in Cell and Developmental Biology, 2010 Apr;21(2):148-55.

Moser JJ, Fritzler MJ, Rattner JB. Primary ciliogenesis defects are associated with human astrocytoma/glioblastoma cells. BMC Cancer, 2009 December 17;9:448.

Ou Y, Ruan Y, Cheng M, **Moser JJ**, Rattner JB, van der Hoorn FA. Adenylate cyclase regulates elongation of mammalian primary cilia. Experimental Cell Research, 2009 Oct 1; 315(16):2802-2817.

Moser JJ, Chan EKL, Fritzler MJ. Detection of components of GW Bodies by immunoprecipitation and western blot analysis. Nature Protocols, 2009 Apr 16; 4(5):674-685.

Li S, Lian S*****, **Moser JJ***, Fritzler ML, Fritzler MJ, Satoh M, and Chan EKL. Identification of GW182 and its novel isoform TNGW1 as translational repressors in Ago2 mediated silencing. Journal of Cell Science, 2008, Dec 15; 121(Pt 24):4134-4144. *****Authors contributed equally to this work.

Moser JJ, Eystathioy T, Chan EKL, Fritzler MJ. Markers of mRNA stabilization and degradation, and RNAi within astrocytoma GW bodies. Journal of Neuroscience Research, 2007 Jul 30; 85(16): 3619-3631.